2014-06-04

Neotectonics on the Edge of the Cuban Fold and Thrust Belt

Deniz Kula
University of Miami, denizkula@hotmail.com

Recommended Citation

UNIVERSITY OF MIAMI

NEOTECTONICS ON THE EDGE OF THE CUBAN FOLD AND THRUST BELT

By

Deniz Kula

A THESIS

Submitted to the Faculty
of the University of Miami
in partial fulfillment of the requirements for
the degree of Master of Science

Coral Gables, Florida

August 2014

UNIVERSITY OF MIAMI

A thesis submitted in partial fulfillment of
the requirements for the degree of
Master of Science

NEOTECTONICS ON THE EDGE OF THE CUBAN FOLD AND THRUST BELT

Deniz Kula

Approved:

_____
Gregor P. Eberli, Ph.D.
Professor of Marine Geology
and Geophysics

_____
Chris Harrison, Ph.D.
Professor of Marine Geology
and Geophysics

_____
Ralf J. Weger, Ph.D.
Associate Scientist of Marine Geology
and Geophysics

_____
M. Brian Blake, Ph.D.
Dean of the Graduate School

_____
Thomas Luedmann, Ph.D.
Research Assistant of Geological Sciences
University of Hamburg

KULA, DENIZ   (M.S. Marine Geology and Geophysics)
<u>Neotectonics on the Edge of</u>   (August 2014)
<u>the Cuban Fold and Thrust Belt</u>

Abstract of a thesis at the University of Miami.

Thesis supervised by Professor Gregor P. Eberli.
No. of pages in text (118)

The Santaren Channel separates Cuba and Cay Sal Bank, the westernmost platform of the Bahamian archipelago, from Great Bahama Bank. Multichannel seismic data from the southern Santaren Channel reveal that the outer edge of the Cuban Fold and Thrust Belt is situated within the channel. Newly acquired 2D high-resolution multichannel seismic data east and north of Cay Sal Bank reveal that the bank itself is part of the Cuban Fold and Thrust Belt. In addition, seafloor displacements, observed in the seismic data, the multibeam-bathymetry, and sub-bottom (parasound) profiles, document neotectonic activity in the area.

The data sets acquired during the M95 cruise on the R/V *Meteor* in 2013 are combined with the old regional seismic profiles and tied to the borehole information from ODP LEG 166 and the deep industrial Great Isaac-1 well on the northwestern tip of Great Bahama Bank. These combined data sets allow the tectono-stratigraphic evolution of Cay Sal Bank and its adjacent seaway to be delineated. Careful processing that included migration of the newly acquired seismic data produced high-quality seismic images that improve the imaging of the various structural elements and the stratigraphic correlation of facies and tectonic changes in the study area.

The Santaren Channel is a long-lived, deep-water re-entrant into the shallow-water platform area that formed after Jurassic rifting but it experienced morphologic alterations from the Cretaceous to the recent time. The horizon map of the top Albian reflection illustrates a wide and deep channel that was bordered on both sides by the steep slopes of the adjacent platforms. In the Turonian, compressional forces fold part of the deep-water sediments into a NNW-SSE trending anticline that remains a high until the Early Miocene. With the onset of the Florida Current and the concomitant onset of drift deposition in the Santaren Channel, the anticline is buried. The increased sedimentation rate from the drift deposition results in a shoaling of the seaway and the transformation into a V-shaped form. Seven depositional systems are identified in the seismic facies analysis in the region. Most pronounced is the near vertical juxtaposition of the chaotic-transparent seismic facies of shallow-water carbonates with the more continuous seismic reflections of the deep-water sediments. Within the deep-water facies, high-amplitude reflections (turbidites), chaotic-transparent intervals (slump units) and down-cutting channels are seismic expressions of mass-gravity flow processes. Wavy seismic facies and large mounded sedimentary bodies are the result of current processes such as sand waves and drift deposits. Acoustic pipes are detected within the deep-water sediments associated with pockmarks and coral mounds, and are interpreted as fluid escape features.

The structural analysis reveals two types of fault systems; deep-rooted fault systems and strata-bound faults. The latter are the dominant structural feature in the southern profiles and the most dominant type in this system are polygonal faults that are interpreted as having formed by fluid escape. They are detected mostly in the drift deposits. The polygonal faults are associated with acoustic pipes and some end, like the

acoustic pipes, underneath pockmarks, indicating that they are also pathways for migrating fluid and hydrocarbons.

The deep-rooted fault systems are reminiscent of wrench faults but also display characteristics of thrust faults. These reactivated deep-rooted faults and growth anticlines on the eastern side of the Cay Sal Bank clearly place the edge of the Cuban Fold and Thrust Belt east of Cay Sal Bank into the Santaren Channel. An anticline protruding from Cay Sal Bank to the NE is the northeastern tip of the deformation. The position of these tectonic elements confirms that Cay Sal Bank is part of the Cuban Fold and Thrust Belt. A sea-floor break that is around 40 km in length and 50 m in depth at the northeastern portion of the Cay Sal Bank document neotectonic activity along the outer fringe of the fold belt. Five earthquakes in early 2014 at the eastern edge of the Nortecubana Fault further south within the Fold and Thrust Belt document that present-day tectonism is occurring in the region. Based on all of these findings, a new structural model is proposed as a final product of this study. This model relocates the Cuban Fold and Thrust Belt further east and north and confirms continuous shortening between Cuba and the Bahamas.

ACKNOWLEDGMENTS

University of Hamburg, I had great support for my project and spent great times in Germany.

I am giving my warmest regards to the faculty of the Dokuz Eylul University's Geophysical Engineering Department and Seismic-Lab. Thank you for the high-level education that provided me with a great start for this challenging experience.

I would like to send my deepest thanks and love to my family, which is the beacon of my life leading me towards to the true path forever and a day. Demir and Doruk, my little flames, when the day comes you will become wildfires filling all of us with pride.

TABLE OF CONTENTS

LIST OF FIGURES

LIST OF TABLES

CHAPTER 1. INTRODUCTION

1.1. Introductory Remarks

Before the 1980's, the isolated carbonate platforms of the Bahamas were considered to be static systems, which hardly responded to tectonism. Using multi-channel seismic data from the northwestern part of the Great Bahama Bank, Eberli and Ginsburg (1987, 1989) reported that the modern platform configuration is a consequence of both tectonic activity and subsequent sedimentation.

The late Cretaceous-middle Eocene Cuban-North American collision dominated platform evolution and affected the tectonic regime of the area. Sheridan et al. (1988) proposed that the collision produced a wrench fault system, which controlled the position of the modern platforms. Interpreting the seismic data from the southern Great Bahama Bank also revealed that the collision triggered transtensional faults during the late Cretaceous and affected sediment deposition (Masaferro and Eberli, 1994). The convergence of Cuba and the Bahamas produced the Cuban Orogenic Belt. This convergence affected the area west of Great Bahama Bank with an anticline forming in the Santaren Channel (Ball et al., 1985). The movement of the belt continued northward and subsequently the carbonate platform drowned and was buried by post-orogenic deep-water carbonate sediments (Masaferro, 1997). The collision was triggered by the fault activity that controlled the position of the eastern side of the Cay Sal Bank margin (Masaferro et al., 2002). Re-activation of Jurassic extensional faults forced Cay Sal Bank to backstep. Under the effect of the wrench fault system, the bank backstepped to its modern position in the Middle Miocene and deep-water sediments covered the drowned portion of the platform. The modern Cay Sal Bank is just the remnant of a much larger

platform that stretched south to Cuba (Masaferro, 1997).

The Cuban Fold and Thrust Belt is another result of this collision. This Tertiary age thrust belt which extends throughout the island of Cuba is a result of a shortening in the region. There is a controversy about the location of the Cuban Fold and Thrust Belt. While one group of scientists claims that the belt is located on the northern side of Cuba (Figure 1-1), based on the studies from Ball et al. (1985) and Masaferro (1997), the Cuban Fold and Thrust Bell might go further north.
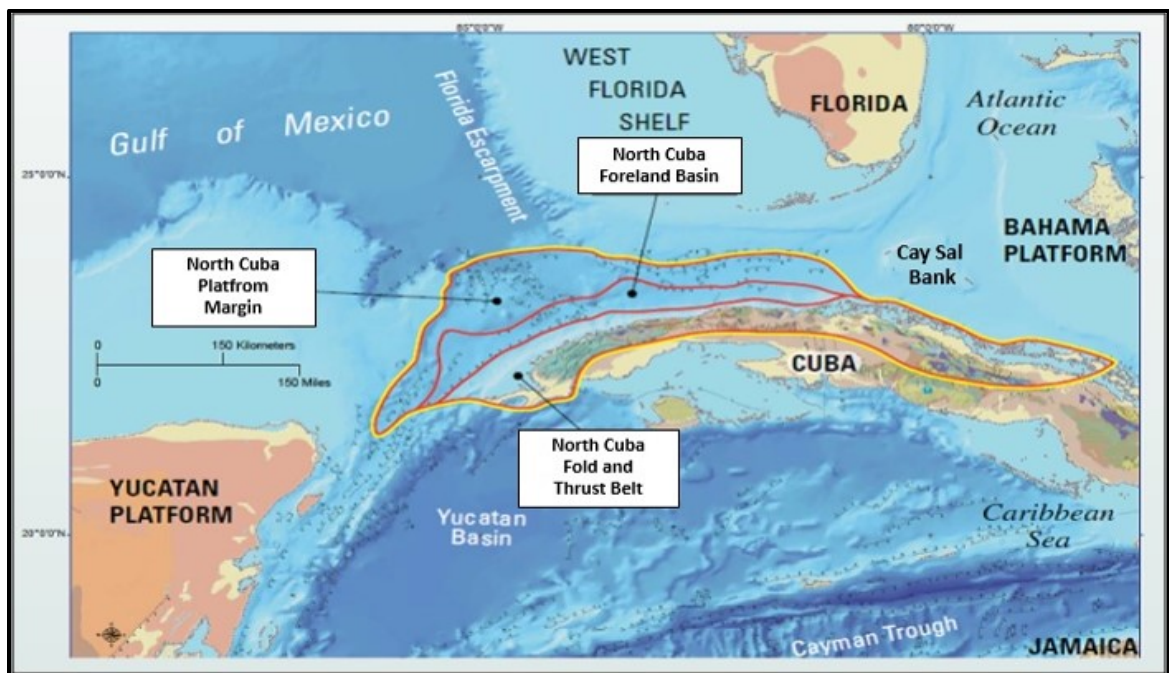
Figure 1-1. Location map of the Cuban Fold and Thrust Belt modified after U.S. Geological Survey, 2004.

1.2. Scope of the Study

This thesis intends to evaluate the known tectonic features and their influence on the sedimentary evolution of the eastern part of Cay Sal Bank. In the course of this study, the following hypotheses are presented:

- Seismic interpretation and bathymetry observations deduce structures such as acoustic pipes, polygonal faults, pockmarks, and bright spots that are indicators of possible hydrocarbon migration within the deep-water sediments.

- The structural analysis reveals compressional structures consisting of anticlines, residual faults and tectonically influenced faults which are interpreted as part of the Cuban Fold and Thrust Belt. Furthermore, the anticline detected at the northeastern part of Cay Sal Bank might be the northern edge of the Cuban Fold and Thrust Belt.

- The sea floor breaks around the Cay Sal Bank and earthquake records indicate that the region is still active today.

In order to test the hypotheses mentioned above, two 2D seismic reflection data sets are interpreted along with the bathymetry and well log data. The first data set is a grid of 1363 km of 2D multi-channel seismic profiles gathered in April 2013 onboard the R/V *Meteor*, during the University of Hamburg research cruise M95. The second data set consists of regional seismic lines collected in the 1980's during industrial activity in the Florida-Bahamas region (Figure 1-2).
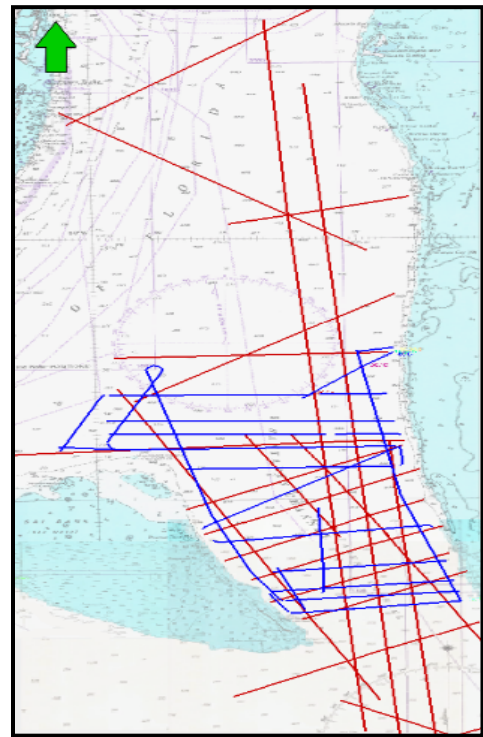
Figure 1-2. Location of the datasets. The newly gathered data set; blue lines, the old regional data set; red lines.

1.3. Outline of the Thesis

This thesis consists of six chapters:

Chapter One: *A general overview of the study area is briefly given in this chapter. The course of this study and methodology for testing proposed hypotheses are described concisely.*

Chapter Two: *This chapter presents background information of the study area and outlines the general geological setting and its tectonic history. Arguments of previous studies in the area are summarized to compare their findings with our new result.*

Chapter Three: The *acquisition of 2D seismic reflection data is briefly described in the first section. The second section addresses the 2D seismic data processing. In particular, the processing of the seismic data using the ProMAX software is explained in detail. The chosen modules, parameters and their effects on the data are illustrated using selected seismic profiles.*

Chapter Four: *This chapter is comprised of seismic interpretation. Well log information will be used to correlate the mapped horizons. Surface maps are created and seismic facies analysis is performed.*

Chapter Five: *This chapter identifies geological elements required to outline the tectonic modification of the study area. Structural maps are created to reveal the connection between the observed deep-rooted fault systems with the Cuban Fold and Thrust Belt.*

Chapter Six: *Summary of the study and discussion of arguments are given in this final chapter.*

CHAPTER 2. BACKGROUND INFORMATION

2.1. Geological Settings and Sedimentology

The Bahamian archipelago is a modern, large carbonate province that is located on the southeastern edge of the North American continent (Mayerhoff and Hatten, 1974; Anselmetti et al., 2000). The carbonate platforms of the Bahamas have been extensively investigated by scientists for a long time because of their enormous areal extent and thickness (Meyerhoff and Hatten, 1974). The Bahamas can be divided into two portions based on topography and structural features: a northwestern area which consists of the largest carbonate platforms, Great Bahama Bank and Little Bahama Bank, and a southeastern area dominated by many small banks (Uchupi et al., 1971).

There are two competing hypotheses about the origin of the Bahamian archipelago. One group of scientists proposes that Early Jurassic rift topography caused the modern pattern of bank-channel morphology. The other group argues that the modern array of platforms and troughs were created by the partial drowning of the megabank in the Mid-Cretaceous as a consequence of a carbonate crisis in the world's ocean (Austin et al., 1988a). Eberli and Ginsburg (1987, 1989) proposed that the Bahamian platforms experienced not only drowning or rifting events, but that tectonic activities and coalescence of platforms play also an important role in shaping the modern platform configuration.

The shallow-water banks and the deep-water areas are the two distinct features that define the modern Bahamian topography. The shallow water areas consist of several flat-topped, steep-sided carbonate platforms. The shallow-marine carbonate platforms of

the Bahamas are isolated and inclusive of a zone around 125,000 km² out of the 300,000

km² of the total area of the Bahamas (Bergman et al., 2010).

The relief of the Bahama banks is low and the average water depth is less than 10

m with water depth slightly increasing to the north; the deep-water regions and channels

isolate the banks in all directions (Boss and Rasmussen, 1995; Bergman et al., 2010):

- In the east, the Tongue of the Ocean divides Andros Island from New Providence Island; as a deep basin example, Exuma Sound divides Exuma Island from Cat Island.

- In the west, the Straits of Florida separates GBB from the North American Continent.

- In the north, the Blake Plateau abuts Little Bahama Bank.

- In the south, the Old Bahama Channel splits Great Bahama Bank from Cuba and the Santaren Channel divides GBB from Cay Sal Bank.
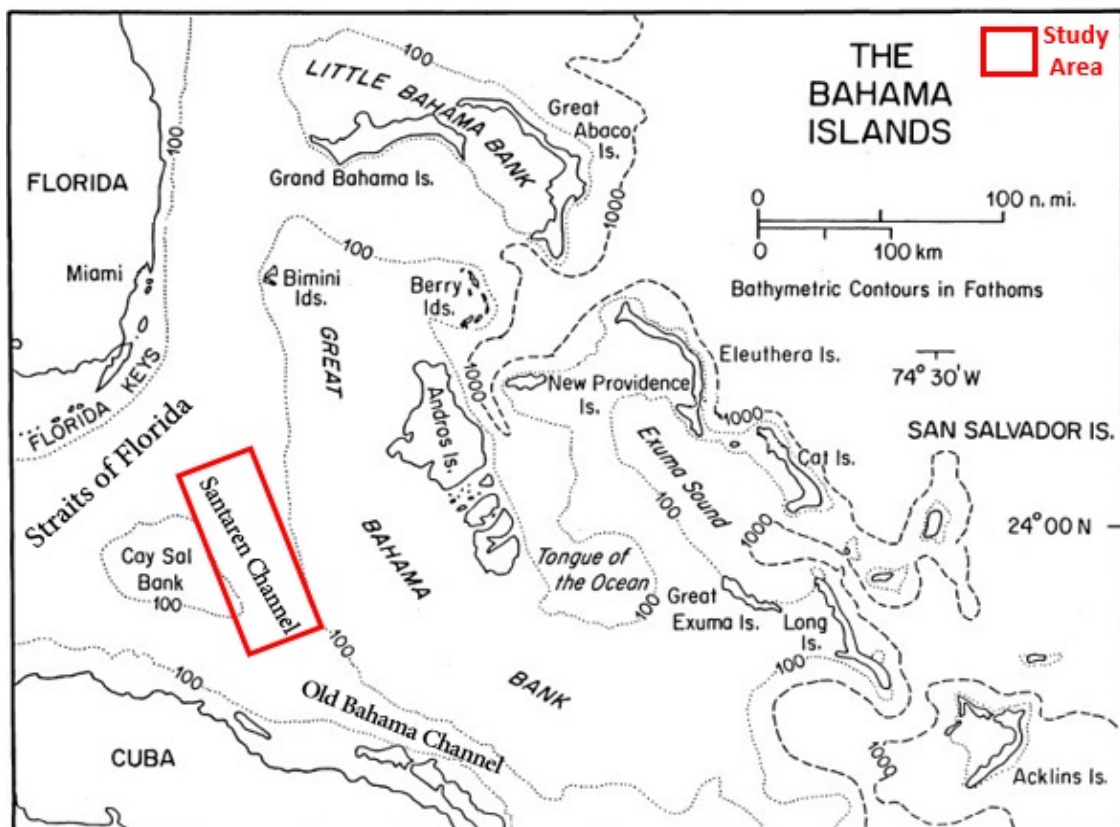
Figure 2-1. Location map of the Bahamas Banks and study area (Curran, 1997)

Cay Sal Bank is the third biggest platform in the region and is located in the westernmost portion of Great Bahama Bank. Unlike GBB or LBB, Cay Sal Bank has neither active sand shoals nor tidal flats. It is a small detached carbonate platform consisting of a restricted reef system and poorly developed margins with a thin sedimentary cover (Hine and Steinmetz, 1984). Because well-developed margins are lacking, the bank-top area is influenced by current energy and strong waves which transport sediments off the platform. Consequently, sediments are dominantly accumulated on the flanks and the platform top is deprived of sediments (Purkis et al., 2014). Cay Sal Bank has a deeper platform top than GBB and LBB, and has no high-energy shoals. Because of the lowered platform top profile Cay Sal is considered "partially drowned" (Hine and Steinmetz, 1984, Schlager 1981).

Sea-level conditions, tides and currents are important factors that control carbonate production and distribution. The production and transportation of sediments are highest, when carbonate platform is flooded (Mullins, 1983; Eberli, 1991; Eberli et al., 2000). Platforms are exposed during sea-level lowstands, and as a result sediment production is restricted to the fringes of the platforms. The Florida current is a strong surface current that flows between Florida and the Bahamas. This current dramatically influences the sedimentation of the region. The Santaren Channel is one of the subsidiary channels that contributes to the transportation of the Florida Current (Leaman et al., 1995). It is dominated by deep-water sediments approximately 10 km thick (Ball et al., 1985). The Santaren Drift lies along the channel. The Miami Terrace and the deposition of thick drift deposits show the effects of both current erosion and deposition (Anselmetti et al., 2000).

Figure 2-2 summarizes the distribution of sediment types on the Bahamas platforms. Bank margins contain skeletal sediments while the interior of the platforms are mostly formed of non-skeletal grains. Some of the platform interior areas protected by the topographic barriers consist of very-fine grained sediments (pelletoidal grainstone and packstone) (Reijmer et. al., 2009). Oolitic sands accumulate in high-energy areas dominated by tidal currents, forming various types of sand bodies. Broad fields of sand waves occur in more stabilized areas (Imbrie and Purdy, 1962). Cay Sal Bank is in the pathway of the Florida Current that influences the sedimentation around Cay Sal Bank. The northern and eastern sides of the bank consist of deep, rocky, sediment-barren terraces with restricted reef systems (Hine and Steinmetz, 1984).
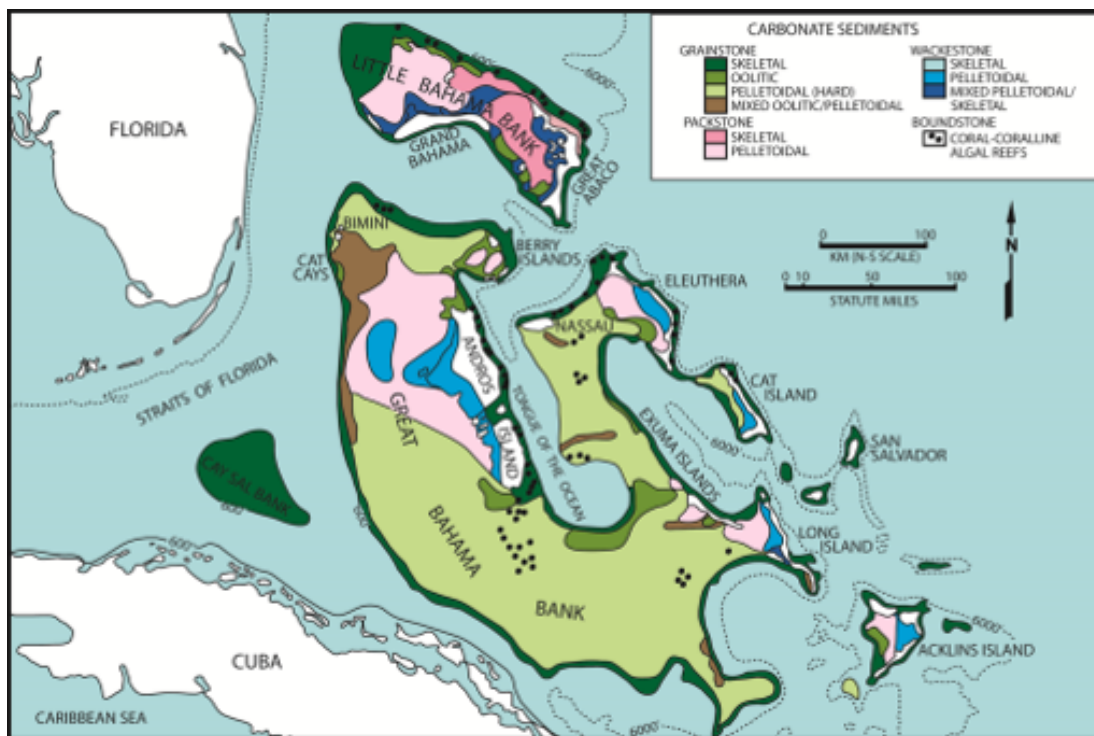
Figure 2-2. Sediment facies map of the northern platforms of the Bahamian archipelago. The top of Cay Sal Bank is all skeletal gainstone facies (Enos, 1974).

2.2. Plate Tectonic Settings

The platforms of the Bahamas archipelago were modified by several tectonic events (Masaferro and Eberli, 1999). In the Early-Middle Jurassic, North America and Africa began to drift apart; the Bahamas were most probably created on the rifted margin during this break up. The early configuration of carbonate platforms depends on the rift geometry consisting of half grabens, strike-slip and extensional faults in the Bahamas-Cuban area (Ross and Scotese, 1988; Sheridan et al., 1988; Masaferro and Eberli, 1999).

The Bahamas is tectonically bordered by the Cuban Orogenic Belt to the southwest and the Caribbean lithospheric plate to the south (Mullins and Lynts, 1977). Lewis (1990) and Walles (1993) characterized the paleographic setting of the southern edge of the Bahamas archipelago and northeastern Cuba as a large evaporite basin until the early Cretaceous. These evaporites indicated a restricted marine environment and shallow-water conditions throughout the Early Cretaceous (Masaferro and Eberli, 1999). Deep-water sediments have been recovered in the Cayo Coco area and in the northeast Providence Channel and south of San Salvador. In addition, the seismic facies in the southern portion of the Santaren Channel also indicates the presence of a deep re-entrant in this area (Masaferro and Eberli, 1999).

Relative plate motions changed in the Mid-Cretaceous not only in the Caribbean but also world-wide (Burke et al., 1984; Ross and Scotese, 1988; Meschede and Frisch, 1998). A change in polarity of the subduction zone (from NW to NE) induced a movement of the Greater Antilles towards the northeast in the Caribbean region (Ross and Scotese, 1988). This arc movement and the proto-Caribbean crust consumption stopped when the arc collided with the southern edge of the Bahamas platform in the Late

Cretaceous-Paleocene (Ross and Scotese, 1988; Pindell and Barrett, 1990; Mann et al., 1995).

As a result of this collision, the Cuban orogenic belt formed and the Bahamian region transformed into a foreland basin (Figure 2-3) (Masaferro, 1997; Masaferro and Eberli, 1999). Due to the plate rearrangement and associated fault activity, the margins of Andros and Bimini Banks were reactivated (Eberli and Ginsburg, 1987; 1989). Another result of this rearrangement was that interplate volcanism increased the volume of oceanic plate in the Pacific, creating a relative sea-level rise and increasing global spreading rates (Mullins et al., 1992). Evidence from Cuban geology suggests that the collision continued into the Middle Tertiary where younger Middle Eocene sediments unconformably overlay the greatly deformed collisional deposits (Masaferro and Eberli, 1999).

The collision decreased dramatically in the late Eocene. The NW part of the Bahamas-Cuban area became tectonically more stable as the Cuban Island arc detached from the Caribbean plate and became a part of the North American plate (Masaferro and Eberli, 1999). This collision reactivated reverse faults and growth anticlines throughout the Neogene. Continuous shortening throughout the Neogene indicates that the Cuban-American plate boundary might still be active (Masaferro et al., 1999).
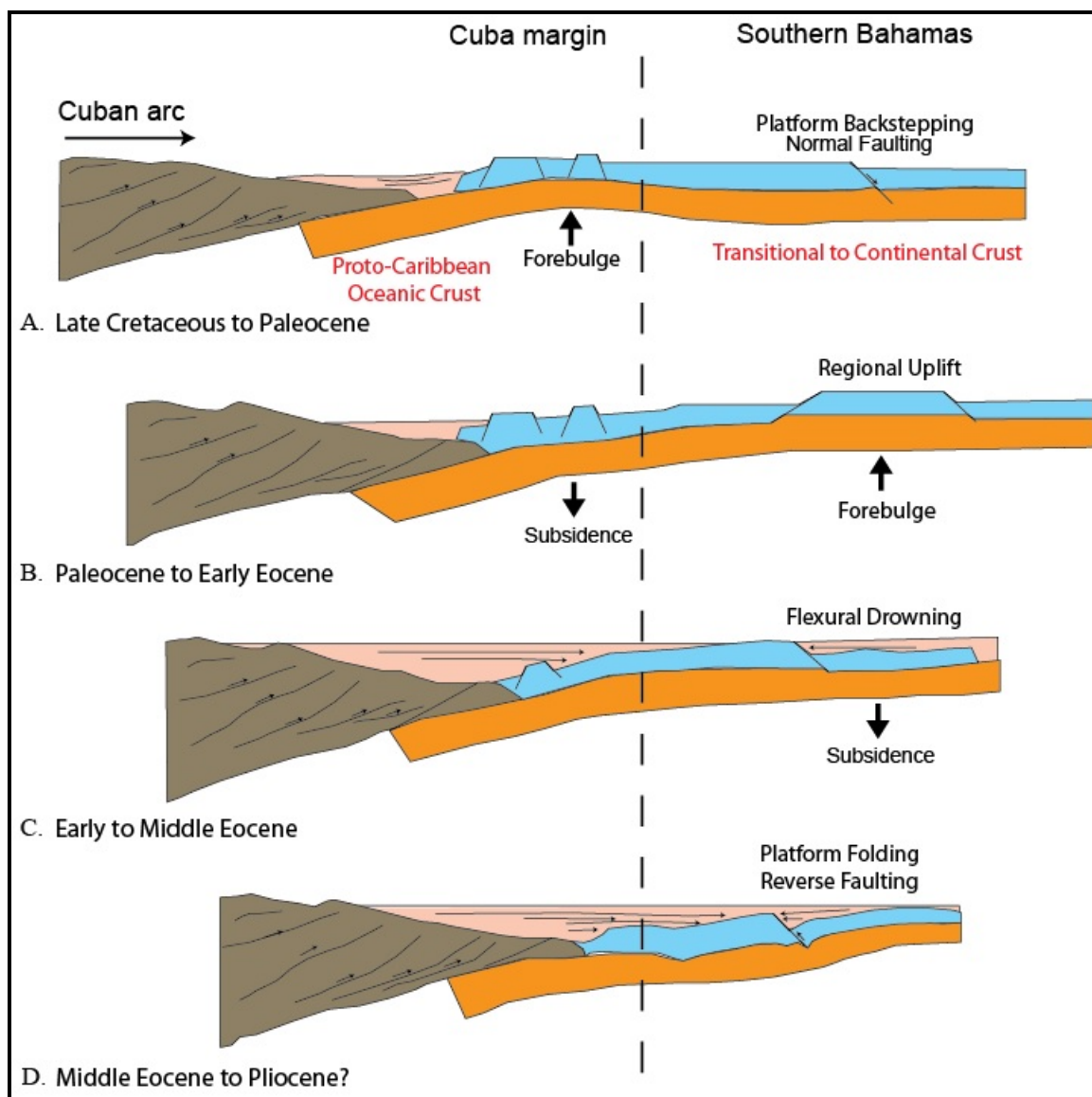
Figure 2-3. Interpretative geodynamic model of the evolution of the southern Bahamas area (proposed by Masaferro 1997 modified after Bergman 2005). In the late Cretaceous, the Caribbean plate collided with the North American plate forming the Cuban orogenic belt, which was a thrust system, and transforming the Bahamas into a foreland basin. During the Paleocene to Early Miocene, continuing northeastward migration created a regional uplift. Due to the loading of the Cuban orogeny, flexural drowning continued until the middle Eocene. By the late Eocene, collision decreased and folded the platform. The Cuban island arc was attached to the North American plate.

The Cuban Fold and Thrust Belt

The Cuban Fold and Thrust Belt was created as a result of the collision between the Caribbean and the North American plates during early Tertiary times (Gordon et al., 1997). It belongs to the Greater Antilles Island Arc formed from the Late Cretaceous continuing to Early Eocene times (Iturralde-Vinent, 1994). The origin of the convergence motion between the plates was farther to the west (Pindell and Barrett, 1990). Later on the thrust belt was dissected by the left-lateral strike-slip faults and the deformation front moved to the east (Saura et al, 2008). Reactivated reverse faults and growth anticlines in the Cuban Fold and Thrust Belt indicate that continuous shortening occurred at the most external part of the Cuban Fold and Thrust Belt throughout the Neogene and probably during the Quaternary (Masaferro et al., 1999). Despite this shortening, the Cuban Fold and Thrust Belt is seismically very quiet and few earthquakes have been reported in the last 50 years.

The Cuban orogeny consists of metamorphosed margin sediments, abducted ophiolites, imbricated platform carbonates, mélanges, and arc derived volcanic rocks (Masaferro, 1997). Two main structural units are defined in Cuba: foldbelt and neo-autochthon (Itturalde-Vinent, 1994). The foldbelt unit is mainly subdivided into continental (Bahamas and Yucatan platform) and oceanic units (volcanic arcs and ophiolities). The Bahamas platform and southwestern terrains formed the continental unit; whereas, the oceanic unit is composed of Cretaceous aged volcanic arcs, a northern ophiolitic belt and Paleocene island arc. The oldest element of the northern ophiolitic belt is considered Late Jurassic in age (Saura et al, 2008). The foldbelt unit is overlain by the neo-autochthon unit that consists of sedimentary rocks with latest Eocene to Recent ages.

A pronounced curvature causes diversity in the structural grain from eastern and central Cuba to western Cuba. The Florida-Bahamas margin in the west and the Yucatan margin in the east shaped the deformed Cretaceous North American margin observed today (Saura et al, 2008). The recent shape of the thrust belt can be defined as various outcrop areas divided by several post-orogenic sediments (Saura et al, 2008). The Island of Cuba along with the major structural units and tectonic elements are featured in Figure 2-4.
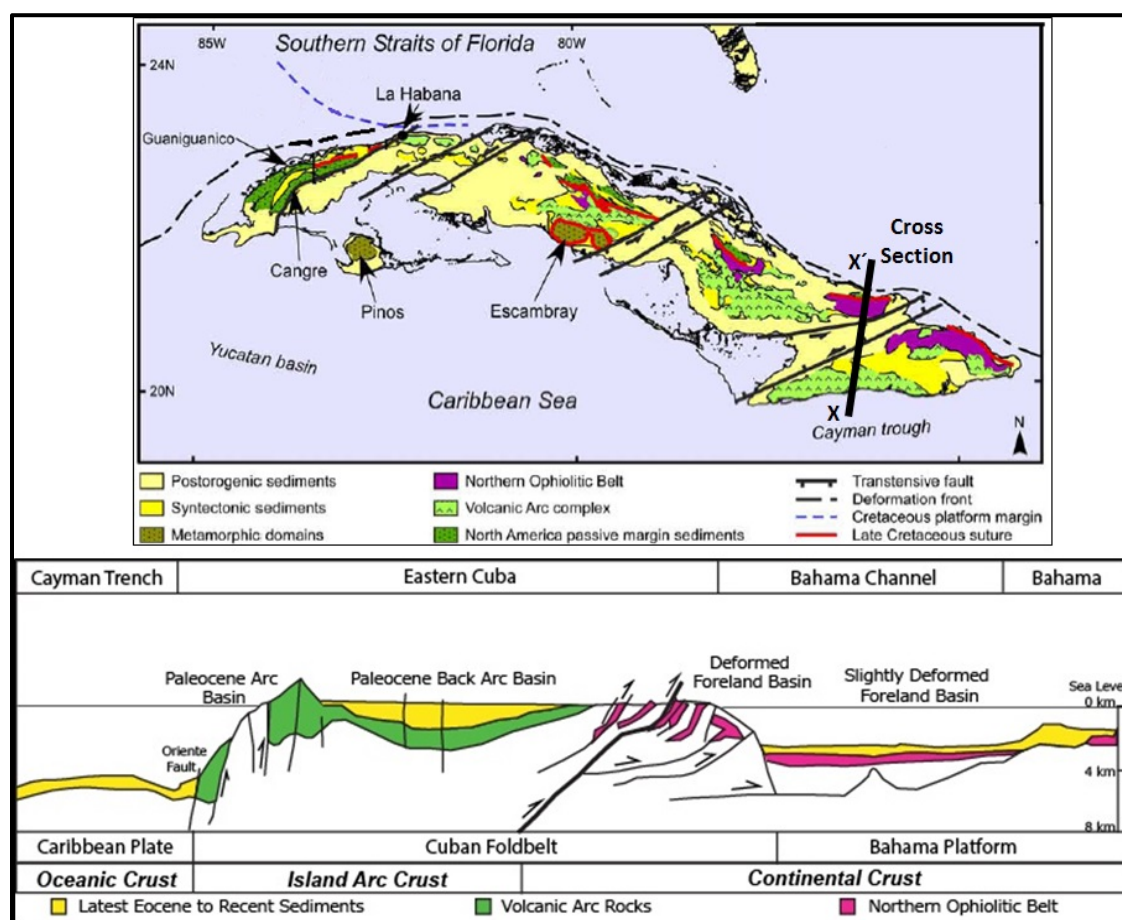
Figure 2-4. Geological framework map of Cuba (modified after Saura et al. 2008). Main structural units are defined, and different tectonic units are seperated by transtensional conjugated faults. Cross section from Cayman trench to the Bahamas foreland is represented by the black X-X´ line (modified after Iturralde-Vinent 2003). See text for discussion.

At present the motion of the Caribbean plate is eastwards relative to North America at a rate of 2 cm/year (Mann and Burke, 1984). The Cayman trough became an active spreading center in the Early Miocene, resulting in a strike-slip motion between the Caribbean and North American plates which continues today (Leroy et al., 2000). It is approximately 120 km wide, 5 km in depth and 1600 km in length (Draper et al., 1994). Its current spreading rate is about 15 mm/year (Rosencrantz et al., 1988). The northern plate margin stretches over the northern coast of Hispaniola, Puerto Rico and the western coast of the Lesser Antilles where the new subduction zone has formed (Dillon et al., 1987; Pindell and Barrett, 1990).
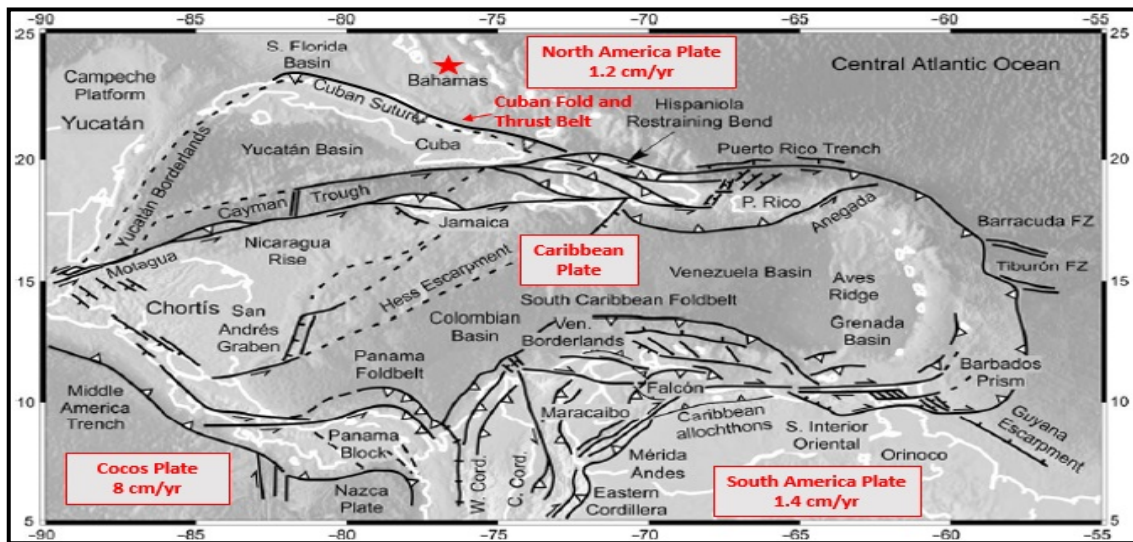
Figure 2-5. Tectonic sketch map of the Caribbean area (modified after Pindelland Kennan 2009). Plate motion directions and rates with respect to the Caribbean plate are from Gordon et al. 1997.

Masaferro and Eberli (1995) claimed that the compressional forces reactivated the main extensional fault on the eastern side of the Cay Sal Bank. Later on Masaferro (1997) observed some faults that emerged within younger horizons. This study contributes to these findings by investigating the active fault systems in the Santaren Channel and other compressional structures using a newly gathered high resolution seismic dataset.

CHAPTER 3. 2D SEISMIC DATA PROCESSING

3.1. Seismic Data Acquisition

The 2D seismic reflection data were gathered during the M95 cruise on board the R/V *Meteor* in April 2013 (Figure 3-1). The data set consists of 27 seismic profiles with a total length of 1393 km. Most profiles are oriented west to east crossing the Santaren channel between Great Bahama Bank and Cay Sal Bank. Three long profiles are oriented north-south in the center of the channel. In order to connect the borehole age information of the cores taken during the Ocean Drilling Program (ODP) Leg 166, one seismic profile (4) passed through the three sites drilled by ODP Leg 166 in 1996.

Detailed information regarding the seismic acquisition equipment is given by Dr. Thomas Luedmann in the R/V Meteor M95 CICARB's cruise report in the geophysics section. Two streamer systems were deployed. One 144-channel digital streamer had an active length of 600 m; the second one was a shorter 18-channel analog streamer. The depth of the long streamer was controlled by 4 birds and kept at 4 m. The guns were fired every 12.5 m. Data was sampled with a rate of 1 ms in the seven 24-channel digi-modules of the streamer to a record length of 3 s. The results in this thesis are based mostly on the data from the long streamer.
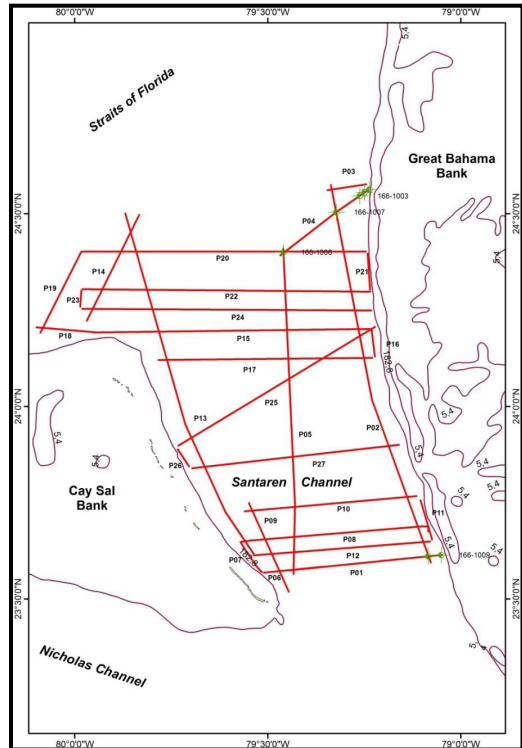
Figure 3-1. Base map of seismic sections (M95 cruise report of CICARB)

15

3. 2. Seismic Data Processing

Overview

Field records contain reflections, coherent noise and random ambient noise. The effect of noise on the signal during data gathering cannot be totally eliminated. Sideswipe and diffractions are also gathered. The main goal of seismic data processing is to increase the signal to noise ratio and to eliminate sideswipes, multiples and false reflection so that the acquired data is manipulated into an image which can be used to infer the sub-surface structure.

All 2D seismic reflection profiles were processed using Halliburton-Landmark ProMAX software. ProMAX is considered to be the industry standard seismic data processing software, having a wide variety of different modules and sections. Processing success depends on choosing the right routine and proper parameters. For this reason, seismic processing requires a substantial amount of time and precision. The processing flow used for this data set is given in Table 3-1.

Table 3-1. General Seismic Processing Flow
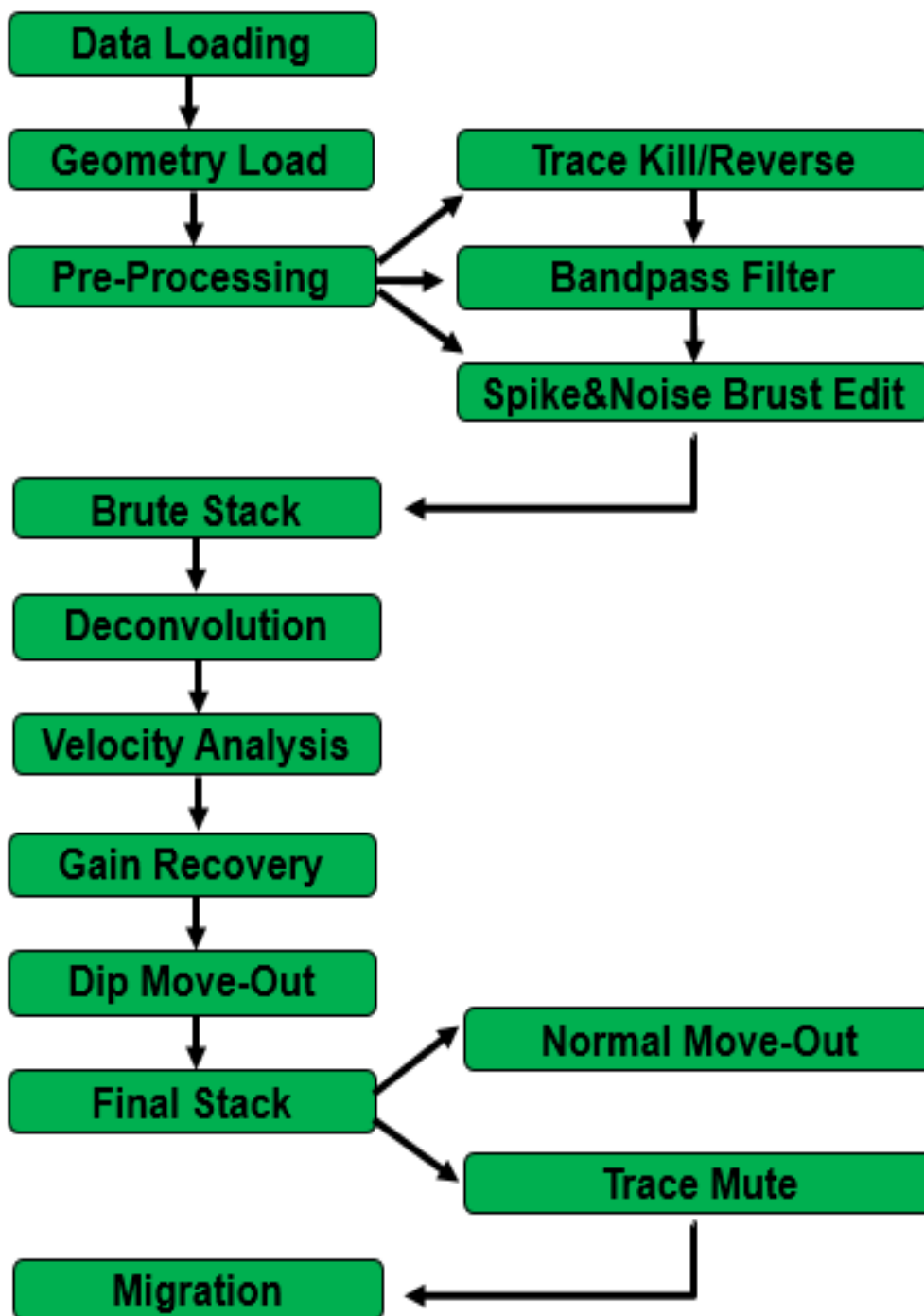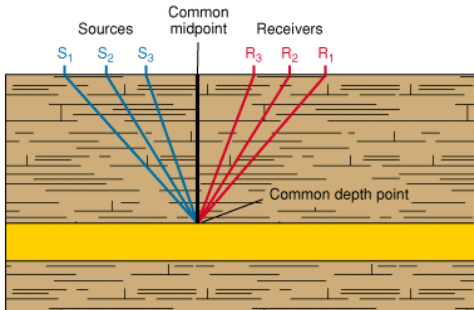
3.2.1 Data Loading

Seismic data are gathered in SEG-D format, a specific, legacy tape data format defined by the Society of Exploration Geophysicists. The first requirement for processing is converting the data from SEG-D format to a ProMAX internal data format. As an initial step, the data are uploaded to the ProMAX system and converted to the internal data using the tape-input process.

3.2.2. Geometry Load

The next step is integrating the survey data with the field geometry. Field geometry is merged with the seismic data using observation logs. Geometry assignment is a process that applies a trace number, a shot number, a receiver number, a common depth-point (CDP), an inline number, and a bin number to each trace. Loading the geometry allows the dataset to be sorted into single shots, CDP, or common offset bins. This is one of the most important processing steps that must be done very carefully before any other processing can be performed. In order to obtain accurate, geologically useful, quality images, accurate acquisition geometries (streamer length, shot interval, offsets between shots and receivers) must be defined. Some of the most important parameters and their explanations are given in Table 3-2.

Table 3-2. Parameters for Geometry Assignment

PARAMETERS	*VALUE*	*DEFINITION*
Channel Number	144	The number of channels located in the streamer
Receiver Interval (Group Interval)	6.25 m.	Distance between receiver (in meters)
Source Interval (Shot Interval)	12.5 m.	Distance between shots (in meters)
FFID/ SIN/	1-4591	FFID is the field file ID. This is usually the tape file number assigned to each shot at time of recording. SIN is the source index number.
Offset Bin Center Increment	6.25 m.	Offset is the distance from the source to the receiver (in meters).
Min and Max. CDP	2-9241	CDP (Common Depth Point) is the sum of seismic traces which reflects at the same point. *(picture is taken from Schlumberger online dictionary)*
Distance between CDPs	6.25 m.	The interval between CDPs. Generally it equals half of the shot interval (in meters).

3.2.3. Pre-processing

3.2.3.1. Trace Kill/ Reverse

Since only high quality data traces should be used for stacking, noisy traces and dead channels need to be eliminated from the data. This can be done using the "Kill/Reverse" module. A sequence of randomly chosen shot gathers is displayed in wiggle trace mode in order to determine the channels that have problems. The channel numbers of 3, 14, 55, 73,97 and 121 are found to be faulty and are deleted from the data. Figure 3-2 illustrates three noisy channels (channel number 3, 14 and 55) and their removal.
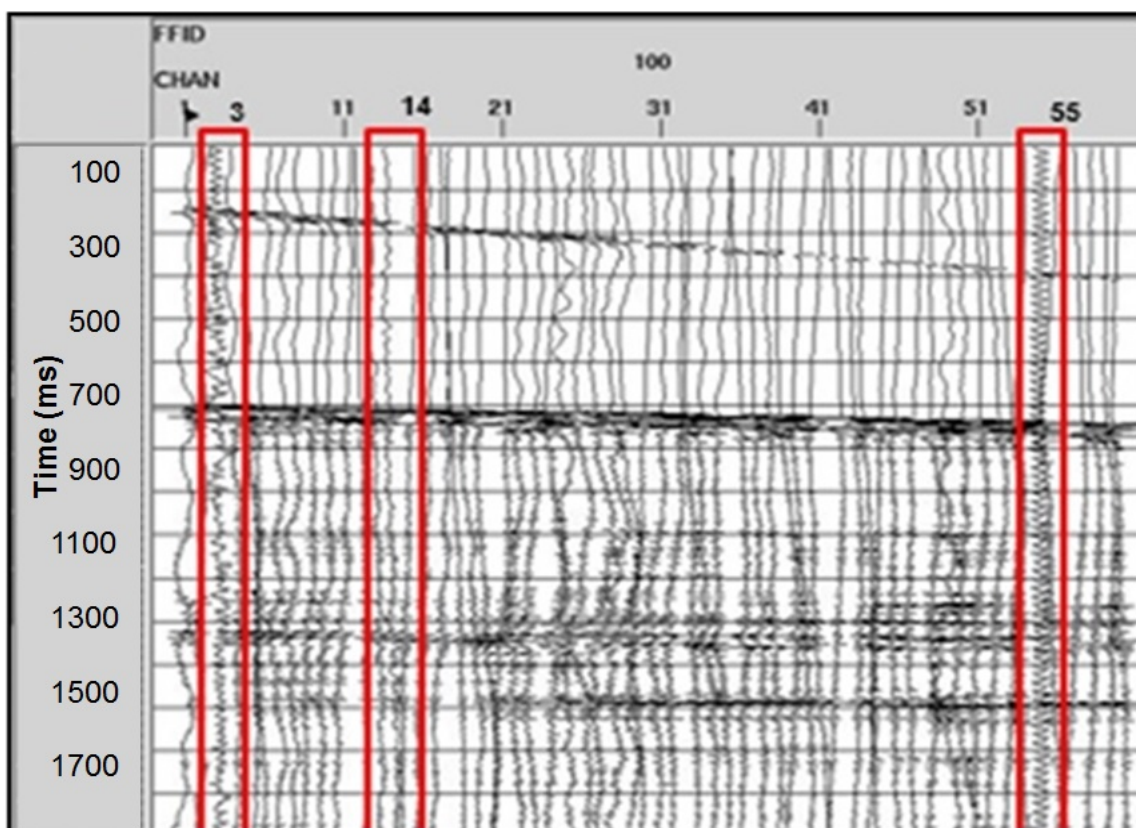
Figure 3-2. Wiggle trace display mode for Profile 27 FFID 100. Red boxes highlight three noisy channels identified as 3, 14, 55. These noisy traces are deleted from the data.

3.2.3.2. Bandpass Filter

A seismic trace typically contains some low frequency noise (swell noise and cable noise) and some ambient noise. Bandpass filtering is used to remove these extraneous noises. "Butterworth Bandpass" is selected as filter type and requires 4 corner frequencies as input parameters. These frequencies are chosen using the "Interactive Spectral Analysis" module (Figure 3-3) and are determined to be 10, 20, 200, and 220 Hz.
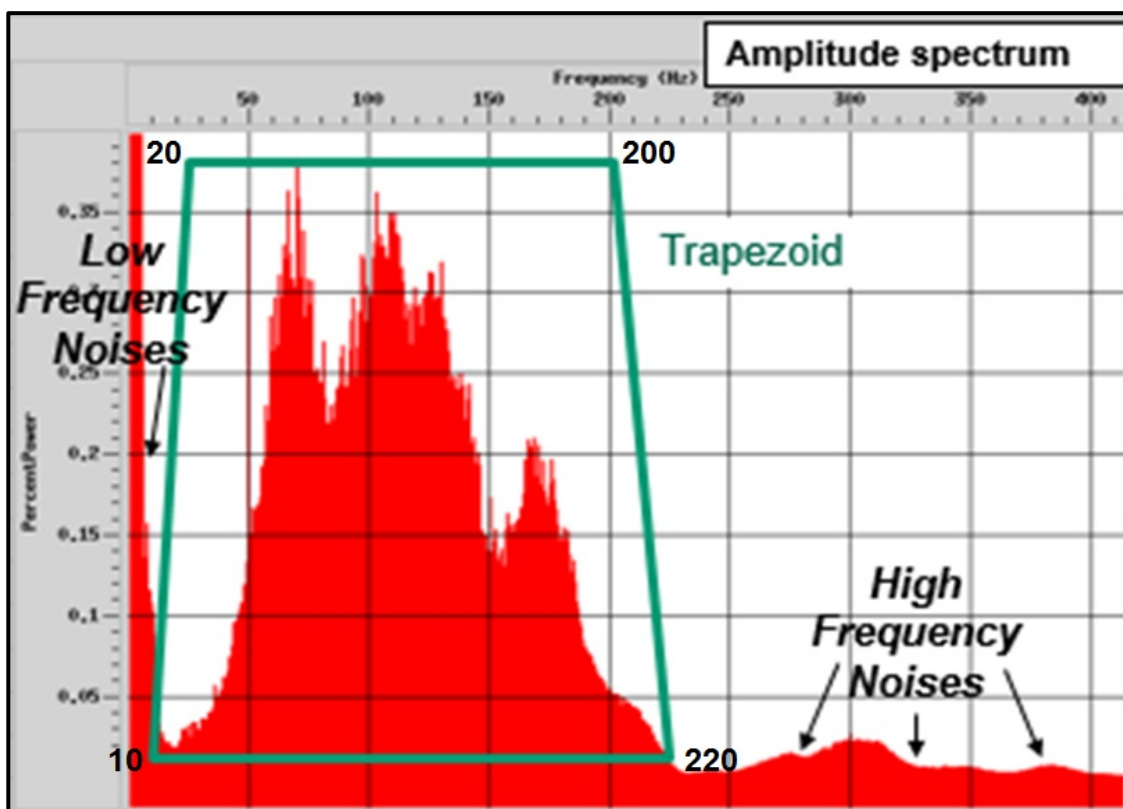
Figure 3-3. The Interactive Spectral Analysis Module. A trapezoid, which covers the information area is hypothetically drawn to eliminate low and high frequencies. The corners of this trapezoid specify four frequencies for Bandpass filtering.

3.2.3.3. Spike and Noise Burst Edit

ProMAX provides a sophisticated filtering module called "Spike and Noise Burst Edit". Although it does not always perform with equal effectiveness on all data types, it achieves excellent results on our profiles. The module localizes and eliminates simple spikes and multiple sample bursts of noise. Figure 3-4 shows one example of how data quality can be improved by applying "Spike and Noise Burst Edit".
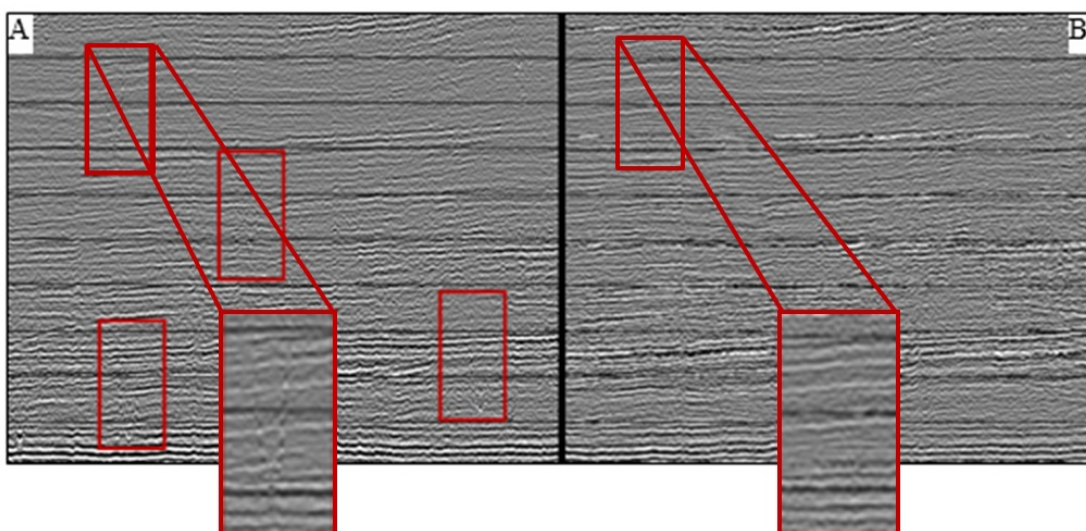
Figure 3-4. (A) Shows a section without application of the "Spike and Noise Burst Edit" module, and (B) shows the section with application of the same module. The spikes are indicated with red boxes.

3.2.4. Brute Stack

The aim of a brute stack is to provide an initial look at the structure of the line (Figure 3-5). Traces from common midpoint gathers are added together and Normal Moveout correction (NMO) is applied as a first attempt with a constant velocity field (1500 m/s). The details of the NMO module and the creation of the velocity field will be explained in detail in the following sections.

Figure 3-5. Brute Stack of Profile 27.

3.2.5. Deconvolution

Deconvolution is a filtering process that can be used to remove repeating signals called multiples from the recorded seismic trace. ProMAX offers several different deconvolution algorithms. In this study a targeted predictive deconvolution is used because it appears to produce the most accurate results. This algorithm also corrects the amplitude traces by using a separately calculated scale factor as deconvolution operator. The steps required during application of this module are explained below and listed in Table 3-3.

1. Picking the sea floor: A brute section is opened and the sea floor is picked. The resulting sea floor horizon is saved and named as WB_Time (water bottom time) (Figure 3-6).
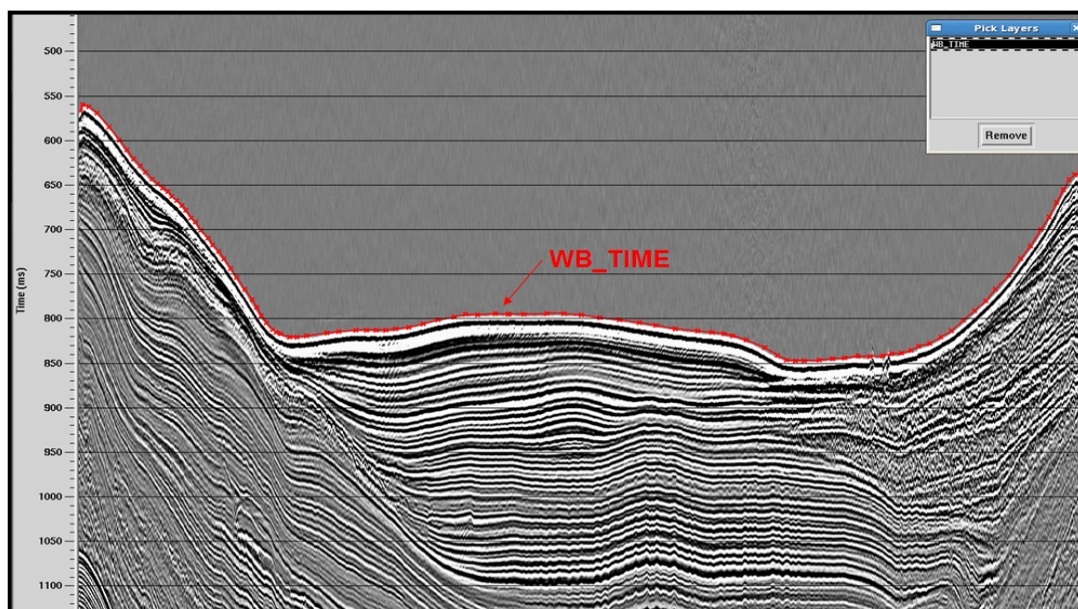
Figure 3-6. Picking WB_Time Horizon at profile 27.

2. The water bottom time horizon needs to be transferred to a database in order to be readable for the system. To achieve this, the database/horizon module is chosen.

3. The "Targeted Predictive Decon" module reads the required parameters from the trace headers. Specific equations are used to define the required decon parameters based on trace headers values. There are 6 trace headers needed to define 5 required decon parameters in the module. Their equations are given below.

- Decon window time   = [DECSTART=WB_TIME*0.89]

- Prediction distance   = [WB_MINUS= WB_TIME*0.4]

- Operator Length   = [WB_SLIDE= WB_TIME*0.6]

- Sliding window length = [TD_SLIDE= WB_TIME*0.9]

- Window step size   = [TD_STEP= WB_TIME*0.9]

(All numerical constants used above have been determined using parameter testing)

3.1. The "Targeted Predictive Decon" module is applied twice to improve the results. The first time it is used to calculate the "scale factors". The scale factor optimization parameters are determined using parameter testing (Figure 3-7).

3.2. In the second run, the scale factor determined in the first run is now used as an input for the optimization parameters in the "Targeted Predictive Decon" module (Figure 3-8). The errors in the amplitudes are fixed more accurately using this two-step "scale factor" optimization procedure.
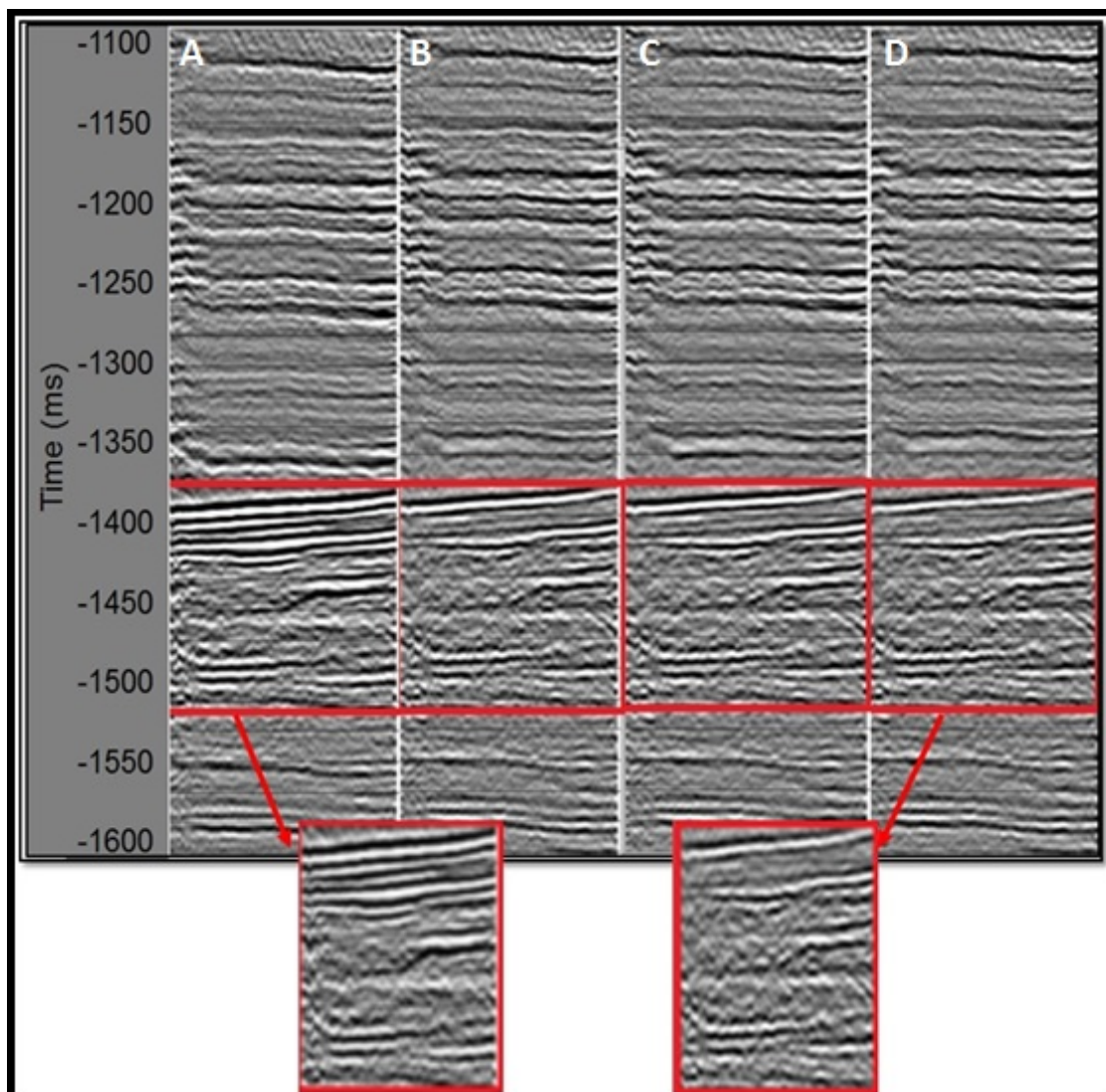
Figure 3-7. Comparison of parameter testing results. For each section the same FFID number (1100) is selected, and the first multiple zone, highlighted within a red box, is zoomed out at the same scale. Part (A) is before the application of deconvolution. Part (B) represents a section after the application of deconvolution; the scale factor parameter is selected as starting at 1 and ending at 17. Part (C) represents a section after the application of deconvolution; the scale factor parameter is chosen as starting at 0.01 and ending at 17. Part (D) represents a section after the application of deconvolution; the scale factor parameter is given as starting at 0.1 and ending at 17. Parameters that are used in Part D are selected for the module.
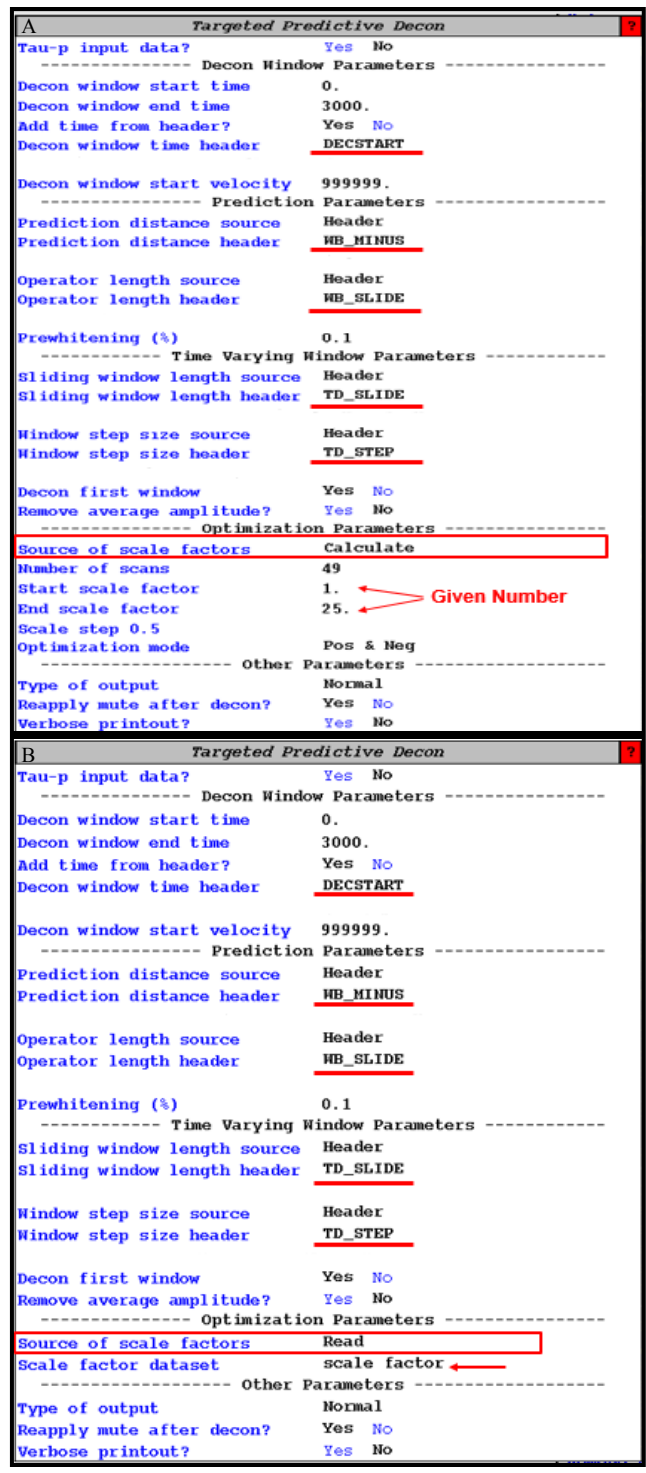
Figure 3-8. Section A is the first use of the module for calculating "scale factor". Section B is the final use of the module. Calculated scale factor is used as optimization parameters.

Table 3-3. General flow of the Deconvolution Module

Tool	Entry
Disk Data Input	Filter
Trace Header Math 1	Decon window time
Trace Header Math 2	Prediction distance
Trace Header Math 3	Operator Length
Trace Header Math 4	Sliding window length
Trace Header Math 5	Window step size
Targeted Predictive Decon	Scale Factor
Disk Data Output	Decon

As a result of "Targeted Predictive Decon", the dominant multiples are suppressed almost perfectly. However, signals adjacent to the multiples were slightly affected by this suppressing procedure. The impact of targeted predictive deconvolution can be seen in Figure 3-9. The sections are shown as brute stack (the near offset trace is used for each shot to see the sea floor and the strata below) with band-pass filters applied before and after deconvolution.
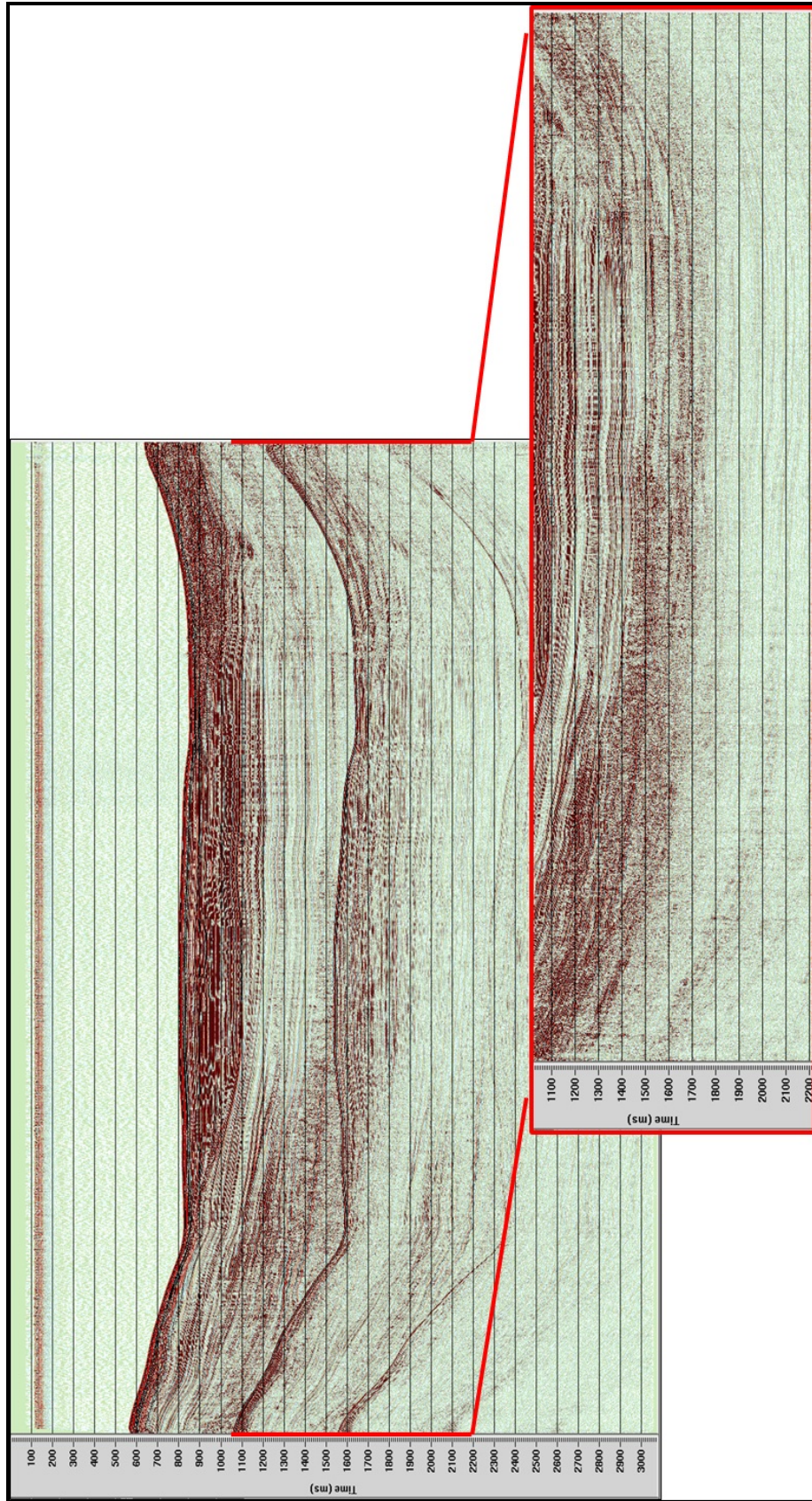
Figure 3-9. (A) Brute stack of Profile 27 before deconvolution is applied. Red boxes highlight the first and second multiple. (B) Brute stack of profile 27 after deconvolution is applied. The multiples are removed successfully.

3.2.6. Velocity Analysis

The product of seismic velocity and density is called acoustic impedance. The contrast between the acoustic impedance of different layers creates the contrast that reflects acoustic waves and forms the basis for seismic reflection. Velocities are extremely important for seismic processing and interpretation partially because velocity variations can be much larger then density variations. More importantly for seismic processing, the acoustic velocity of the strata is needed to compensate for the travel time differences between near and far traces. If the subsurface is composed of several layers with different elastic properties, seismic waves will pass through these layers with varying one way travel times that is often measured as Root-Mean Square (RMS) velocity (Dondurur, 2009). The RMS velocity is used in the travel time equation to eliminate arrival time differences between traces (Figure 3-10). This process is called Normal Moveout (NMO) Correction. The complete NMO is performed when producing the final stack; therefore, the details of the module will be explained in the final section.
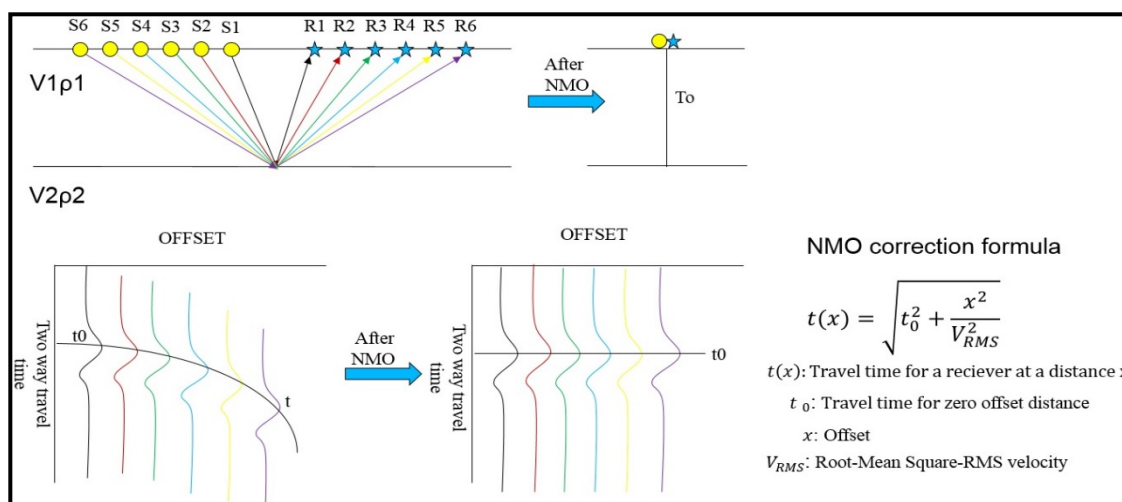
Figure 3-10. NMO Correction on CDP Gather. See text for discussion.

Velocity analysis is performed on the CDP (Common Depth Point). Figure 3-11 shows how RMS velocities are selected on a semblance plot and CDP gathers. A semblance is calculated by dividing the square of summed stack amplitudes by total gate power and is plotted as a function of time and velocity (Gadallah and Fisher, 2005). A semblance plot visually helps to generate the velocity model. The approximate velocity range for our data was determined to be between 1500-4250 m/s based on the ages of these units (from Pleistocene-Holocene to the base of Neogene).
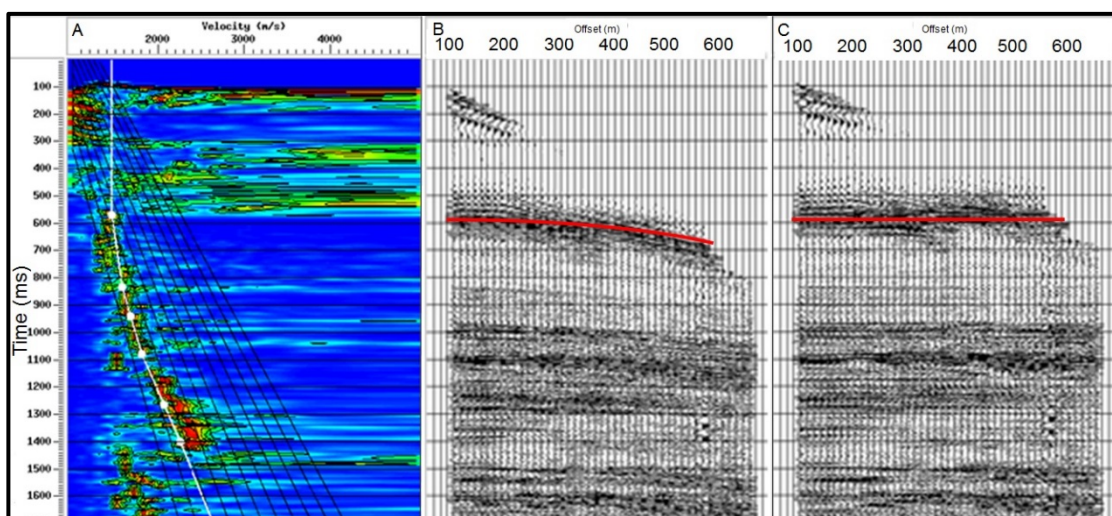
Figure 3-11. Velocity Analysis windows for Profile 27. Panel A shows a semblance plot; the white line with picks is our velocity function for the CDP 141. Panel B shows a common offset supergather of 5 stacked CDPs before NMO correction is applied. Panel C shows the same section after NMO correction is applied using selected velocities from panel A.

After velocity selection for a specified series of CDPs is completed, the program interpolates these 1D picks for the entire line to create a 2D velocity model. We named this model "brutestack" and saved it in table format. Velocities are expected to change smoothly rather than abruptly. To suppress abrupt changes, highlighted in Figure 3-12, a quality control module is applied. As a result, the velocity model is smoothed. The new velocity model is named "brutestacksmooth" and will be used in the DMO flow.
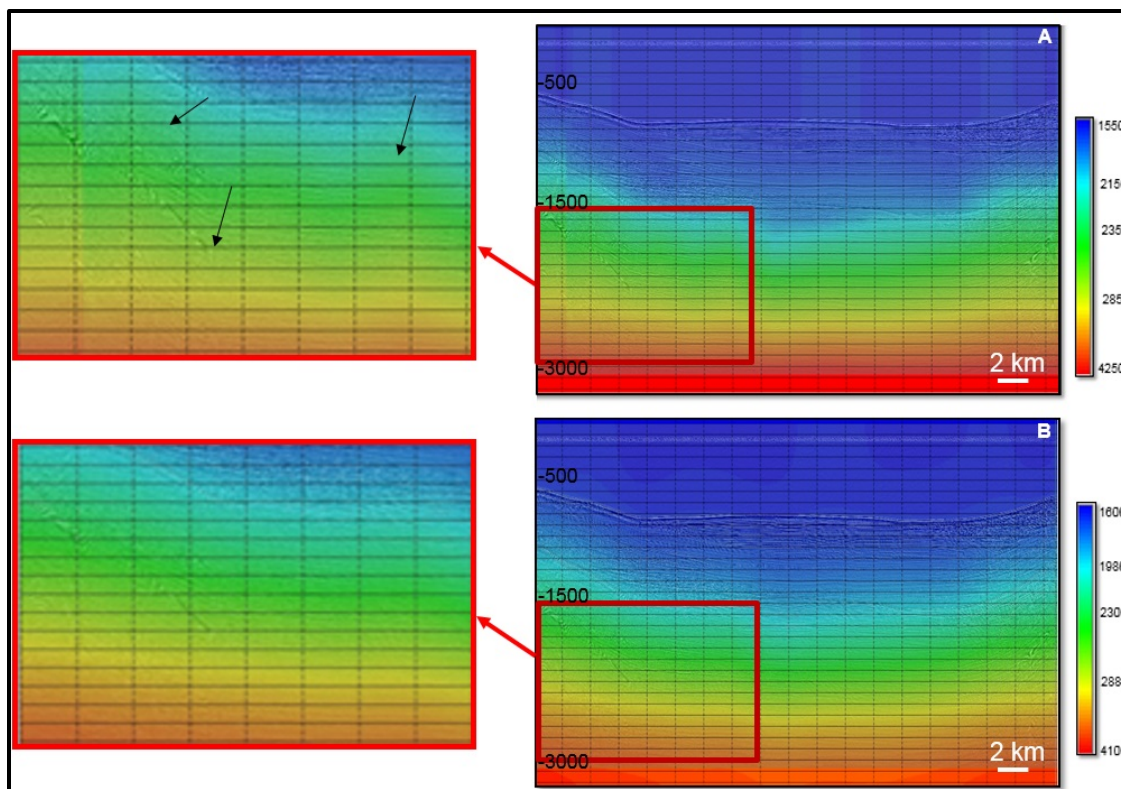
Figure 3-12. Section A and B illustrate the velocity field from profile 27. (A) The "Brutestack" velocity model is used as an input to create this section. Instantaneous velocity changes are shown with arrows. (B) The "Brutestacksmooth" velocity model created after smoothing is used as an input to create section B. The abrupt picks are eliminated.

3.2.7. Gain Recovery

Due to a variety of factors, seismic amplitude weakens as a seismic wave travels away from its source. Two of these factors are spherical divergence and absorption. Spherical divergence is the apparent loss of energy from a wave as it spreads during travel. Absorption depends on the physical properties of the dispersing medium. Consequently, traces recorded at far channels or sampled at later times show lower amplitudes than traces recorded at near channels or sampled early (Figure 3-13).
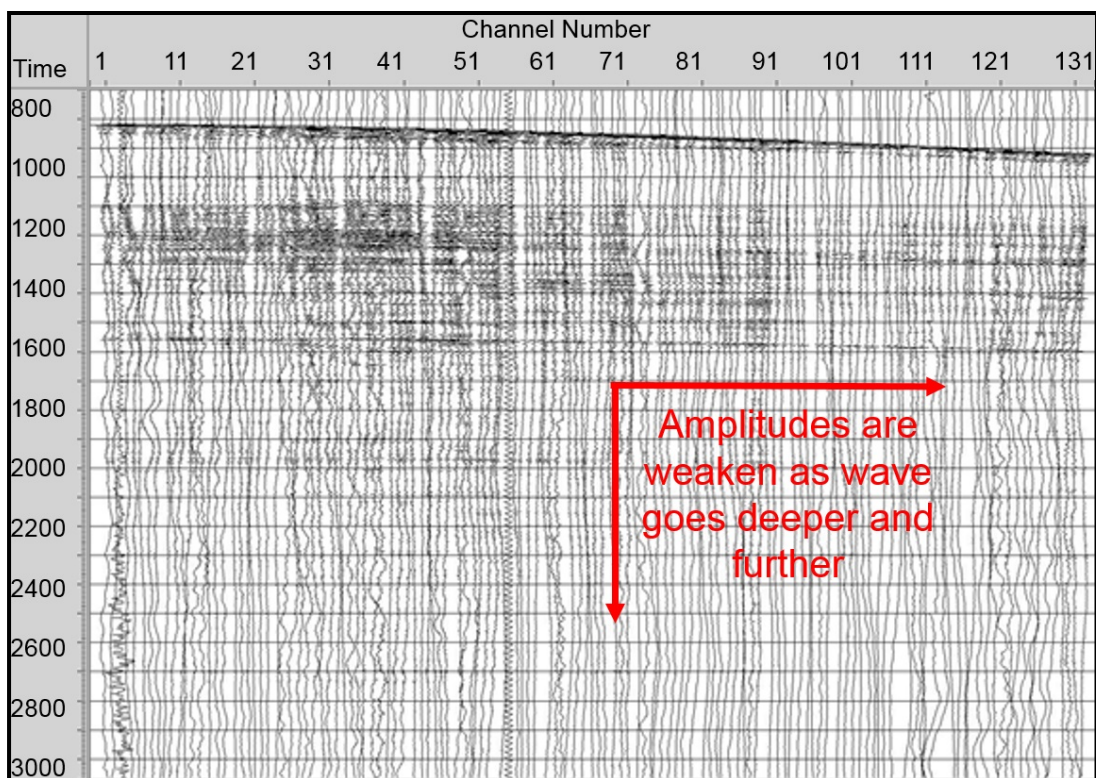
Figure 3-13. Trace display in wiggle trace mode for raw data. One FFID (800) is selected randomly and all channels are displayed in order to illustrate the amplitude loss at far channels and in late times.

There are several methods available to recover amplitudes that have been lost due to attenuation or spherical divergence. In our workflow, "True Amplitude Recovery" (TAR) and "Surface Consistent Amplitude" (SCA) are used to remedy these effects. Another type of gain recovery is called "Automatic Gain Recovery" (AGC). AGC was used during migration and a short explanation will be given there. A short description of the TAR and SCA procedures are given here:

1. True Amplitude Recovery helps to recover amplitudes that are weakened due to spherical wave front spreading. It uses a velocity model and a constant time correction to compensate for differences in amplitude caused by differences in travel distance.

The previously established RMS (stacking) velocity model is used as the basis for this calculation. Likewise, the previously picked water bottom is used as the starting time for single decibel per second amplitude corrections (dB/sec). In addition, a correction constant is determined using parameter testing (in our case 3).

2. Surface Consistent Amplitude: This process determines statistically the combined effects of amplitude loss and the attempts to eliminate them. It is commonly used twice; once in "Input" mode and once in "Compute and Apply" mode. The "Input" mode estimates trace amplitudes over a user defined time gate and saves the results to the database. Here the time gate is chosen to be the absolute value offset range of 0 to 700. The "Compute and Apply" mode reads the database, decomposes amplitudes by shot and channel, and applies the specified parameters for correction.
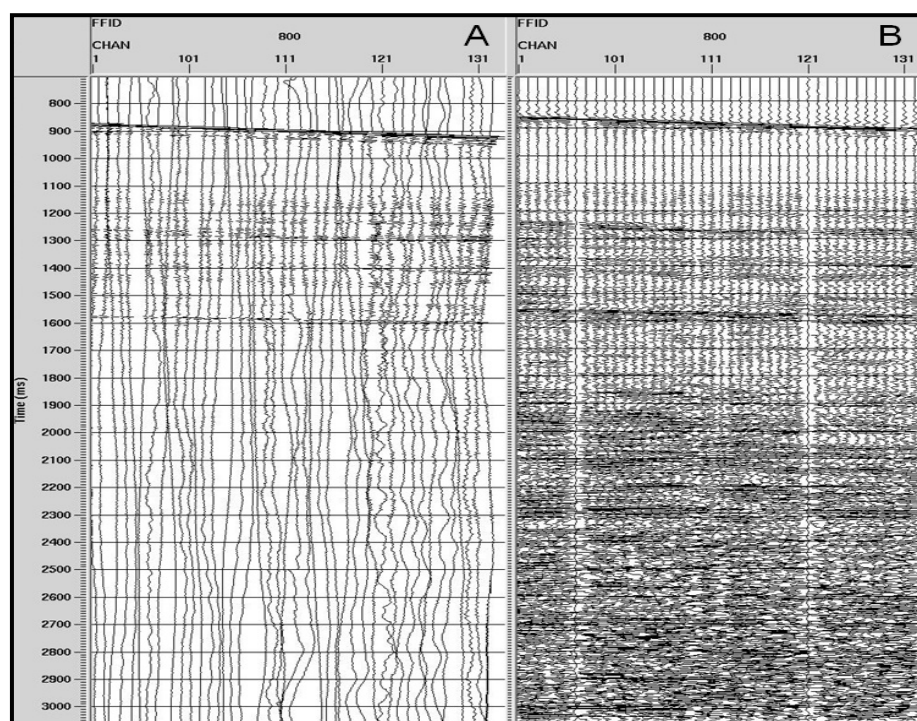
Figure 3-14. Gain recovery comparing raw and gained data of Profile 27. (A) wiggle trace display of raw data FFID 800 (Channel 91 - 131). (B) wiggle trace display of gained data FFID 800 (Channel 91 - 131). Several deeper lying seismic reflection horizons become visible after gain application.

3.2.8. Dip Moveout (DMO)

Stacking of NMO corrected, gain recovered data, assumes a simple, horizontally layered earth model. Given that real-world data is rarely collected on perfectly horizontal layers, the result is a less-accurate stack that exhibits reflection artifacts (Figure 3-15). To correct for this, a dip moveout correction has to be applied.
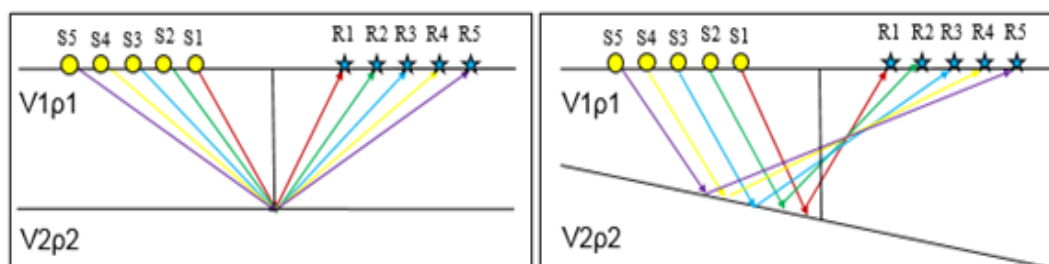
Figure 3-15. Illustration of basic assumptions for NMO and DMO corrections.

This correction will move reflection events to their correct subsurface position. However, it requires a new velocity analysis after the application of DMO. To perform DMO, the input data must be previously NMO corrected, and time shifts have to be removed prior to performing DMO. Velocity analysis is then repeated on the DMO output data and should produce more accurate stacking velocities. Generally, this is an iterative process where the new velocity model will be used for the second run of the DMO. This procedure is performed in four steps:

The first step is trace binning. DMO correction can work on larger bins to save computing time, thus a special binning for the DMO is applied and used as an input for the following steps.

The second step is the application of dip moveout corrections. The reflections from dipping layers must be corrected for true position in order to improve stacking accuracy.

Application of this module and input parameters are briefly explained in the following paragraph.

DMO correction is applied on NMO corrected CDP's. Pre DMO, NMO is applied in a "forward" direction with a stretch mute of 30% (found by parameter testing). The previously created "brutestacksmooth" velocity model is used for this procedure. The "Ensemble DMO in T-X Domain" module automatically calculates the CDP interval, CDP spacing, and maximum offset using user determined parameters for mute time (here 500 ms found by parameter testing) and RMS velocity (here 1600 m/s). After the application of DMO, the previously applied NMO correction is removed using the NMO correction in inverse mode.

The third step is a repeat velocity analysis. Velocities are picked again on semblance panels, saved and smoothed. Here we perform velocity analysis on super-gathers, which are the sum of 5 CDPs. The entire dataset is analyzed in CDP super gather increments of 10. (That is CDP increments of 50). As a result, the final velocity model is substantially more precise. The new velocity model was called "dmo". A smoothed version of this final model is saved as "dmosmooth". This final velocity model will be used for the fourth and last step of DMO.

The fourth step is almost identical to step two but uses the new velocity model. All other parameters remain the same. The resulting new dataset called "dmo" is created. This DMO corrected data is consistent with the final velocity model and will be used for final stacking.

3.2.9. Final Stack

Stacking in general is the process summing up traces with varying offsets to improve the signal-to-noise ratio of the data. In contrast to the brute stacks, where normal-moveout correction was only a first attempt and only initial, coarse velocity analysis had been performed, the final stack will be based on our detailed DMO corrected velocity model.

In this step, NMO is corrected and trace mute applied before being stacked to create the final stack. Although still not perfect, final stack data are suitable for interpretation if the environment is nearly horizontally layered, and little to no faulting that would cause diffractions of the seismic wave is present (Dondurur, 2009). The study area shows substantial amounts of dipping layers and faults. As a result, our final stack requires migration.

3.2.9.1. Normal Moveout

The Normal Moveout describes the effect of longer seismic travel time to receivers further away from the source (Figure 3-16). As a result, reflections created by an impedance contrast at a given depth will occur at a later time in traces with larger offsets. NMO correction will adjust the data so that reflection from common impedance contrasts will occur at the same point in time. After NMO correction is performed, traces belonging to the same CDP can be stacked. Stacking (adding the traces) creates one resulting trace commonly referred to as a "Stacked Trace". NMO correction is performed using the "NMO correction" and "CDP/ensemble stack" modules. The "dmosmooth" velocity model is used for this procedure, and a stretch mute of 30% is applied. The "CDP/ensemble stack" module is used to sort the input data into CDP order.
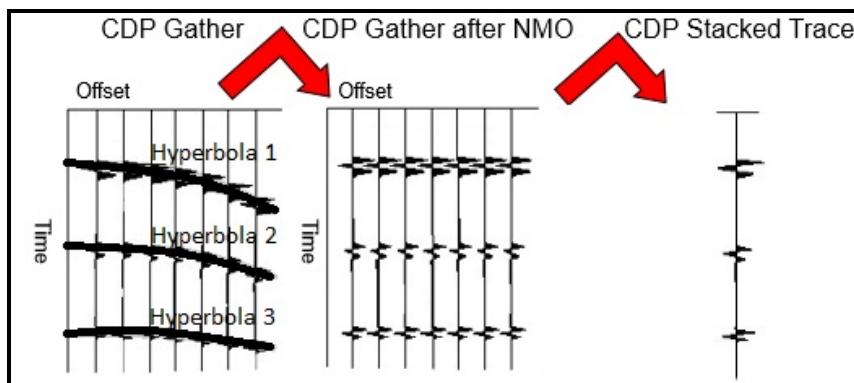
Figure 3-16. Steps for creating a stacked trace.

3.2.9.2. Trace Mute

The "trace mute" module is used to remove from the data the noise contained in the water column. This is usually done by picking the sea floor and muting all data content above it. Since the sea floor was already picked for deconvolution, we used these picks as reference. Figure 3-17 illustrates the results of this procedure.
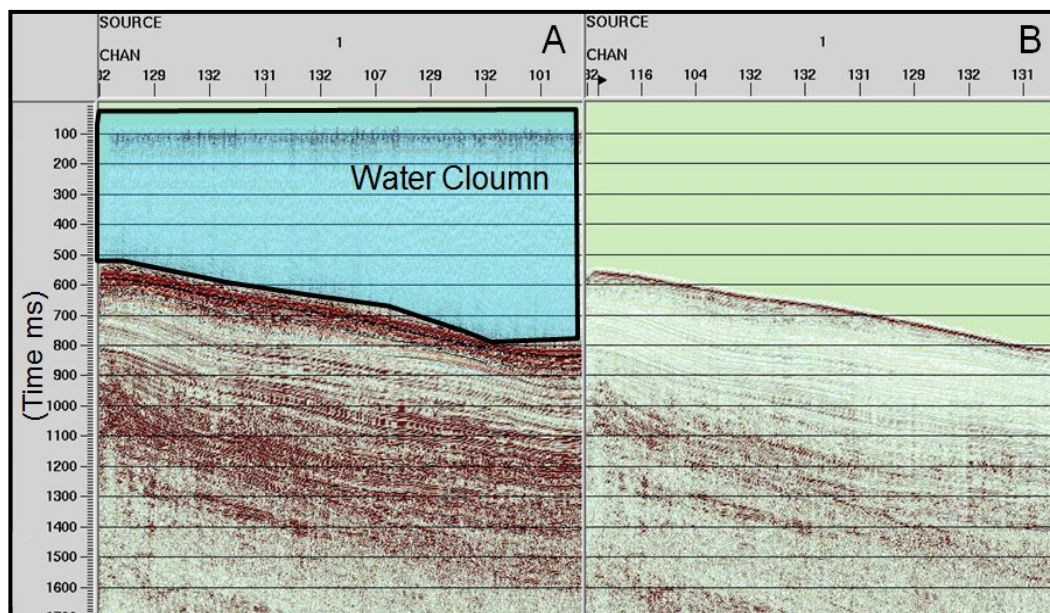
Figure 3-17. (A) The water column is indicated with a light blue box. (B) All noises in the water column are removed after the trace mute module is applied.

3.2.10. Migration

Migration is the process by which seismic reflections are placed at the actual location where they occur in the subsurface. It is often performed on final stacked seismic sections. In geologically complex areas, reflections are diffracted or absorbed and their signal patterns carry misplaced information from the subsurface. The aim of migration is to increase the lateral resolution by collapsing these diffractions and moving dipping events to their true subsurface positions (Figure 3-18).
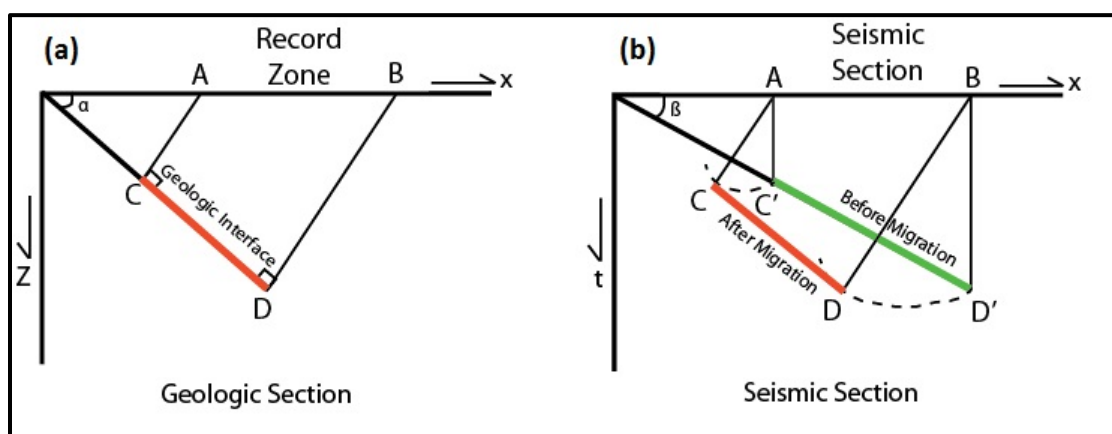
Figure 3-18. Section (A) reflects the location of the geologic interface which is originally found along the line CD. Section (B) shows the location of the geologic interface along the line C'D'. Using migration, this interface is repositioned under its appropiate subsurface location and correct time (modified after Dondurur, 2009).

There are many different Migration Algorithms with a variety of different benefits and shortcomings. In order to choose the most appropriate migration for our data, we tested 3 different alternatives, compared the results, and used a table from the ProMAX manual as the basis for selecting which algorithm to use (Table 3-4). The three algorithms compared are "Phase Shift 2D", "Fast Explicit FD Time", and "Kirchhoff Time" migration. The "Fast Explicit FD Time" migration appeared to produce the best results.

Table 3-4. Poststack 2D migration characteristics (Modified from ProMAX manual)

Migration Name	Category	Type	Velocity	V(x)	V(t/z)	Steep Dip	Run Time
Stolt 2D	F-K	Time	$V_{RMS}(x,t)$	Poor	Poor	Fair	0.2
Phase Shift 2D	Phase Shift	Time	$V_{INT}(x,t)$	None	Good	Good	1.0
Steep-Dip Explicit FD Time	F-D (70 deg) (50 deg)	Time Time	$V_{INT}(x,t)$ $V_{INT}(x,t)$	Fair Fair	Good Good	Good Fair	21.0 10.0
Fast Explicit FD Time	F-D	Time	$V_{INT}(x,t)$	Fair	Good	Fair	9.6
Explicit FD Depth	F-D	Depth	$V_{INT}(x,z)$	Good	Good	Good	21.7
Kirchhoff Depth	Kirchhoff/Im Explicit Mult. Arr.	Depth Depth Depth	$V_{INT}(x,z)$ $V_{INT}(x,z)$ $V_{INT}(x,z)$	Fair Good Excel.	Good Good Excel.	Good Good Excel.	7.3 12.0 64.0
Kirchhoff Time	Kirchhoff	Time	$V_{RMS}(x,t)$	Fair	Good	Good	14.6
Reverse-Time T-K	Reverse Time	Time	$V_{INT}(t)$	None	Good	Good	2.5

The "Fast Explicit FD Time" module requires interval velocities to migrate the data. The interval velocity is a constant velocity in any given layer. It is generally lower than the RMS (stacking) velocity. The difference between interval and RMS (stacking) velocity analysis is that interval velocity analysis is performed on stacked data rather than CDP gathers. The chosen interval velocities for migration are shown in Figure 3-19.
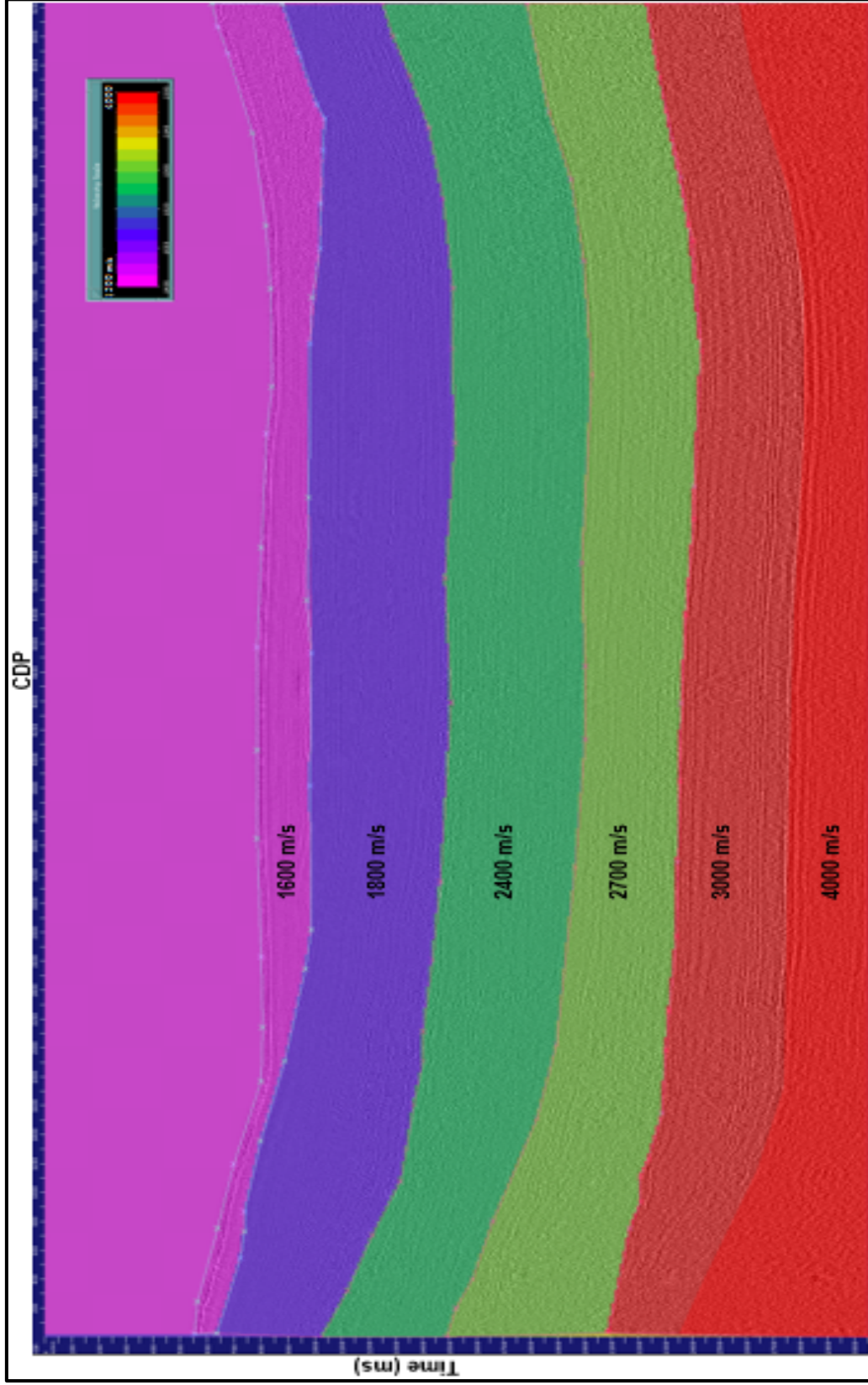
Figure 3-19. Interval velocity selection on Finalstack section of Profile 27. Velocity analysis is performed on each profile individually.

3.2.11. Automatic Gain Control (AGC)

"Automatic Gain Control" is applied as a final step after migration of the data. The "AGC" module is a gain recovery module; it helps to strengthen weak amplitudes by automatically varying the gain applied to trace samples as a function of sample amplitude within an AGC time window. The input parameters for the module are standard.
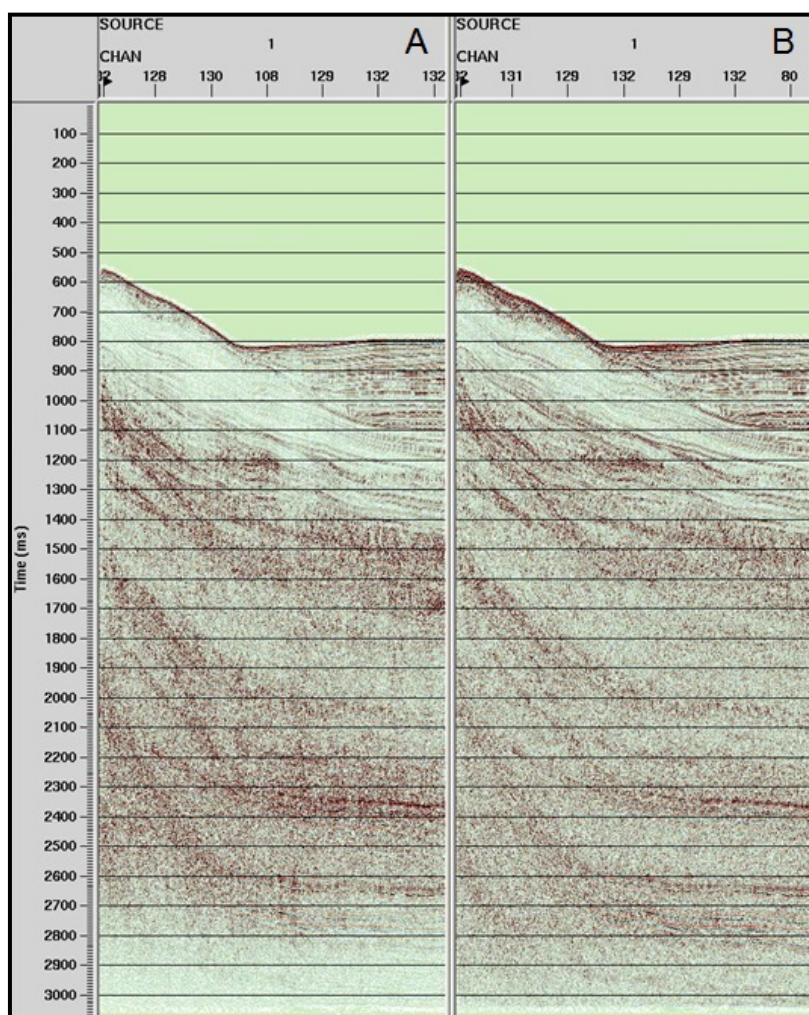
Figure 3-20. The effect of AGC module. (A) Shows the migrated section of Profile 27 without AGC applied. (B) Illustrates the same section with AGC applied. The resulting section shows much more balanced amplitude distribution than the original.

Figure 3-21. The end product of our seismic processing is a post stack migrated section with AGC applied and muted water column; Example Profile 27.

Summary

A set of 27 high resolution 2D seismic profiles were gathered onboard the R/V *Meteor* in the Santaren Channel. Despite our best efforts, coherent and ambient noise, effects of sideswipes, multiples, and false reflections could not be completely avoided during the acquisition. Since these unwanted events decrease the quality of the data, special attention to correcting for these effects is required during processing to achieve high quality images representative of the subsurface structure.

Processing is performed using Landmark ProMAX software. Initially the dataset is uploaded to the software database, and field geometry parameters are defined for each profile individually. The rest of the processing flow can be divided into three main stages: preprocessing, pre-stack, and post-stack. The preprocessing stage focuses on increasing the signal-to-noise ratio. Dead and noisy channels are eliminated, very high and very low frequencies are filtered out, and spikes in the signals are edited out. The pre-stack stage focuses on enhancing the resolution and correcting travel time differences within gathers. Multiples were dominant in our data but have been successfully suppressed using targeted predictive deconvolution. Velocity analysis is performed and the resulting RMS velocity model is used for NMO and DMO correction, in addition, weak amplitudes are enhanced. During the post-stack stage, NMO corrected traces are added to create the final stack. Post-stack time migration is used to increase the lateral resolution and to move dipping events to their true subsurface positions. Water column noise is muted in the data and automatic gain control is applied to balance the amplitudes. All used ProMAX modules and their effects on the data are summarized briefly in Table 5 and Figure 3-22.

Table 3-5. Seismic Processing Flow Summary

Flow Name	Selected Module in ProMAX	Effect of the Module
Trace Kill/Reverse	Trace Kill/Reverse	The faulty channels (3, 14, 55, 73,97,121) are deleted.
Bandpass Filter	Butterworth Bandpass Filter	10, 20, 200, and 220 Hz are used as frequency range. Frequencies below and above this range is eliminated.
Spike&Noise Burst Edit	Spike and Noise Burst Edit	Simple spikes and multiple noise bursts are edited.
Deconvolution	Targeted Deconvolution	Multiples are suppressed, yet adjacent signals were slightly affected. In some profiles third multiples are seen as a strong reflection.
Velocity Analysis	Velocity Analysis	RMS velocities are determined to be 1500 and 4250 m/s.
Gain Recovery	TAR/ Surface Constant Amplitude	Weak amplitudes are enhanced using both "brutestacksmooth" velocity model and time gate 0-4000 ms.
Dip Moveout	DMO Correction	Time difference between far and near traces for dipping layers is corrected. Velocity analysis is repeated on DMO corrected data. "dmosmooth" velocity model is created.
Final Stack	NMO Correction/ CDP/Ensemble Stack	NMO correction is performed using "dmosmooth" velocity model. Hence all CDP gathers are flattened and added to create the stacked section.
	Trace Mute	Water column noise is deleted.
Migration	Fast Explicit Time Migration	Interval velocity model is created and data is migrated. Lateral resolution is increased. Dipping events are relocated.
	AGC	Overall automatic amplitude balancing is performed.
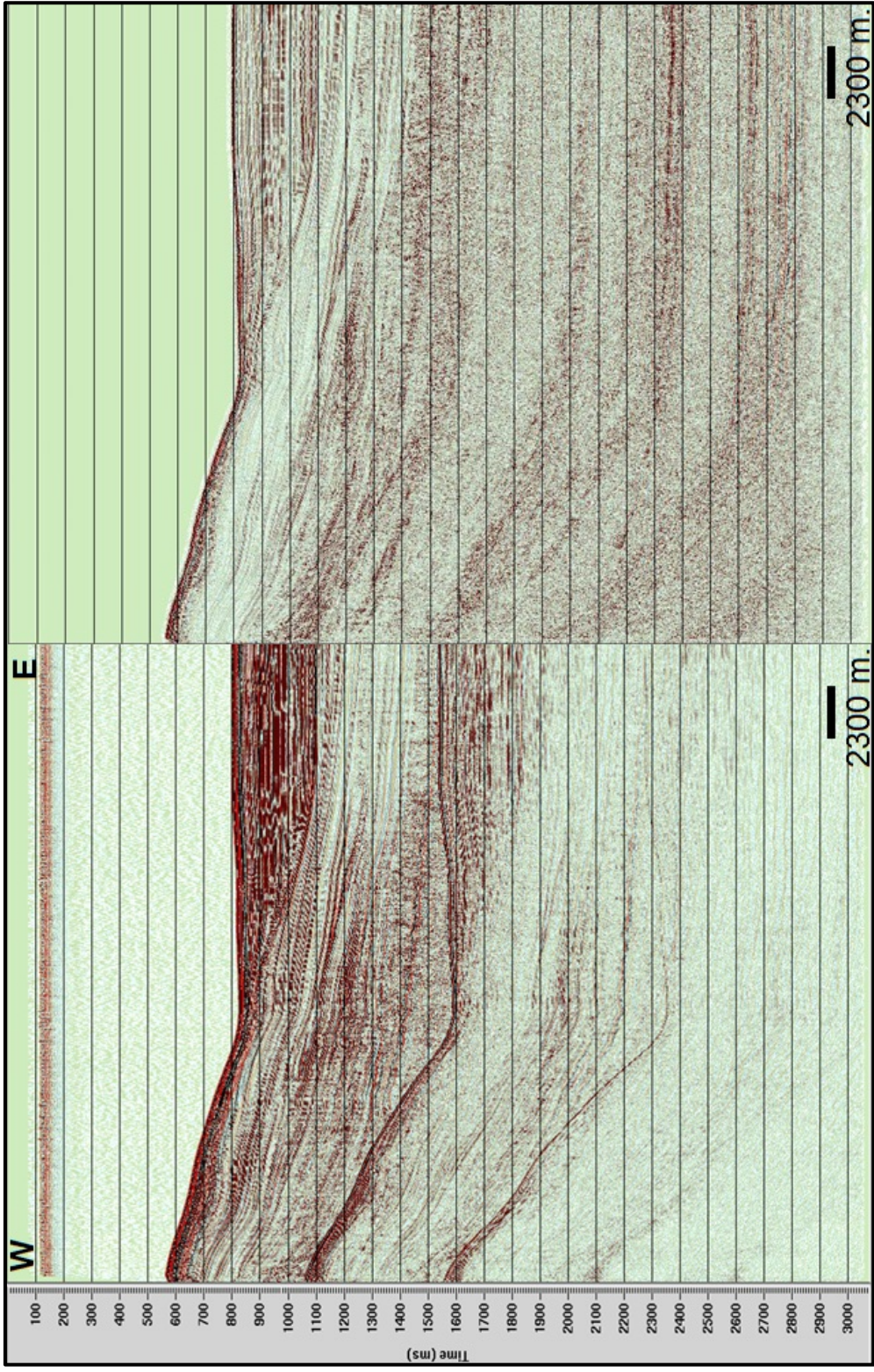
Figure 3-22. Comparing the brute stack and the final post-stack time migrated section from Profile 27 illustrates the benefits of our processing; multiples are suppressed, water column noise is eliminated, the amplitudes from deeper parts are enhanced and noise in the shallow part are filtered out.

CHAPTER 4. SEISMIC DATA ANALYSIS

Overview

The Bahamian platforms have been exposed to the effects of both 1) periods of platform expansion and coalescence and 2) tectonic segmentation since their creation on the extended crust when the Atlantic opened in the Late Jurassic (Eberli and Ginsburg, 1987, 1989; Eberli and Masaferro, 1999; Eberli et al., 2004). A major segmentation of the Bahamian platform system occurred in the late Cretaceous when the Caribbean plate collided with the North American plate (Melim and Masaferro, 1997). After this collision, transtensional faulting reactivated deep-seated extensional faults, and enhanced subsidence due to the loading of the North American plate increased the accommodation space (Melim and Masaferro, 1997; Masaferro 1997). Because prolific carbonate sediment production healed the tectonic segmentation, the tectonic effects remained unclear until seismic sections across the shallow banks became available. Several seismic data sets now display the effect of tectonism.

Masaferro (1997) reconstructed for the first time the influence of the Cuban collision on the platforms of the Bahamas. Based on seismic data from the Santaren Channel and on the southern portion of Great Bahama Bank he documented that during the northeastward advance of the Cuban orogenic front, the southern Bahamas encountered backstepping, uplifting and drowning events of carbonate platforms. Drowning events are recognized on seismic sections as covered by deep-water sediments. Masaferro (1997) states that Cay Sal Bank, the focus of this study, is a residual platform, which survived this drowning event. This is the key assumption for our study.

In the course of this chapter, seismic data will be utilized to reveal the morphologic evolution of the Santaren Channel, and to analyze the depositional settings of the region. The seismic interpretation is performed in two steps. First, the seismic data is described and five seismic horizons are selected and mapped. Their ages are assigned using a core-seismic correlation from the cores drilled during ODP Leg 166 and supplemented by data obtained from Site 626 on ODP Leg 101. Surface maps are created using these horizons in order to reveal the thickness and distribution of the sediments in two way travel time (twtt). In a second step depositional facies are interpreted based on the seismic facies in the Santaren Channel. In the following chapter the structural and tectonic interpretation of the seismic data will be illustrated and discussed.

Datasets

In addition to the newly gathered and processed high-resolution 2D seismic reflection lines, 4000 km of un-migrated regional seismic lines are incorporated in to the seismic interpretation. This seismic data set was gathered by Geophysical Service Inc. (GSI) in the 1980s. A 96 channel streamer with a length of 3200 m was used. The record time was 6-9 s. For the processing parameters: the velocity filter was set at 80 Hz and the time variable filter was given a range of 5-50 Hz. The data was not migrated (Bergman, 2005). Multibeam bathymetry data and parasound profiles collected during the R/V *Meteor* M95 cruise provide information on near surface and seafloor topography, respectively. Cores from 4 sites drilled during ODP Leg 166 provide lithological and biostratigraphic information for the seismic data.

The parasound system of R/V *Meteor* recorded the high frequency sub-bottom profiles. The system operated with two frequencies of 18 kHz and 22 kHz. The interference of two frequencies in the water column caused a parametric effect, which increases the penetration of the high frequency signal into the subbottom (Westervelt, 1963; Betzler, 2013).

The multibeam data were acquired with the hull-mounted multibeam systems Kongsberg EM710 and EM122. The EM710 is a high-resolution system that can be run in water depths up to 2000 m with sonar frequencies that are in the 70 to 100 kHz range. The EM122 is a system designed for medium to deep-water having a sonar frequency of 12 kHz. The locations of these datasets are given in Figure 4-1.
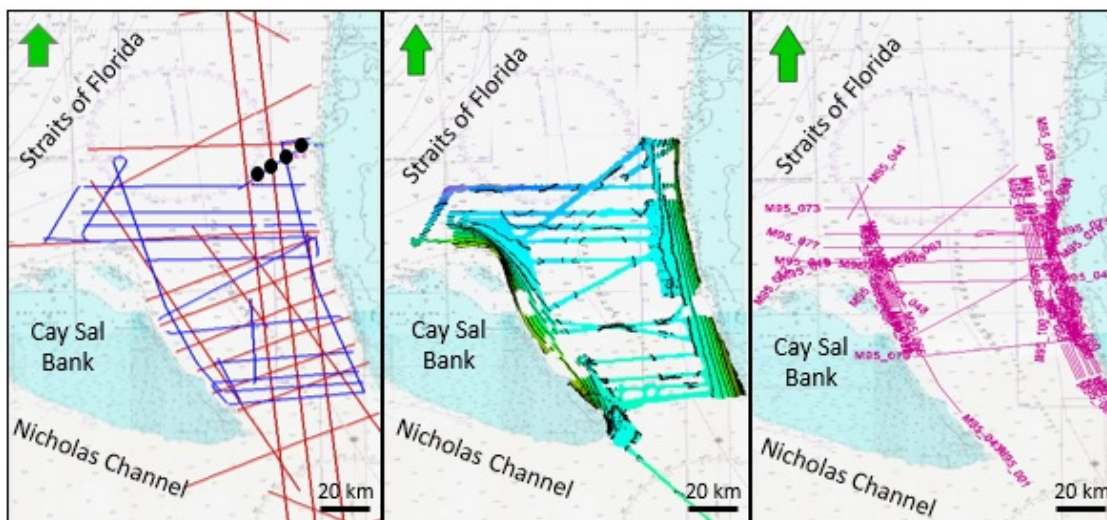
Figure 4-1. Location of the datasets. Left: Locations of two seismic reflection datasets; newly acquired data are shown as blue lines while the old regional data is given in red lines. Black dots give positions of the 4 cores of ODP Leg 166 that are situated on profile 4. Middle: Coverage of the multibeam bathymetry data. Right: Locations of parasound profiles acquired on R/V *Meteor*. Green arrow indicates North.

4.1. Seismic Interpretation

The seismic data interpretation is performed using Petrel software. As an initial step all the datasets, including 2D seismic reflection, bathymetry and parasound profiles and borehole information, are uploaded to the software. The horizon dating and the horizon mapping are performed on the following steps.

4.1.1. Seismic Horizons' Age Assignment

A total of five horizons were selected. They are named as C, H, P, 4 and 4' referenced to Ball et al. (1985), Eberli et al. (1997), and Anselmetti et al. (2000) (Table 4-1). The ages of these horizons are: Pleistocene-Pliocene, Miocene, Early Miocene, Turonian, and Albian. Borehole information is needed to assign age. Seismic profile 4 is positioned on ODP sites 1003 through 1007; therefore, the first three horizon selections and their age attribution started on this profile. Figure 4-2 shows seismic profile 4 along with the four borehole locations. Site 1007 is the deepest well from ODP Leg 166, continuing to a depth of 1779 m. The other two selected horizons are deeper, hence ODP Leg 166 cannot be used for age correlation for these horizons. The borehole Great Isaac 1, located on the northwestern corner of the Great Bahama Bank, is the deepest well in the Bahamas and of sufficient depth (2000 m) for age correlation of pre-Neogene strata. Schlager et al. (1988) analyzed the well down to the mid-Cretaceous. Although the regional seismic line that passed through ODP Leg 101 sites is included in this project, due to the lack of borehole information from Great Isaac, the age correlation of the last two horizons (Turonian and Albian) is started at the most northerly regional seismic line 81-22B, comparing the Bergman study of the same line (dissertation, 2005). Figure 4-3 displays how strata horizons from the Pre-Neogene are correlated with seismic lines.

Table 4-1. Comparing horizon selection between this study and previous studies (modified after Poiriez, 2004).

STUDY	Present Study		Bergman, 2005		Schlager et al., 1988	
STUDY AREA	Eastern part of Cay Sal Bank, Santaren Channel		Northern Straits of Florida, Northwest Providence and Santaren Channels		Northwestern Great Bahama Bank and Northern Florida Straits	
DATASET	1) 1393 km multi-channel seismic (MCS) data, tied to ODP Leg 166 sites1003-1007 2) 3000 km MCS dataset tied to Great Isaac-1		1) 1200 km MCS tied to ODP Leg 166 sites 1003-1007 2) 3000 km MCS dataset tied to Great Isaac-1		Ca. 50 km MCS data tied to Great Isaac-1	
SELECTED HORIZONS AND THEİR AGES (Ma.)	C	1.7 Ma	C	1.7 Ma	C	1.7 Ma
			D	3.1		
			E	3.6		
			F	5.4		
			G	8.7		
	H	9.4	H	9.4	H	9.4
			I	10.7		
			K	12.2		
			L	12.7		
			M	15.1		
			N	15.9		
			O	18.3		
	P	19.4	P	19.4	P	19.4
			P2	23.2		
			Q	23.7		
	4	Turonian			4	Turonian
	4'	Albian			4'	Albian
	Age assignment based on previous studies.		Age assignment based on ODP Leg 166 Anselmetti et al., 2000.		Age assignment is based on Great Isaac 1 borehole	
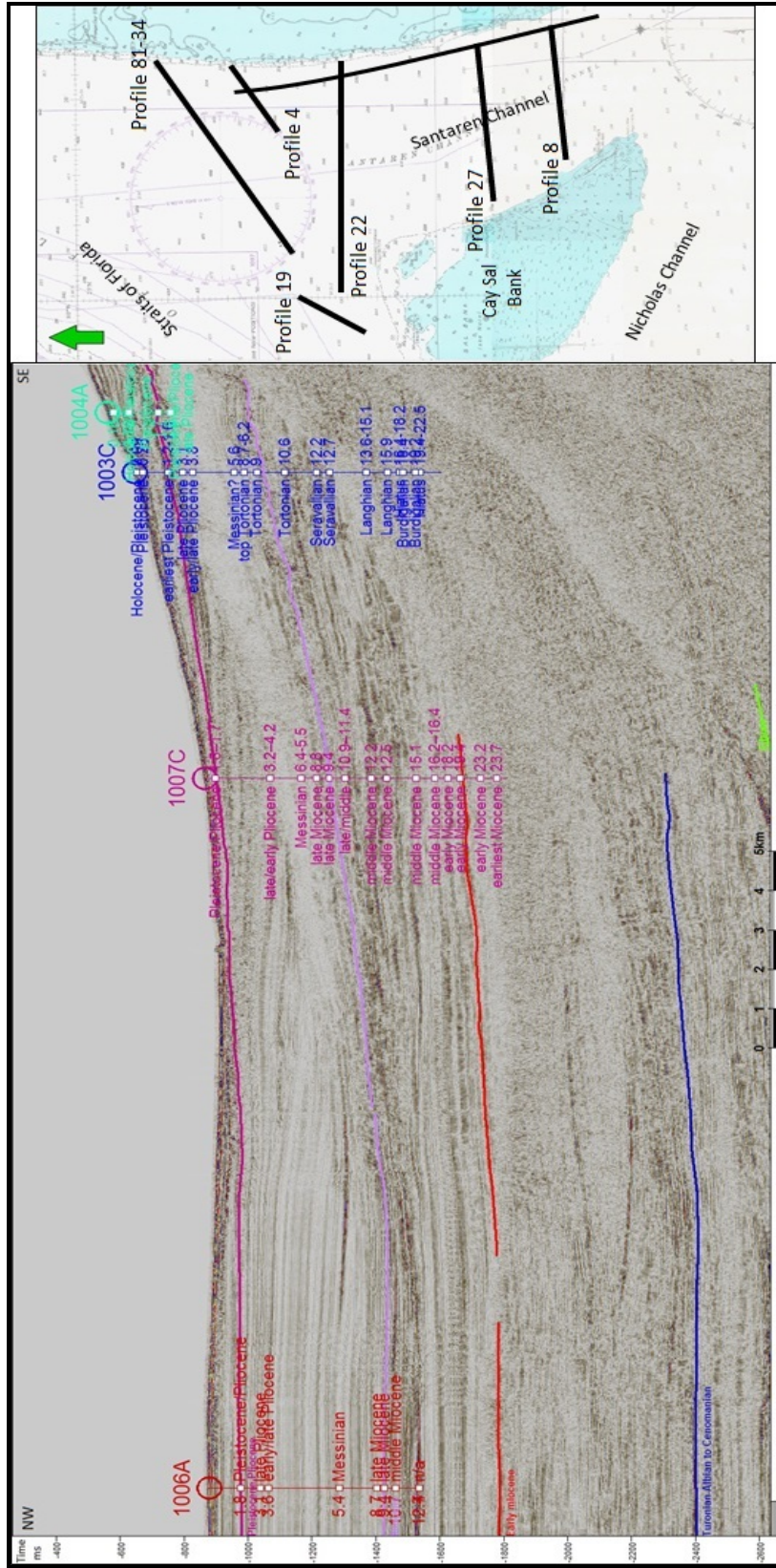
Figure 4-2. Left: Correlation of biostratigraphic ages to seismic reflection horizons along profile 4. The seismic horizons mapped in this study are Horizon C (1.7 Ma) in pink; Horizon H (5.4 Ma) in purple and Horizon P (19.4 Ma) in red. Right: Location of the 2D seismic profiles that will be used for examples in this chapter.
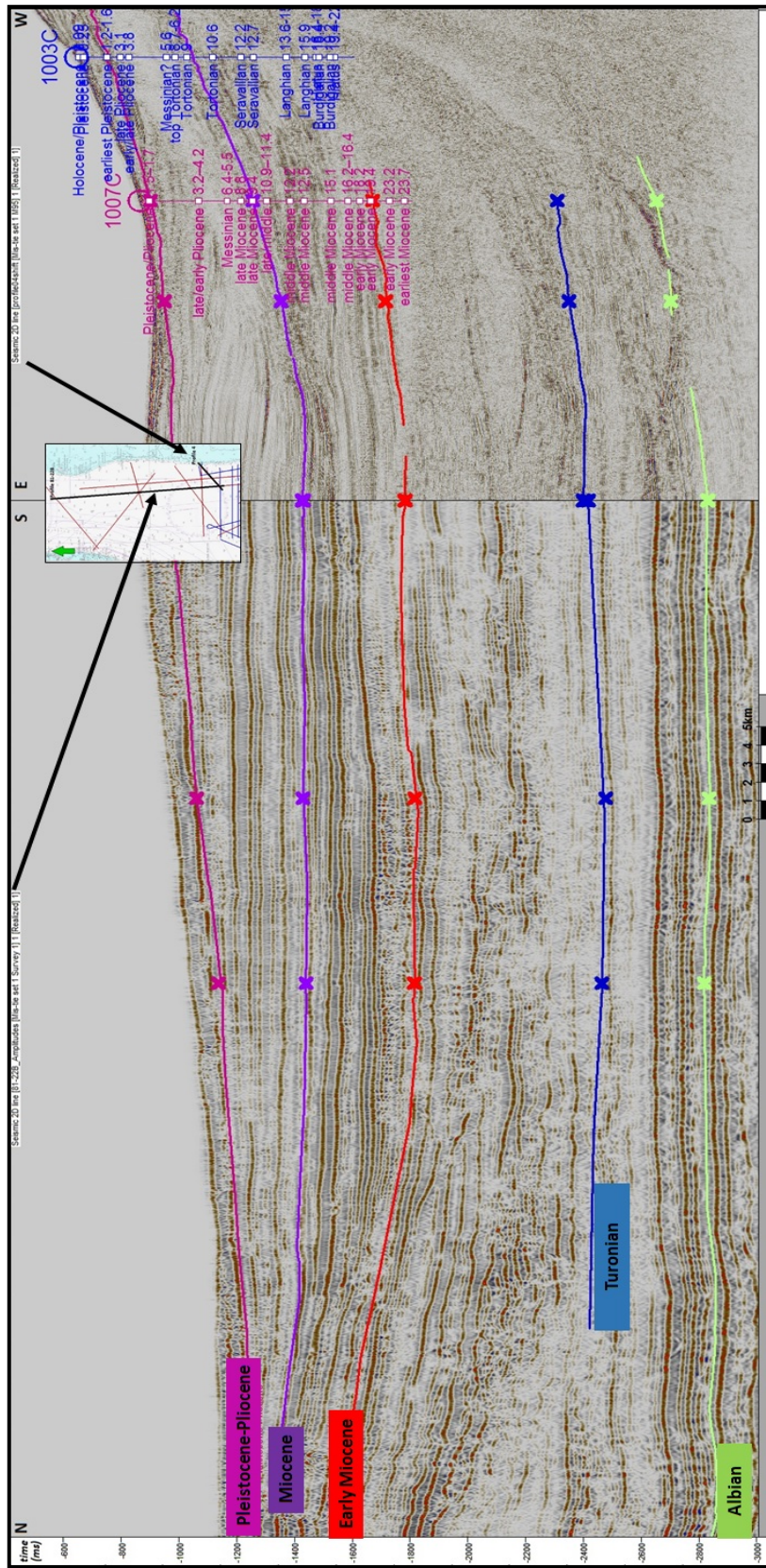
Figure 4-3. Correlation of Profile 81-22B (old seismic line) and Profile 4 (newly gathered seismic line). The Turonian (blue) and the Albian (light green) seismic reflection horizons are carried from the north (Great Isaac-1) to the study area.

4.2.1. Seismic Horizon Mapping

Pre-Neogene Strata

The base of the Neogene was reached at Site 1007 of ODP Leg 166 (Fig. 4-2). In the pre-Neogene strata two strong reflections are mapped. The deepest and oldest reflection mapped is identified as 4' (4prime). The age of this horizon is Albian (Schlager et al. 1988). The younger horizon 4 is Turonian in age. None of the ODP Leg 166 sites extend below the Neogene; therefore, the age assignment of these two horizons are based on correlation from Great Isaac-1 located on northern Great Bahama Bank, to the older seismic data set that had one line crossing this borehole. The biostratigraphy of the Great Isaac-1 relies on cuttings and is thus not very refined (Schlager et al., 1988). The two pre-Neogene horizons are carried from the most northern regional seismic line southwards, reaching the newly processed seismic lines. These two reflections are seen as high amplitude-low frequency, parallel reflections along the Santaren Channel. They dip slightly towards the west from the western part of GBB to the eastern part of Cay Sal Bank. They are both high amplitude-low frequency, which implies a large acoustic impedance change across this horizon (Sheridan et al., 1981; Denny et al., 1994; Anselmetti et al., 2000).

Stratigraphic interpretation of these horizons is done using jump correlation of Great Isaac-1. Correlation of the seismic profile 7N and the Great Isaac-1 well description is illustrated in Figure 4-4. The horizons from Pre-Neogene strata show medium amplitude, semi-continuous reflections. Biostratigraphic data shows that in the mid-Cretaceous a carbonate-evaporate sequence occurred; subsequently overlapped by deep-water chalks until the mid-Miocene (Schlager et al., 1988).
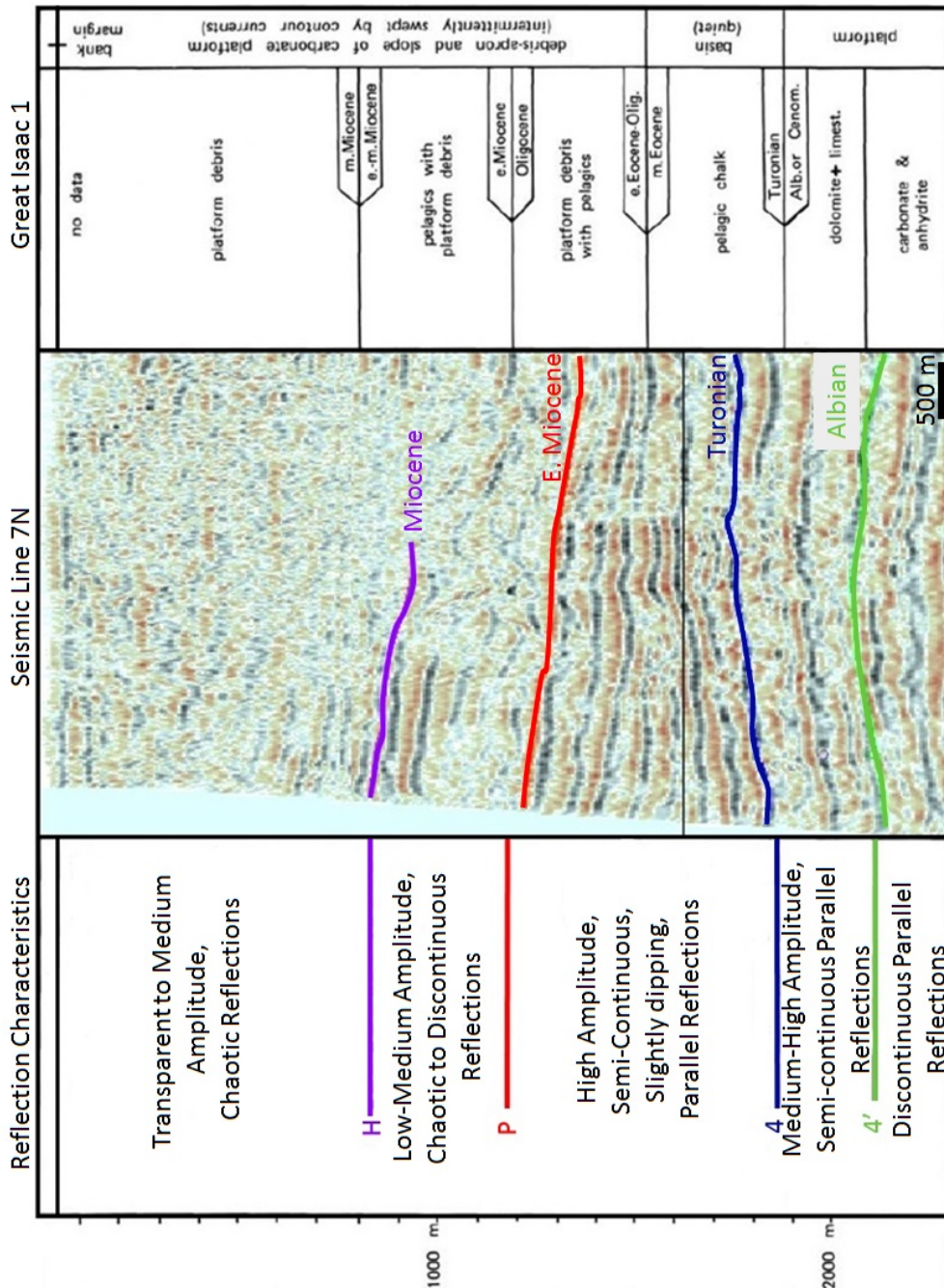
Figure 4-4. Correlation of the seismic line 7N with Great Isaac 1 lithology prepared by Schlager et al., 1988. Lithologic description for platform and basin is done referencing this information since Great Isaac 1 is the deepest well in the area. In the lower part of the seismic profiles, facies lithology is defined using ODP LEG 166.

Miocene Strata

In the Miocene section two seismic horizons labeled as P and H by Eberli et al. (1997a) are mapped. The age assignment of these two horizons relies on the biostratigraphic dating of ODP Site 1007 and the correlation of this well information to newly processed seismic data. The age of seismic horizon P is 19.4 Ma, within the Early Miocene; while the age of seismic horizon H is 9.4 Ma, within the Late Miocene. In the study area the early Miocene strata contains the slope strata along GBB and Cay Sal Bank and basinal deposits in the Santaren Channel. Horizon P is interpreted as a semi-continuous, slightly eastward dipping, high amplitude reflection. The internal characteristic of horizon H is defined as highly continuous, with strong parallel reflection in the drift deposits, and slightly dipping, semi-continuous reflection in the slope. Miocene strata is mostly dominated by the deep-water sediments. The main element is the alternation of light grey and dark grey wackestones and packstones, which reflects seal-level changes (Eberli et al., 1997a).

Pliocene-Pleistocene Boundary

Seismic horizon C, marking the Pliocene-Pleistocene boundary, has an age of 1.7 Ma. Horizon C is a laterally continuous, high amplitude reflection in the drift deposits, and a high to medium amplitude semi-continuous reflection on the slope. Because of its high amplitude reflection character, it can be easily traced on every seismic profile. The succession from the Pliocene to Pleistocene sequences shows unlithified to lithified peloidal mudstones and wackestones (Betzler, 1999). A transparent zone resulting from the entrance of homogenous sediment is observed in the upper part of the Pleistocene strata (Anselmetti et al., 2000).
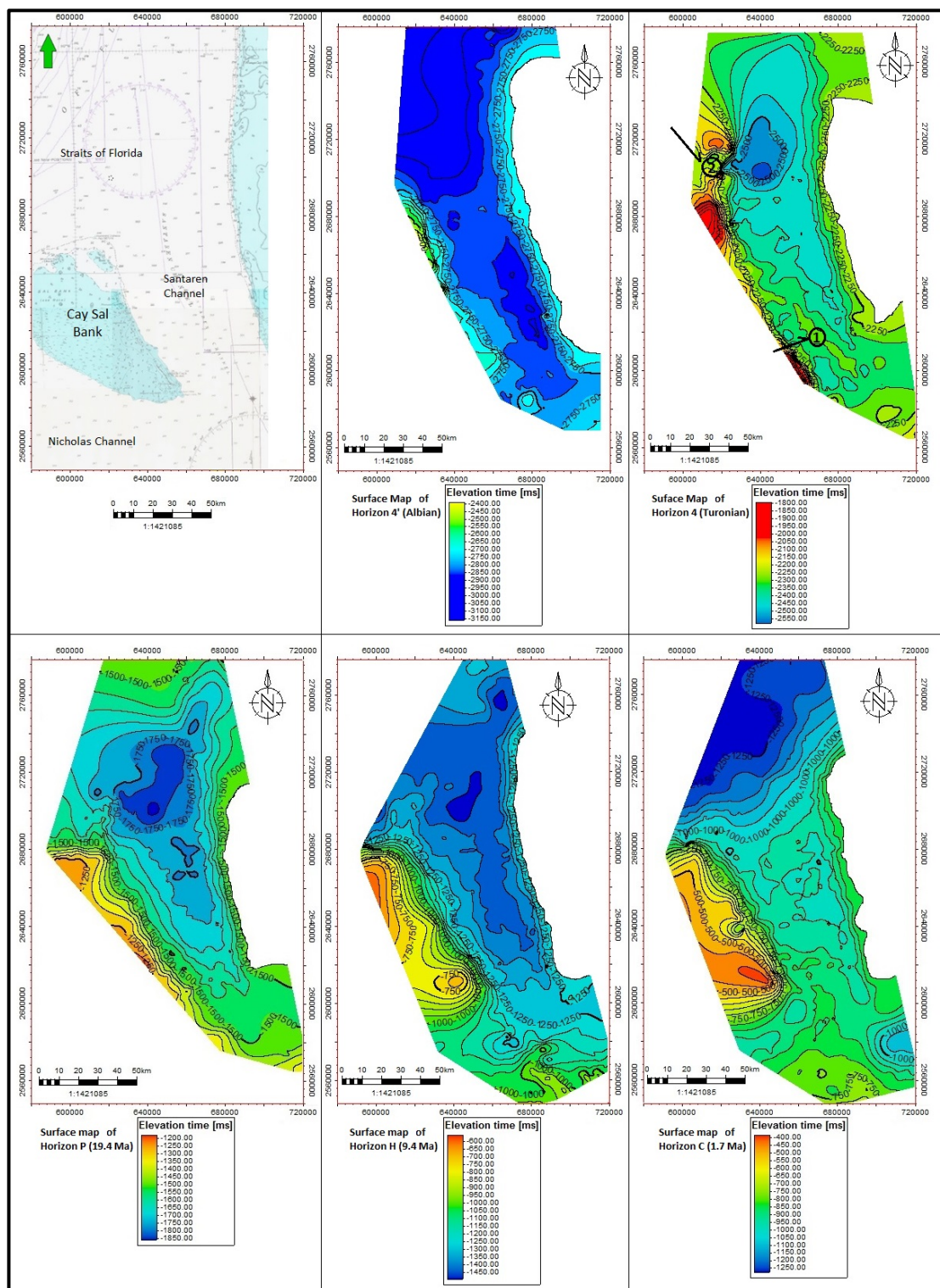
Figure 4-5. Surface maps of the selected seismic horizons illustrate the evolution of the Santaren Channel through time. The location of the surface maps is given in the first figure. The anticline structures are indicated by arrows in the surface map of seismic horizon 4. See text for discussion.

Figure 4-5 illustrates the evolution of the Santaren Channel's morphology through time. The surface contour map of the Albian age seismic horizon (4') shows the northward deepening of the Santaren Channel. The relief of the Santaren Channel is an indication of adjacent carbonate platforms. The thickness difference between the Cay Sal Bank platform margin and deep-water sediments located in the Santaren Channel is approximately 300 ms (twtt). Using an interval velocity of 4000 m/s that was determined in processing, the depth between these two facies is calculated to be around 1200 m. Two anticlines are detected in the surface map of the Turonian. The first one is located parallel to margin of Cay Sal Bank and the second one is situated on the northeastern side of the Cay Sal Bank. Detailed information regarding these structures will be given in the structural analysis chapter. A distinctive decrease in elevation is also observed towards the northern end of the Santaren Channel. Its presence can be traced consistently until the Pliocene-Pleistocene boundary (1.7 Ma). The surface map of the Horizon P (19.4 Ma) indicates that the anticlines were covered and the sea floor was smoothed. The map that is created from the other horizon within the Miocene (seismic horizon H, 9.4 Ma) reveals a NW-SE trending basin axis. The map also indicates the slope expansion, which modified the basin to a slightly V-shaped form. The surface contour map of horizon C implies that the Santaren Channel is shoaling southward. The elevation of the Santaren Channel basin distinctly decreases due to the accumulation of drift deposits. The basin axis is observed to follow the same NW-SE direction seen in the Miocene.
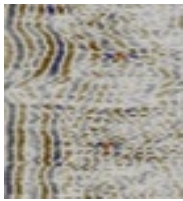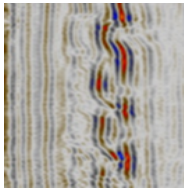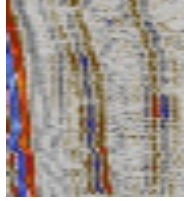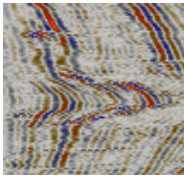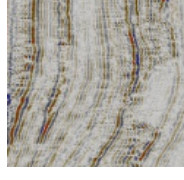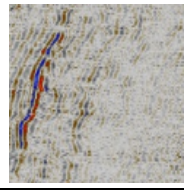
4.2. Seismic Facies Analysis

Seismic reflection characteristics in terms of configuration, continuity, amplitude, frequency, and interval velocity are used to interpret the depositional environment (Mitchum et al., 1977). Seismic facies are divided into units, groups of seismic reflections with characteristics in common, including internal geometry, external form, amplitude strength, etc. The characteristics of these seismic facies units are then related to the lithologic facies.

The first seismic facies analysis in the Bahamas region was done by Ball et al. (1985). He defined two facies in the Northwestern Bahamas; the basinal facies and the platform facies. Masaferro (1997) described four seismic facies in Santaren Channel. Later Masaferro and Eberli (1999) identified five facies units, which are platform carbonates (recent ages), periplatfrom basin fill, platform carbonates (late Cretaceous ages), evaporites, clastics and carbonates and continental to transitional crust.

The resolution of the seismic data is about ½ or ¼ of the wavelength (interval velocity/frequency) of the seismic signal. Higher resolution improves interpretation of the seismic section. The two seismic data sets in our study are of different ages and were acquired employing different frequencies. The older data source had a central frequency of approximately 25 Hz while in the newly acquired data the frequency approximates 100 Hz. As a result, the resolution of the new seismic data is approximately four times higher than the old one. The seismic facies units are thus defined in the newer data set. Seven seismic facies units are defined in three depositional systems; basin, slope, and platform system. Each of these seismic facies units and their descriptions are given in Table 4-2.

Table 4-2. Seismic facies units and their description

Seismic Facies Units	S1	S2	S3	S4	S5	S6	S7
Description of Reflections	Transparent to chaotic, parallel strong top reflections	Semi-continuous, medium to high amplitude, dipping reflections	High to medium amplitudes, cut and fill geometry	Continuous, transparent to high amplitude, parallel reflections	Highly continuous, medium amplitude	Intra-continuous, high amplitude	Dis-continuous to semi-continuous, Semi-transparent amplitude
External Form	Build-up	Inclined Wedge shape		Flat-sheet	Mounded	Wavy	Hummocky
Interval Velocity(m/s)	30000-4000	1600-4000	1800-2200	1600-4000	1600-2600	2500-2600	1600-2600
Interpretation of Seismic Facies	Shallow-Water Carbonate Platform	Slope Facies	Sub-marine Channels	Basinal Sediments	Drift Deposit	Sediment wave	Debris/Slump Flow
Seismic Image							

4.2.1. Seismic Facies Description and Interpretation

4.2.1.1. Platform Facies

Seismic Facies Unit S1. Shallow-water carbonate platform

The internal reflection character is mostly transparent to chaotic capped by horizontally layered continuous high amplitude reflections. The shallow-water carbonate facies is observed throughout the eastern side of Cay Sal Bank and the western part of GBB. Most of the Santaren Channel is old re-entrant that never had shallow-water facies. The seismic horizons 4 and 4' are easy to detect in deep-water facies, yet it is hard to follow these reflections in platform facies. Fortunately, we are able to track horizon 4, which is the top reflection for shallow-water carbonate facies in the four seismic profiles located in the northern part of Cay Sal Bank. From this observation, we may date the northern part of the drowning Megabank platform as Early Miocene in age. High amplitude, semi-continuous, thin (generally 500 ms in twtt) packages, consisting of regional parallel reflections are occasionally found within the carbonate platform. They are interpreted as carbonate-anhydrite alternations (Schlager et al, 1988). The low amplitude sections observed in the platform facies might be related to the differences in acoustic impedance resulting from alternating limestones and dolomites in the lower Cretaceous, and evaporates in the upper Cretaceous (Eberli et al., 2004).

62
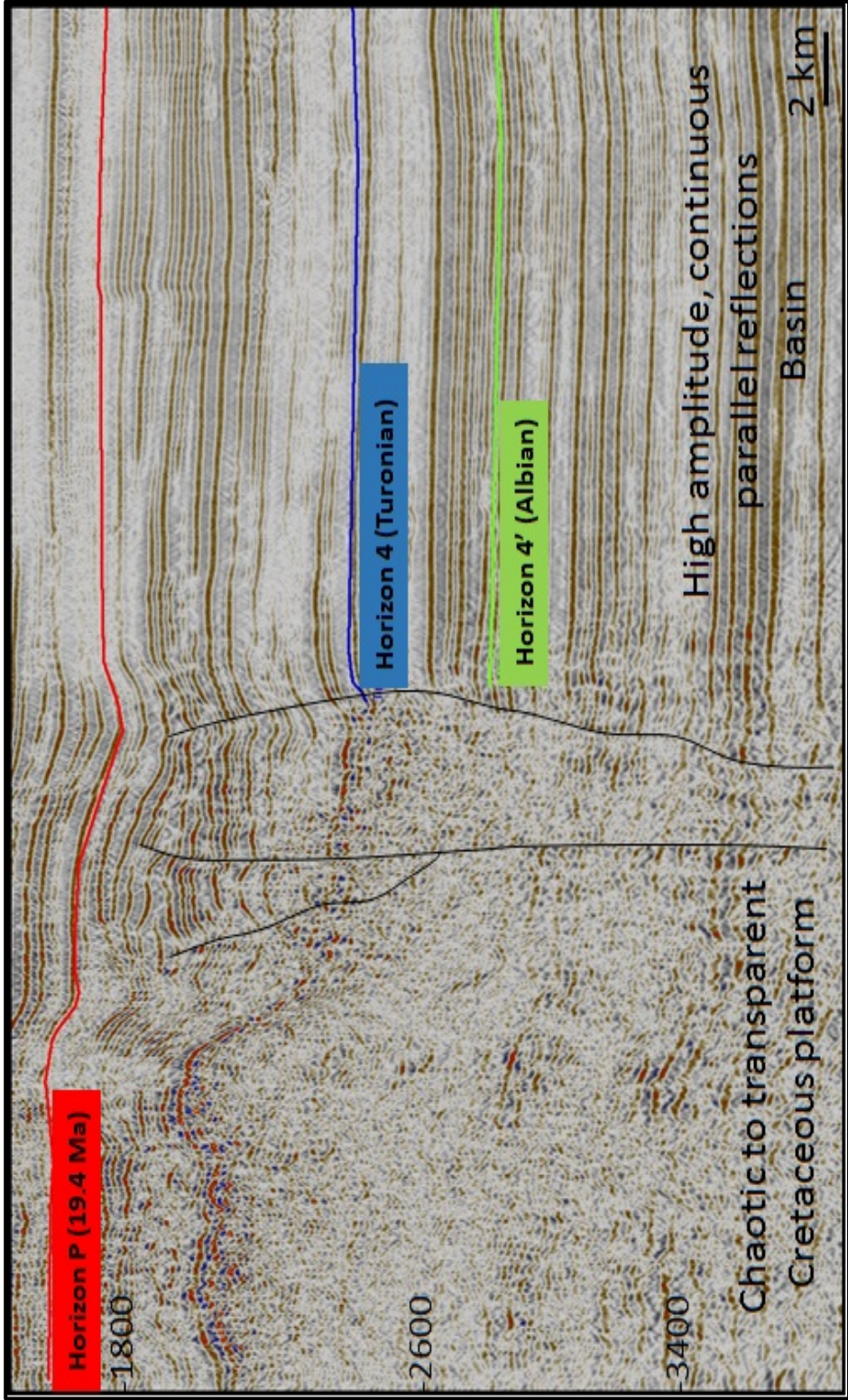
Figure 4-6. The squeezed section from profile 81-34 is located in the northern part of Cay Sal bank. The shallow-water carbonate platfrom is represented by highly chaotic to transparent reflections. The horizons from Pre-Neogene strata show slight dipping towards the platform. The transition zone between the basin and the platform is controlled by deep-rooted fault systems which will be elaborated in the structural analysis unit. The top of the carbonate platform is represented by Horizon H (Early Miocene age). For the location of the profile see Figure 4-2.

4.2.1.2. Slope Facies

Slope facies consist of inclined reflection packages with different amplitude and sub-marine channels (Figure 4-7). The slope is well developed on the western side of the Great Bahama Bank. The slope geometry is mostly wedge-shaped during early Miocene to late Pliocene times. The slope facies are mostly turbidite depocenters and drift deposits (Betzler et al., 1999).
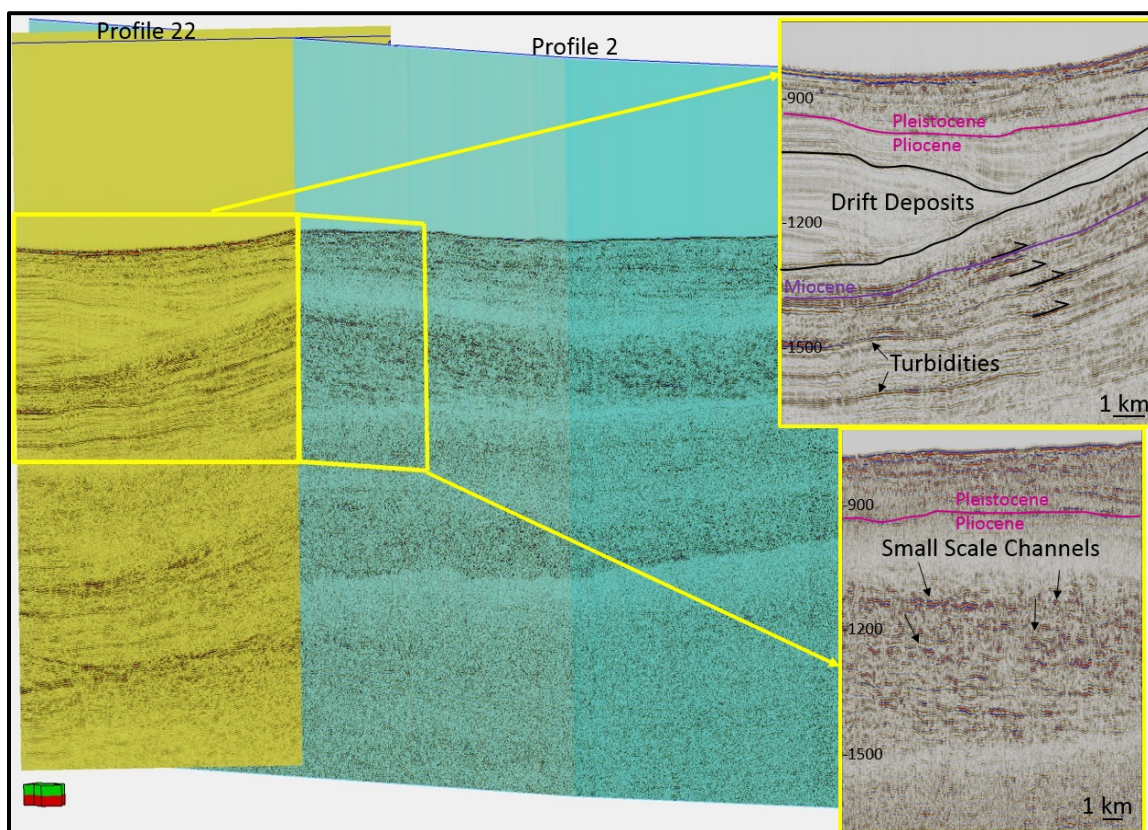
Figure 4-7. 3D view of seismic profile 22 (dark yellow shaded-perpendicular to the slope) and seismic profile 2 (light green shaded-parallel to the slope). North is indicated by the green-topped arrow located at the bottom. The zoom-out part of profile 22 indicates eastward inclined reflections. High amplitude reflections show the velocity increases as a result of transportation of coarser materials by turbidity currents. An approximately 2 km wide deep-water mound, showing low amplitude, very continuous internal characteristics, is observed within the drift deposit. Small-scale channels are dominantly observed along the slope. Black arrows from the zoom-out part of Profile 2 indicate these structures. The internal characteristic of this facies is high amplitude, semi-continuous to discontinuous reflections. See Figure 4-2 for locations.

Seismic Facies Unit S2. Slope Facies

Internal configuration of slope facies is defined as variable continuity, low to high-amplitude, dipping reflections (Eberli et al., 2004). The direction of the inclination is different on the east side and west side of the Santaren Channel. The reflections package gets thinner towards to the basinward direction and interfingers with drift deposits and deep-water sediments (Bergman, 2005).
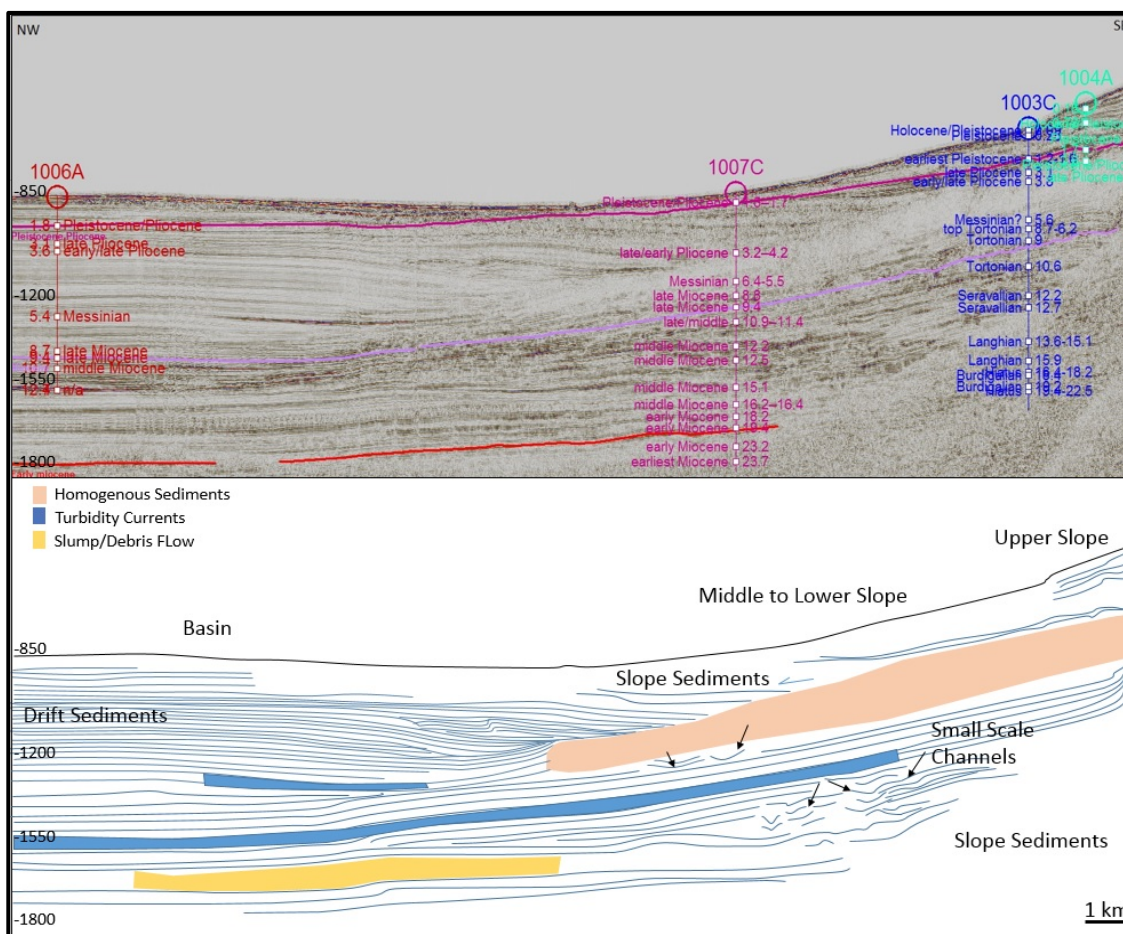
Figure 4-8. Slope and basinal facies are mapped within a prograding sequence along seismic profile 4. The upper slope is composed of platform derived sediments. The middle to lower slope consists of peri-platform ooze. Mass gravity flow deposits, like slump masses debris flows, and turbidities intercalate with these background deposits. Small scale channels act as funnels. The basin is mostly dominated by inclined drift packages. The transparent zone between the Messian and the Pliocene sequence is a result of homogenous sediment deposition.

The lithology of the slope and the basinal sections is derived from cores along the Bahamas transect and two cores at Sites 1008 and 1009 south of the transect. The cores from the Bahamas transect penetrated all the banktop lithology (Borehole Unda) the proximal slope (borehole Clino), three sites on the upper, middle and lower slope (ODP sites 1003 , 1005, and 1007) as well as basinal/drift locations at ODP Site 1006. In core Clino, the uppermost slope facies is composed of a mixture of pelagic foraminifera with skeletal and peloidal grains derived from shallow water (Eberli et al., 1997; Melim and Masaferro, 1997). This mixture of pelagic and neritic components is called the periplatform ooze. It forms the fine-grained portion of the slope and basinal successions in the Santaren Channel. The mass gravity flows are funneled down slope, through small channels and furrows, and form a depo-center on the lower slope and the toe-of-slope with small overlapping lobes. (Eberli et al., 1997; Betzler et al., 1999). The seismic facies of the slope reflect this lithological distribution. The slope facies is composed of continuous reflections that change downslope to more discontinuous facies, indicating an increase in channeling on the lower slope. Likewise, some of the seismic sections display thin packages of chaotic to transparent facies that were confirmed by drilling to be the seismic expression of slump masses (Eberli et al., 1997).

Because of the strong currents in the Straits of Florida and the Santaren Channel, winnowing occurs at the distal slope, producing a wedge shaped geometry to the slope deposits ending in a condensed facies towards the basin (Denny et al., 1994; Betzler et al., 1999, Bergman, 2005). In cores from ODP Leg 166, the turbidities in the slope section are very well cemented, causing over 2000 m/s velocity difference between the turbidities (fast) and the hemipelagic background sediment (slow) (Kenter et al., 2002).
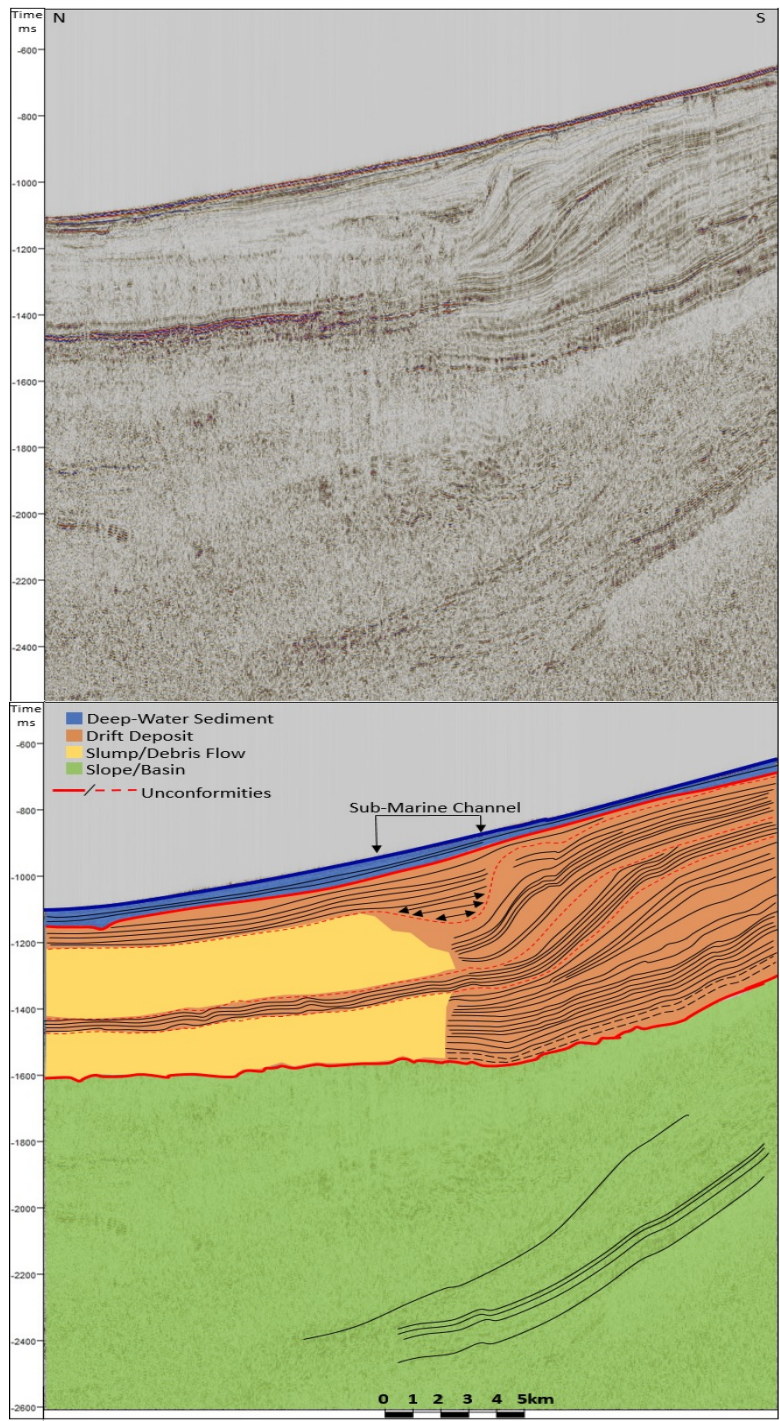
Figure 4-9. The squeezed seismic section from profile 19 shows the facies distribution on the slope. The green shaded area indicates slope/basin deposition. Highly continuous strong parallel reflections indicate drift deposits which are highlighted with brown. The slump/debris flow shows chaotic to transparent medium amplitude reflections shown in yellow; A sub-marine channel approximately 2 km thick is located in the drift deposits. Deep-water sediments, shown in blue, overlie the top of the drift deposit. See Figure 4-2 for the location of the profile.

Seismic Facies Unit S3.Sub-Marine Channels

Large channels that are recognized as a down-cutting erosional truncation of reflections and a subsequent filling of the erosional feature dissect the slope section. Internal configurations of the channels are mostly onlap fill and mounded onlap fill geometry, with strong high amplitude reflections. The channels are filled by shallow-water and slope sediments, which are transported by mass gravity flows (Anselmetti et al., 2000; Bergman, 2005). The maximum depth is 800 m when 2000 m/s interval velocity is used for the time –depth conversion. They are found at different times throughout most of the study area. They are abundant along the eastern side of Cay Sal Bank and the western side of the GBB margin within Miocene and Pleistocene sediments of the upper and middle slope. They are generally V-shaped channels, and show a vertical and lateral stacking pattern, oriented perpendicular to the slope (Anselmetti et al., 2000; Bergmann, 2005) (Figure 4-10). The channels are probably filled by shallow-water and slope sediments, which are transported by mass gravity flows (Anselmetti et al., 2000; Bergman, 2005). They have never been cored.
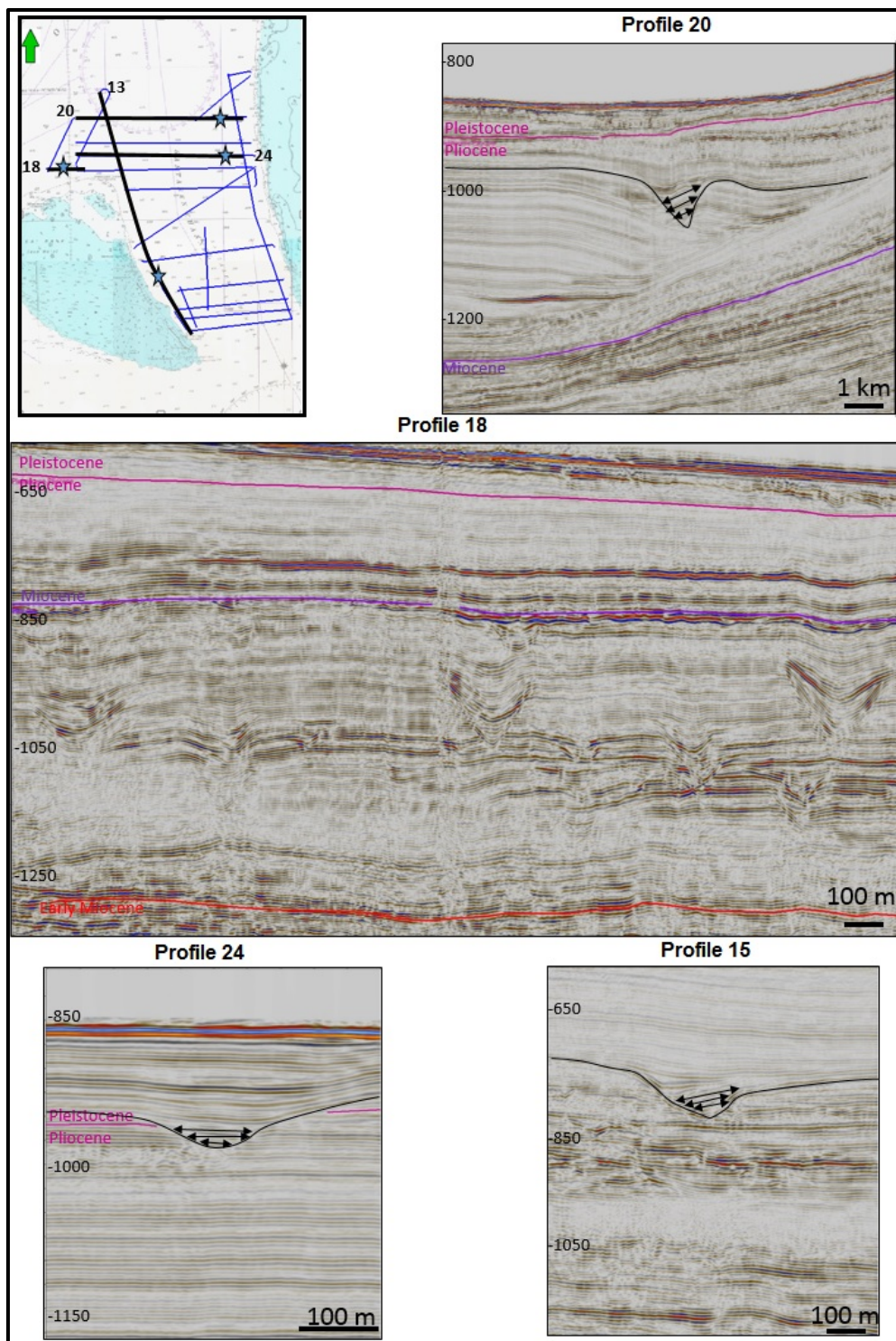
Figure 4-10. Seismic images showing sediments incised by sub-marine channels. Pink (Pleistocene-Pliocene), purple (Miocene) , and red (Early Miocene) horizons indicate the average age for channels. The first three sections are examples of onlap fill geometry channels. The section from profile 18 illustrates the vertically stacked V-shaped channels.

4.2.1.3. Basinal Facies

Seismic Facies Unit S4. Deep-Water Sediments

The basinal seismic facies has an internal reflection character of continuous, faint to high amplitude, horizontally layered reflections (Figure 4-11). The external reflection geometry is defined as sheet-like. The deep-water, basinal facies occurs throughout the Santaren Channel study area, and the Straits of Florida. It onlaps and interfingers with the inclined slope reflection along Cay Sal Bank and GBB. To the west and north of the study area it covers buried shallow-water carbonate platform facies at different depths in different locations. The facies reaches its maximum thickness along the Santaren Channel and gets thinner towards the margins. The lithology of the deep-water, basinal facies is hemipelagic periplatform ooze with intercalation of distal turbidities (Eberli et al., 1997, Anselmetti et al., 2000; Bergman, 2005). The variable amplitudes of the facies is attributed to changes in lithology and diagenetic overprint. Pure periplatform ooze is seismically nearly transparent but intercalations of well-lithified turbidities can create strong impedance contrasts, producing high-amplitude reflections (Anselmetti et al. 2000).
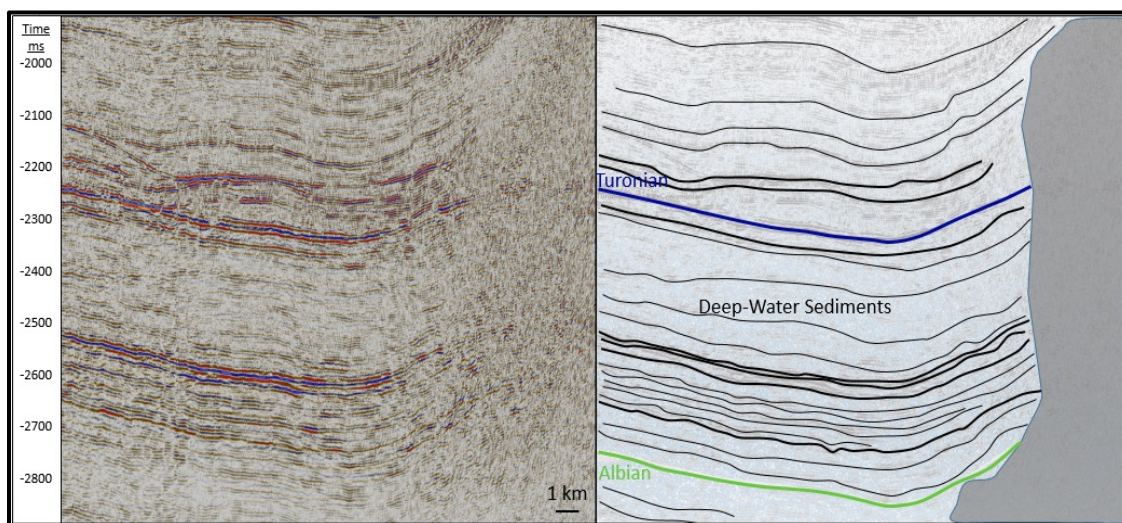
Figure 4-11. Example of the seismic facies of the deep-water, basinal facies. Faint to high amplitude, parallel reflections with a sheeted geometry are the main characteristics of the basinal facies. These deep-water sediments onlap or interfinger with a chaotic reflection package (Light grey area in right panel) (Location for Profile 8 given in Figure 4-2.)

Seismic Facies Unit S5. Drift Deposit

The Santaren Channel and the Straits of Florida are getaways for strong ocean currents. These currents and associated countercurrents and internal tides influence the sediment distribution in the basinal areas, producing both thick accumulations of drift deposits and sediment waves. The seismic facies of the drift deposits is characterized by continuous reflections of low to high amplitude. The external geometries are variable.   In some areas the drift deposits are sheet-like, but in general the geometry is mounded. The two largest drift deposits in the study area are the Santaren Drift, which fills nearly the entire width of the Santaren Channel, and the Cay Sal Drift that is located on the northern slope of Cay Sal Bank (Bergman, 2005).

The Santaren Drift is observed in all the crossing lines in the Santaren Channel. The average thickness of the drift is approximately 900 m when calculated with an interval velocity of 2500 m/s. The Santaren Drift extends over 100 km in length and over 55 km in width (Figure 4-12). The base of the mounded drift deposit is dated as 12.2 Ma, and deposition continues today (Bergman 2005).

The Santaren Drift is, however, a composite drift with three main geometrical elements. The base and main body of the drift, encompassing about 2/3 of the drift, is a wide mounded drift that starts with near horizontal reflections. Laterally the drift reflections interfinger with the inclined slope deposits of Cay Sal and GBB. As the

mounded geometry evolves, several kilometer-wide moats form along both platform slopes (Fig. 4-12).

The seismic amplitudes within this portion of the drift change through time. The basal near horizontal reflections have a medium to high amplitude, whereas in the mounded top, amplitudes are much weaker but still mostly parallel (Fig. 4-14). In the strata between two seismic horizons dated as 3.6 Ma and 1.7 Ma, respectively, the drift sedimentation is shifting into the eastern moat along GBB (Fig. 4-14). The internal geometry of this laterally shifted drift deposit is characterized at the base by a series of up to 2 km wide slightly asymmetric mounds that onlap the eastern margin of the underlying mound and the western facing slopes of GBB (Fig. 4- 12; 4-14). These asymmetric mounds are covered by parallel continuous reflections that form a wide mound with the highest point within the axis of the eastern moat. The strata between seismic horizons is dated as 1.7 Ma and the modern seafloor is the third element of the Santaren Drift. This portion of the drift is again a wide mound in the center of the Santaren Channel with two clearly defined moats on either side (Fig. 4-12, 4-14).

Cores located at ODP Site 1006 are positioned in the middle of the Santaren Drift and, provide the lithologic and stratigraphic information for the drift (Figure 4-13). Correlating borehole 1006 with seismic profile 4, the sediments are divided into three main types as given in log information. Figure 4-14 illustrates the correlation of the seismic horizons of seismic profile 4 and core lithology at Site 1006.
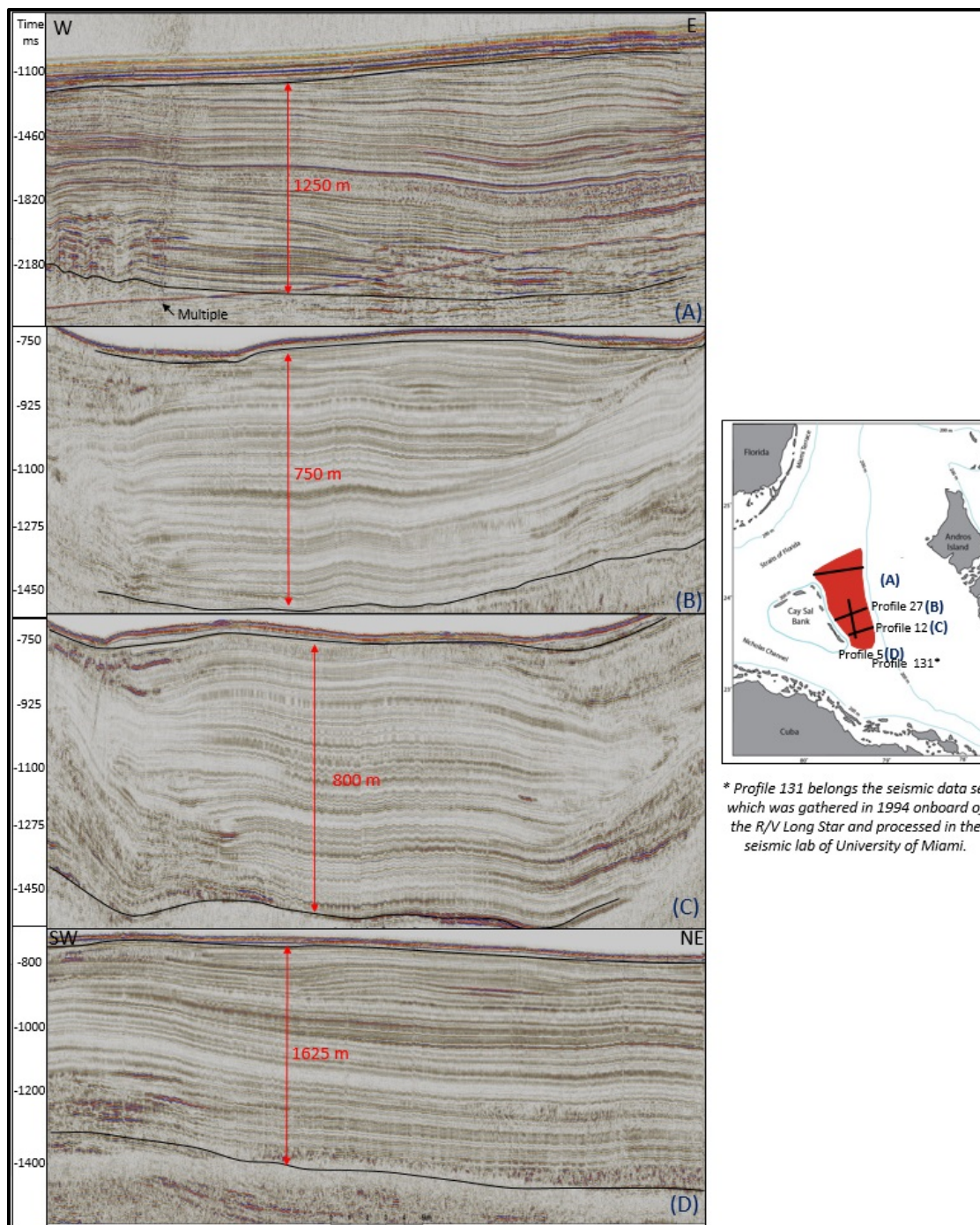
Figure 4-12. Santaren Drift facies in seismic profiles. Drift facies are limited with sequence boundaries shown as black horizons. The thickness of the facies is calculated by the given internal velocity 2500 m/s. Seismic profiles show depositional thickening in the middle of the Santaren Channel.
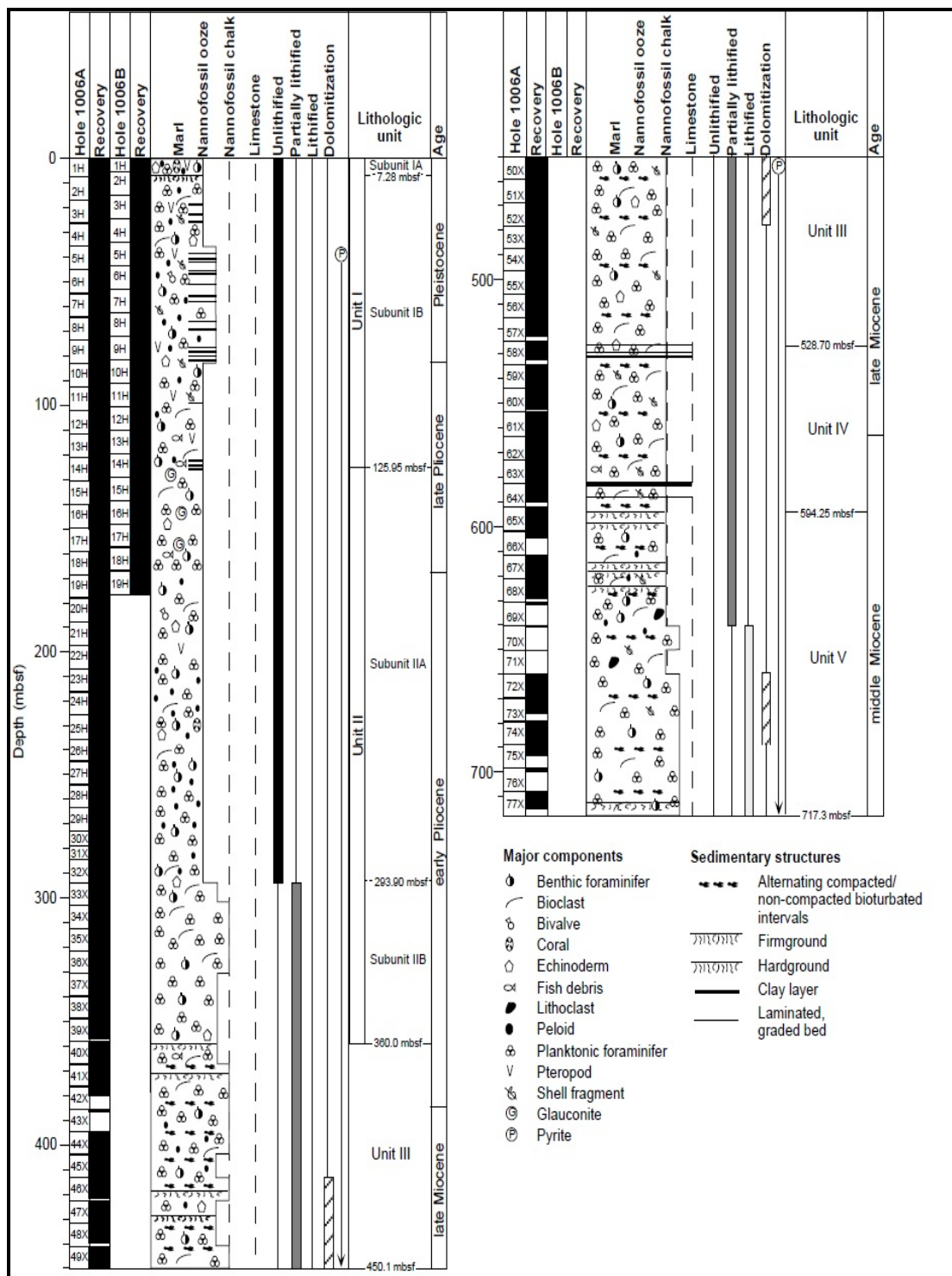
Figure 4-13. Lithostratigraphic synthesis at site 1006 (Eberli et al., 1997).
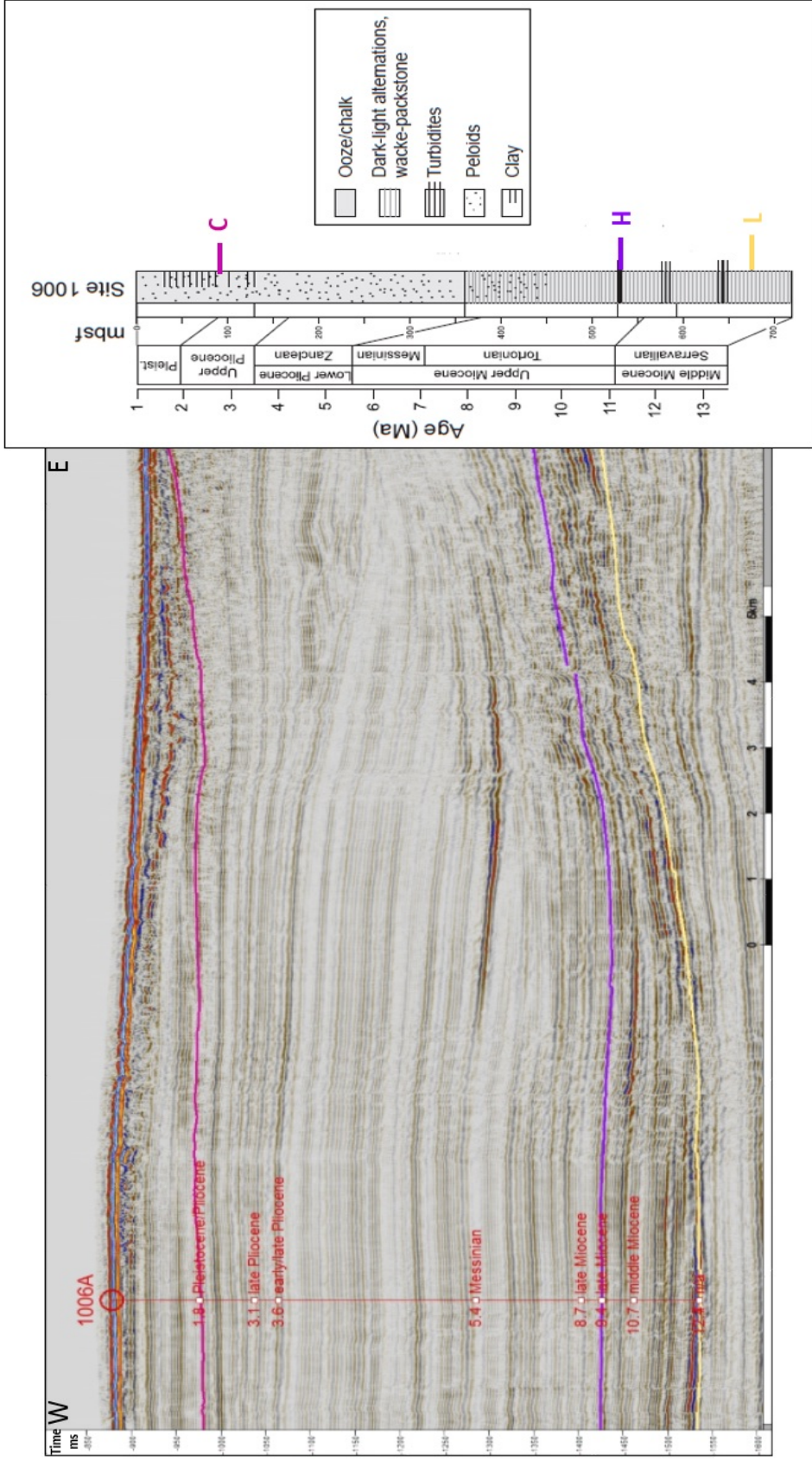
Figure 4-14. Left: Location of ODP Site 1006 on the Santaren Channel with selected horizons on seismic profile 4. Core lithology from Site 1006 with the position of the seismic horizons discussed in the text is to the right (modified after Betzler 1999).

Unit I is Pleistocene in age and is composed of a nannofossil ooze, with foraminifers, and variable amounts of gray clay and silt intercalations (Eberli et al, 1997b). The base of the Unit 1 coincides with Horizon C. The underlying Unit II contains mainly nannofossil ooze and chalk (Eberli et al, 1997b). Sediments from Unit III to Unit V show yellowish gray or greenish gray nannofossil marls of open-water origin alternating with skeletal limestone of shallow-water platform origin (Eberli et al, 1997b; Bergman, 2005). The base of Unit IV is correlated to seismic Horizon H and the base of Unit V is correlated to seismic Horizon L. Seismic Horizon L is selected in the drift deposits as it marks the beginning of the mounded drift development.

Seismic Facies Unit S6. Sediment Wave

This seismic facies has a discrete wavy reflection pattern of highly discontinuous, medium to high amplitude reflections (Fig. 4-15). The wavy seismic facies is limited to thin intervals and is limited in lateral extent, although it can cover several kilometers. Wavy reflections can be produced by several processes. Here the high-amplitude wavy reflections are interpreted to be submarine sand waves, deposited by a strong benthic current with bedload transport. A modern sand wave field that could produce such a seismic facies is documented at the foot of the Miami Terrace (Correa et al., 2012). Sediment wave migration can produce sand wave fields that can be mapped out on seismic data (Bergman, 2005). Amplitude-based seismic plots reveal that the amplitudes of sediment wave facies are higher than the adjacent areas. This can be explained by the fact that coarser material, which causes high acoustic impedance contrast, is transported to form the sediment waves (Figure 4-15).
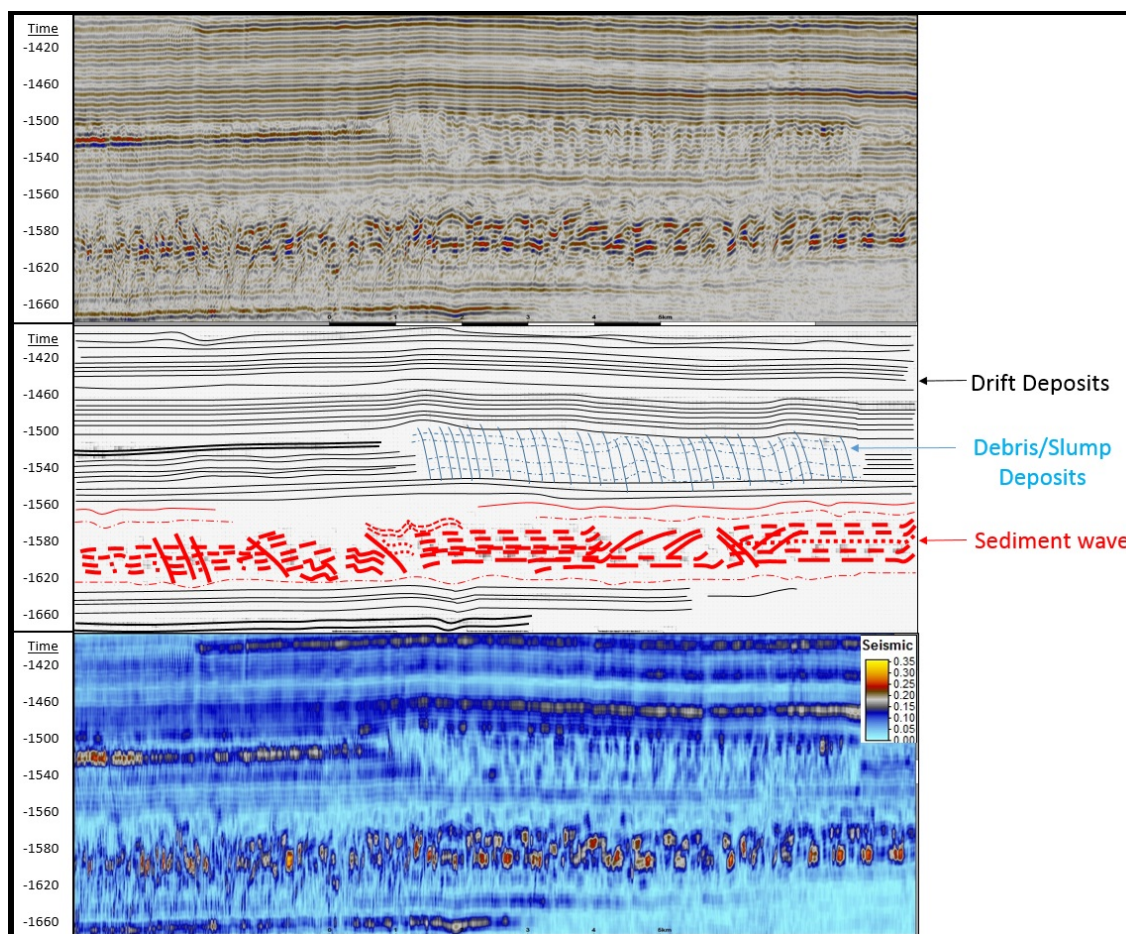
Figure 4-15. Top: Uninterpreted part of seismic profile 22 displaying two types of wavy seismic facies. One is of higher amplitude and has two stacks of wavy reflections the other is more transparent and the wavy reflection pattern is observed mostly in the top. Middle: Interpretation of the seismic facies as sediment waves for the stronger amplitude wavy facies and as debris flow/slump for the low-amplitude wavy facies. Bottom: RMS amplitude display of the seismic section illustrates the amplitude difference in the two wavy facies. Red color indicates high amplitude areas. See Figure 4-2 for the location of the profile.

Seismic Facies Unit S7. Debris/Slump Flow

This seismic facies is mostly represented by highly discontinuous, transparent to chaotic reflections of low to medium amplitudes. The chaotic character can transition into more organized discontinuous reflections that resemble the wavy seismic facies produced by sand waves (Fig. 4-16). A distinct difference in our data set is the muted amplitude in

what is interpreted here as debris flow and slump deposits (Fig. 4-15; 4-16). Debris and slump flows are types of mass gravity flows that produce mass transport complexes (MTC). Slumping moves the entire slope along a basal detachment plane and, depending of the nature and the speed of the movement, results in MTCs that are more or less chaotic. If a slump mass incorporates abundant water it develops into a debris flow in which the matrix carries larger blocks and boulders. A thin debris flow was drilled at ODP Site 1008 and correlated to a chaotic to transparent seismic interval (Eberli et al., 1997). The seismic sections of both the Cay Sal and GBB slopes are punctuated with numerous intervals of chaotic seismic facies that terminate in a basinward direction. The up to 100 ms (twtt) thick packages document major mass gravity flows along the slopes of both banks and the subsequent deposition of large MTCs, similar in size to those observed on the modern seafloor in the Straits of Florida (Mulder et al. 2012).

Turbidity current is another type of mass gravity flow. In the Santaren Channel they originate from the bank top and margin or from slope instabilities. They tend to cement up extensively to produce high velocity layers within the periplatform ooze (Eberli, 1988). As a result of these high acoustic impedance difference within the layers, strong seismic amplitudes are produced. (Fig. 4-16).
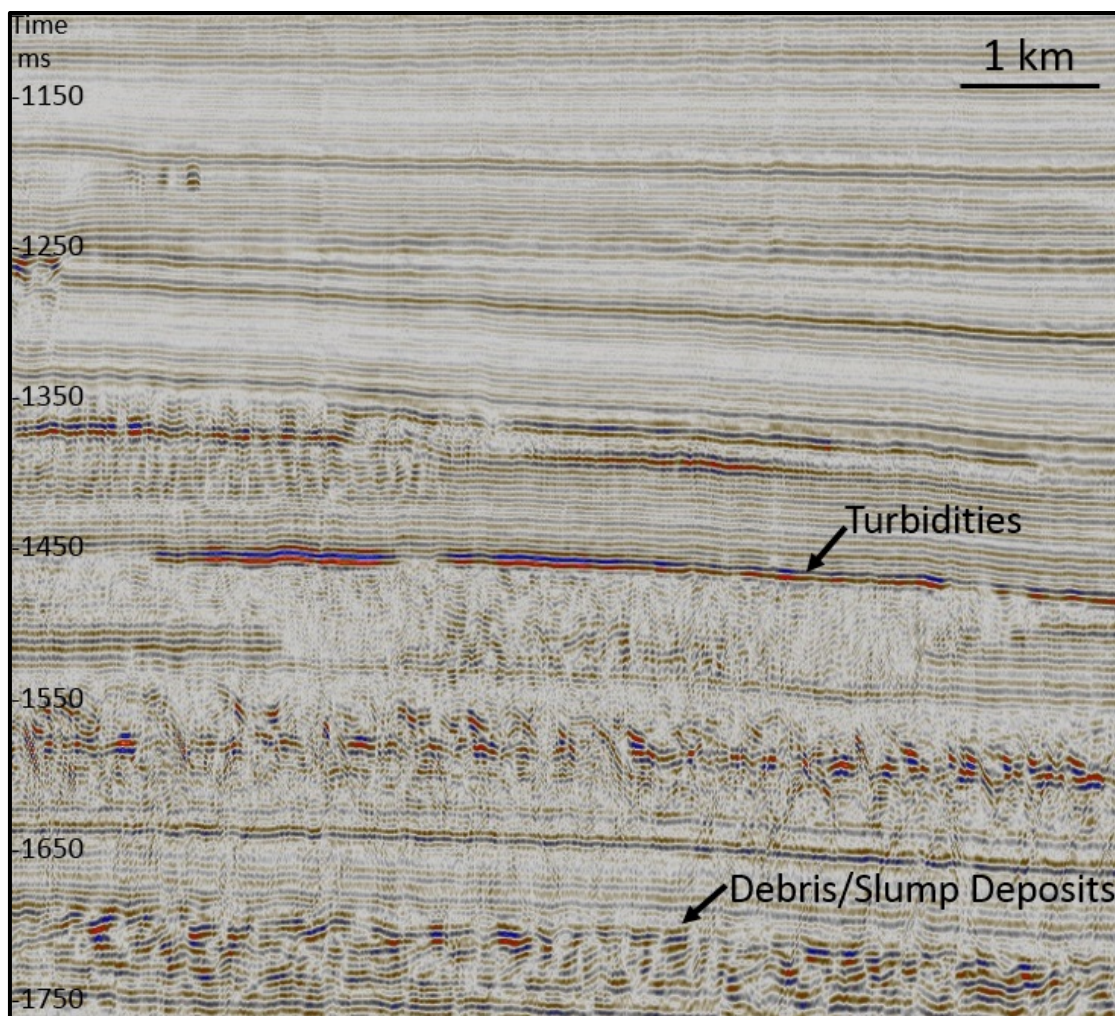
Figure 4-16. Horizontally stacked debris/slump units in seismic profile 22. Turbidities are recognized as high amplitude events within the basinal facies. The chaotic to transparent seismic facies are interpreted to be Mass Transport Complexes (MTC) from slump and debris flows. Likewise the inclined to chaotic facies between -1650 and -1750 ms is interpreted as a large MTC.

Acoustic pipes

High-resolution quality of the newly acquired seismic profiles enables us to detect a common feature within the drift deposits and less frequently in the overlying slope section. The seismic characteristics of these features are narrow and vertical upwardly bended reflections, which are named here "acoustic pipes" (Figure 4-17). The acoustic

pipes are located parallel to each other and they dominantly occur in the southern and the middle part of the Santaren Channel. Their diameters vary between 40 to 160 m. Some of these structures show reflection pull-up while others have a push-down effect. The acoustic pipes generally lead to pockmarks, indicated by a crater in the sea floor. The high-resolution seismic profiles reveal that these structures are also accompanied by polygonal fault systems (see subsequent structural analysis chapter).

Because of the seismic character and the association with pockmarks the acoustic pipes are interpreted to have been caused by fluid flow or gas chimneys (Hovland and Judd, 1988, Løseth et al. 2001, Hustoft et al., 2007). The pipes that show pull-up characteristics have a fill of high acoustic velocity compared to the adjacent sediments, whereas pipes with push-down characteristics have a lower velocity fill compared to the adjacent area, an indicator for free gas (Hustoft et al., 2007). Migrating hydrocarbons are not only indicated by these structures but have also been documented in all coarse sediments in the Straits of Florida, offshore Cuba and Exuma Sounds (Austin et al., 1986, Eberli et al., 1997). Further, hydrocarbon shows in young strata of the Straits of Florida and Exuma Sound indicate that hydrocarbon is actively migrating through the sedimentary column of the deep-water channels. The source of these hydrocarbons could either be Cretaceous or Jurassic in age. Albian carbonaceous limestones in the Northeast Providence Channel document the occurrence of Cretaceous source rocks.
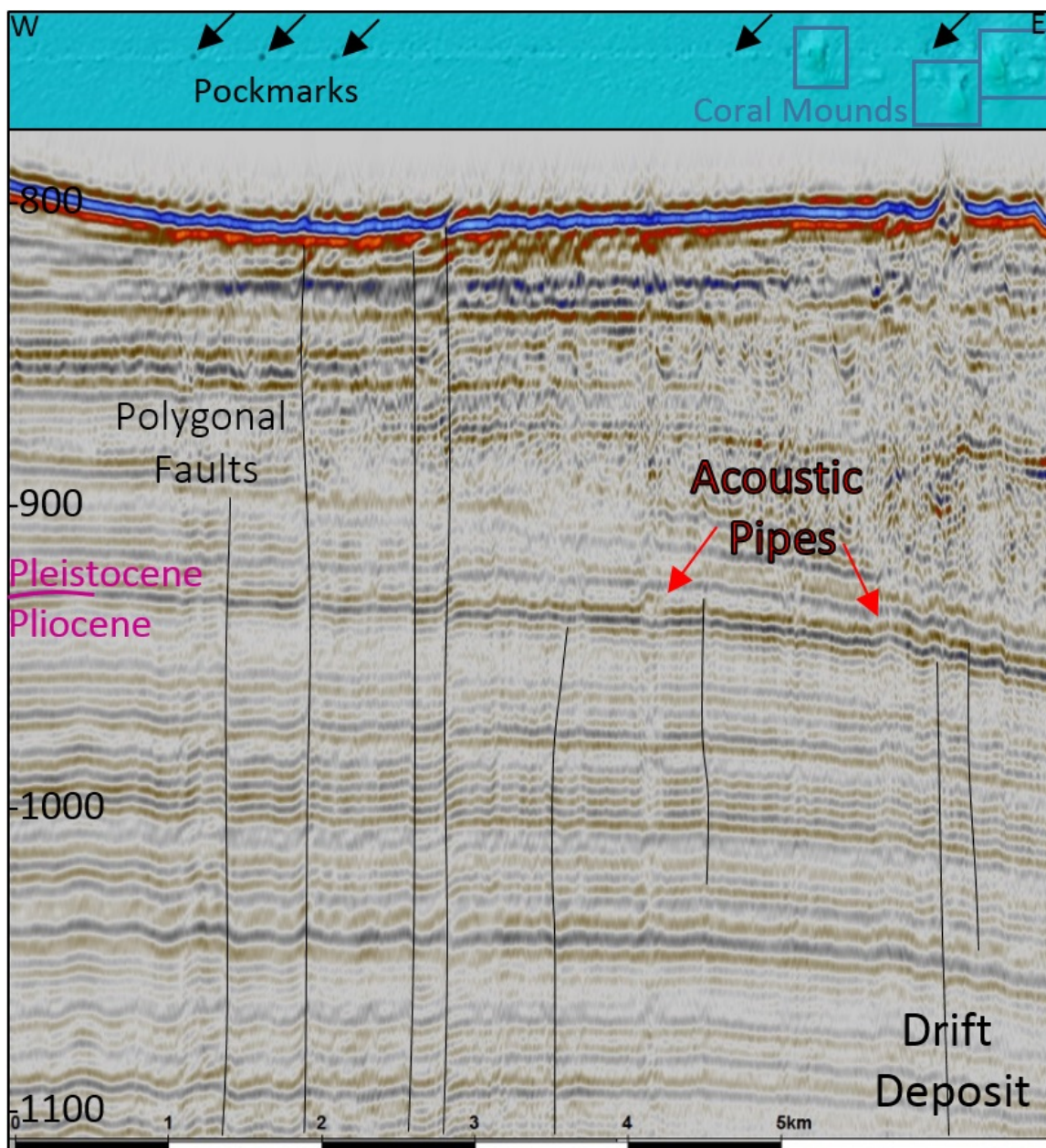
Figure 4-17. The squeezed seismic part from Profile 27 is given along with the bathymetry data on top. The bathymetry profile shows pockmarks as holes and deep-coral mounds. On the seismic section the drift deposit is deformed by a polygonal fault system. Fluid migration is observed towards to the sea floor where the pockmarks are present. Acoustic pipes cause pull-up and push-down on the reflections. The vertical wipe-out zones are mostly results of these structures. The chaotic facies that is located in the left-hand side of the section may arise from the fluid flow or the entrance of the slope sediments derived from the adjacent slope. See Figure 4-2 for the location of the profile.

CHAPTER 5. STRUCTURAL ANALYSIS

Overview

The collision between the Caribbean and North American plates formed the Cuban Fold and Thrust Belt. The collision started in the Late Cretaceous, and culminated in the middle Eocene, but some shortening between the two plates continued throughout the Neogene (Mann et al., 1997, Masaferro et al., 1999). The trend of the Cuban Fold and Thrust Belt and its location are subject to debate. One group of scientists claim that an arcuate Cuban Fold and Thrust Belt is located along the Island of Cuba (Iturralde-Vinent, 1994; Mann et al., 1997; Saura et al., 2008). Another group of scientists expands the belt further to the north, based on a NW-SE trending thrust fault system with compressional structures in the Santaren Channel that they relate to the shortening within the Cuban Fold and Thrust Belt (Ball et al., 1985; Masaferro, 1997). Ball et al. (1985) suggest that the Santaren Anticline, which is located in the southern part of the Santaren Channel, is the northernmost edge of the Cuban Fold and Thrust Belt. Masaferro (1997) reconstructs the evolution of the Santaren Anticline in order to prove the consistency of its timing with Cuban/Bahamas collision. Furthermore, he documents the presence of a reactivated thrust fault system along the eastern side of Cay Sal Bank. Based on these two findings he extends the Cuban Fold and Thrust Belt to the south of Cay Sal Bank, yet insufficient data precludes him from mapping it further north. Figure 5-1 briefly explains these two different hypotheses regarding the trend of the Cuban Fold and Thrust Belt.

In the course of this chapter the different structural elements in the study area are described. The fault systems and compressional structures are placed within the age model derived from the horizon maps and in some cases by correlating other reflections

81

to dated core strata. The structural analysis tests the hypothesis that the observed anticlines, thrusts, and faults, that cause major horizontal displacement in the younger strata and break the sea floor in some places at the northeastern side of the Cay Sal Bank, are related to the Cuban Fold and Thrust Belt. In addition to the compressional structures a polygonal fault system in the drift deposits will be documented. It seems to act as a pathway for fluid flow through this strata. All of these structural units are described in detail and the seismicity of the area is examined in order to demonstrate the possible active tectonism in the area.
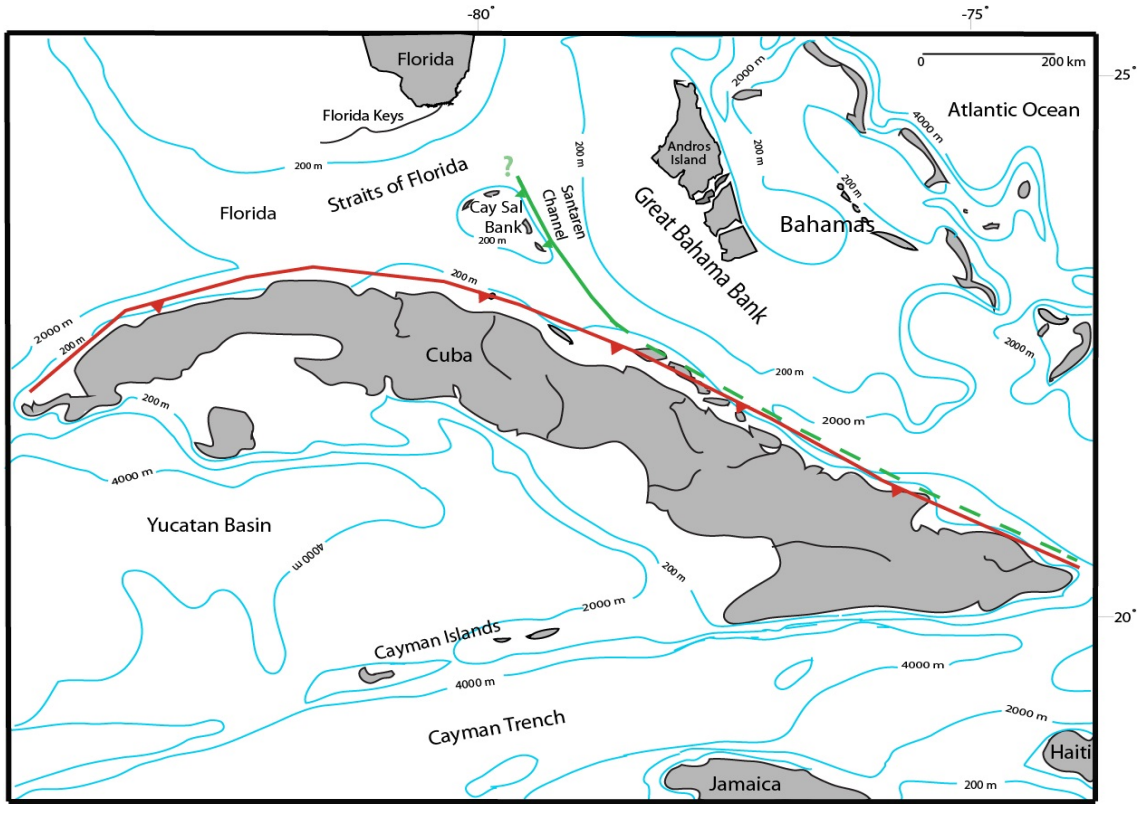
Figure 5-1. Map showing the two competing scenarios of the extent of the Cuban Fold and Thrust Belt. The red line is the outer border of the most accepted structural sketch of the Cuban Fold and Thrust Belt. The green dashed line and continuous line indicate the outer border of a thrust fault system that is also linked with the Cuban Fold and Thrust Belt as proposed by Masaferro (1997).

Figure 5-2. Un-interpreted seismic profile 20 (newly gathered and processed high resolution seismic profile).
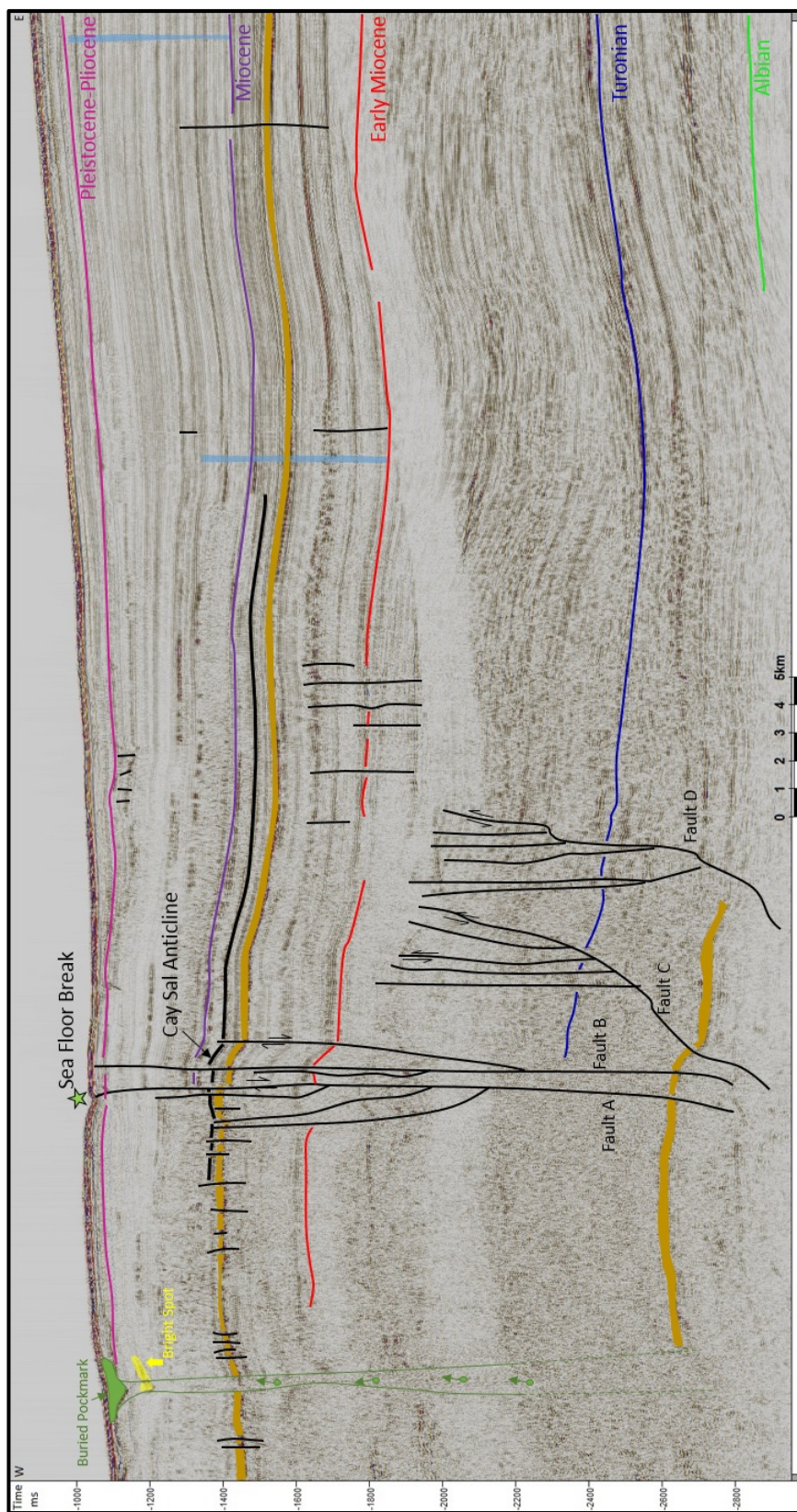
Figure 5-3. Interpreted seismic profile 20. This profile has undergone several deformations with different structural styles. Deep-rooted fault systems are most apparent in the eastern side of the profile. Fault A and Fault B displace the Holocene strata; furthermore fault A breaks the sea floor. Strata-bound faults are also observed with different ages and length. The Cay Say Anticline is indicated with a bold black line. Buried pockmark associated with gas chimney is indicated with green lines. A bright spot is detected within the gas chimney. Possible fluid flow migration is indicated with green arrows. Acoustic pipes found in drift deposits are highlighted with blue strips.

5.1. Fault Systems

The seismic sections reveal two groups of fault systems. One group consists of faults with shallow roots and little vertical displacements. A polygonal fault system, described below, is one type of fault in this group. Faults confined to certain intervals of strata are also included within this group. The other fault group comprises dip-slip fault systems that have deep roots, which in most cases reach the basement or deep portions of the sedimentary strata.

Group 1: Strata-bound faults

The dominant fault system in this group is characterized as a polygonal fault system. They are observed as gently dipping and tightly spaced (ranging from 50 to 1000 m) planar faults (Figure 5-4). The offset range of the polygonal faults varies from 10 to 100 m. Their vertical extension range is around 500 ms (twtt) or approximately 625 m, using an interval velocity of 2500 m/s for the time depth conversion. The faults do not extend into the basement and they do not reach the sea floor (Figure 5-4). They are found along the Santaren Channel in the deep-water sediment deposits, generally within the Pleistocene to Miocene sequences. The faults are found in large numbers within the middle portion of the Santaren Channel in the vicinity of acoustic pipes. Both the polygonal faults and the acoustic pipes act as pathways for fluid flow; yet they show different characteristics. Polygonal faults create slight offsets and the acoustic pipes are observed to function as bending structures. Therefore, changes in offset are considered to be a means of discriminating polygonal faults from acoustic pipes.
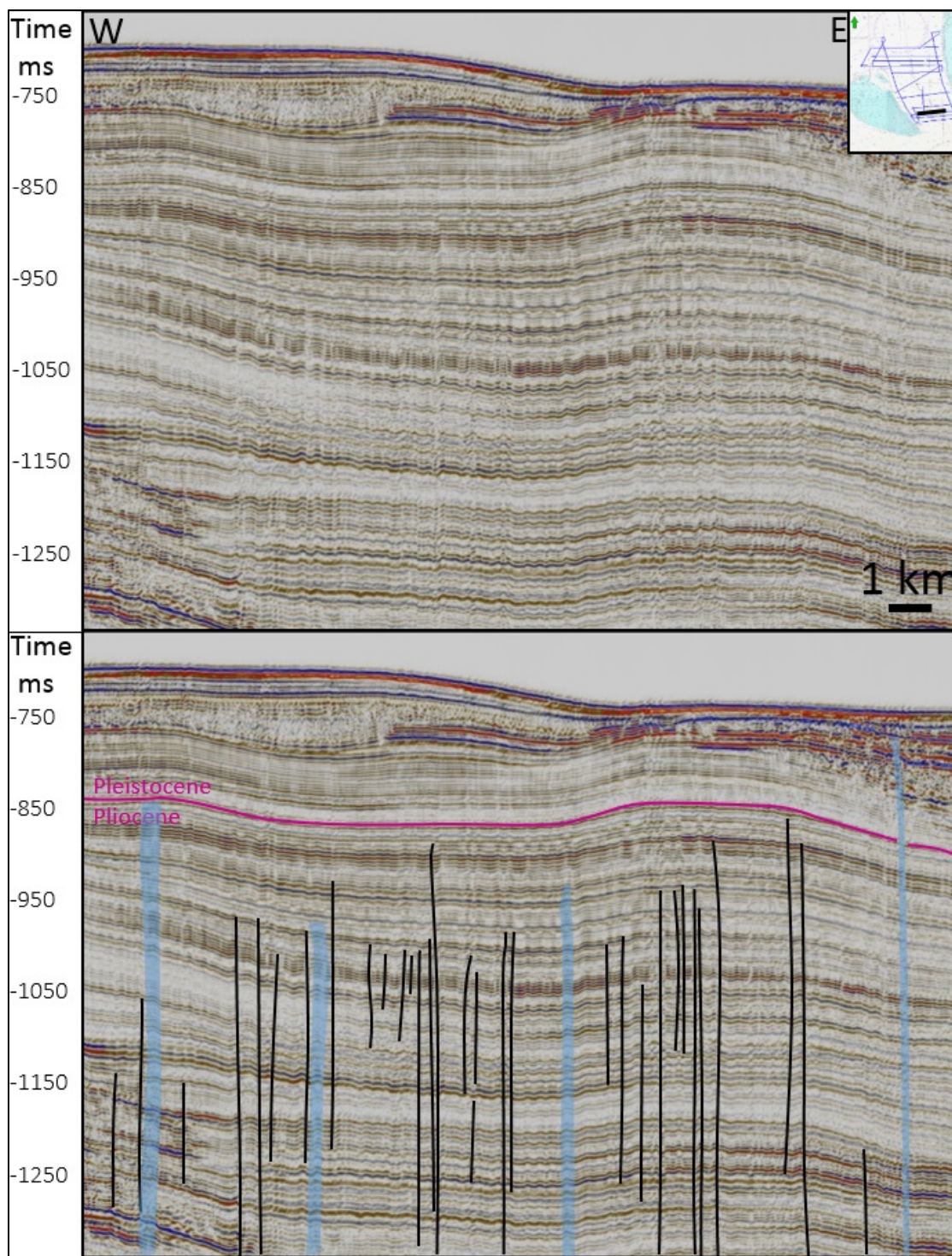
Figure 5-4. Top: Squeezed seismic section from the southern Santaren Channel displaying the Santaren Drift deposit. Bottom: The interpretation of the profile. This figure illustrates two probable structures within the drift deposits. The polygonal faults are indicated with black lines and acoustic pipes are highlighted with blue strips.

The origin of these regularly spaced faults in the basin center is most likely not related to tectonic activity in the region. These types of faults have been better imaged with 3D seismic data, where they display a polygonal pattern (Figure 5-5). According to Cartwright and Dewhurst (1998), polygonal faults are extensional faults, with minimum offset, developed in deep water sediments that act as pathways for fluid flow (Chen et al., 2011). Comparing the features of the faults observed in the Santaren dataset with the literature, they are interpreted as non-tectonic faults that act as pathways for fluid and hydrocarbon migration.
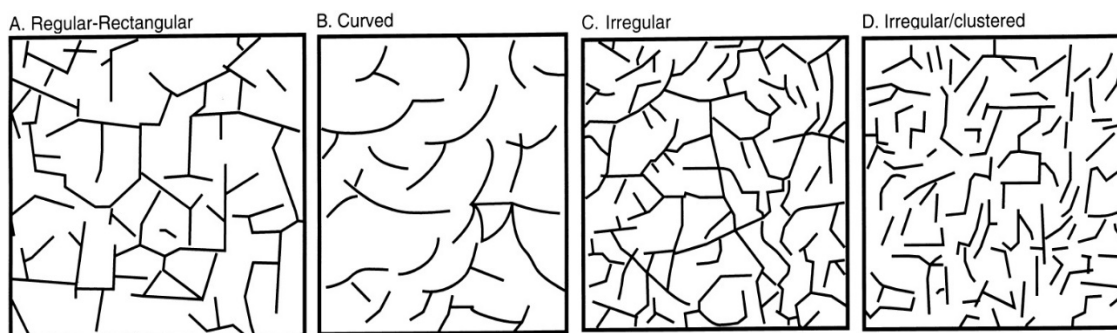
Figure 5-5. Some of the schematic patterns that are observed in the polygonal fault systems (Lonergan and Cartwright, 1998). In order to map the pattern characteristic of our polygonal fault system 3D seismic data is required.

The other fault type in this group also show very small vertical offset. They occur within strata of different ages and have variable length. Some of these non-tectonic faults can be traced for not more than three parallel profiles. Considering that the average distance between two seismic profiles is around 10 km, their length is calculated at about 30 km. Their origin might be compaction related.

Group 2: Deep-rooted faults

The second group of faults penetrates deep into the seismic sections but their point of origin is not always visible on the seismic sections due to insufficient resolution or depth range of the data. These fault types are located on the eastern side of Cay Sal Bank. They have different structures, length, and age but their general trends are NW-SE, the same as the Cuban Fold and Thrust Belt. The faults can be mapped along the entire length of Cay Sal Bank and further north into the Straits of Florida.

The deep-rooted fault systems are divided in two subgroups. The first subgroup consists of Faults A and B which are defined as deep-rooted fault systems showing wrench fault characteristics. The reasons for this characterization are that the fault systems within this subgroup have very steep roots and show strike-slip characteristics over some portions like wrench faults. The second subgroup consists of Faults C and D, defined as deep-rooted thrust fault systems. The second group of thrust fault systems becomes less active eastward from Cay Sal Bank to the GBB. Brief information about each system and a location map is given below.

Fault A is located in the northeastern side of Cay Sal Bank and is observed for a distance of approximately 41 km, trending in a NE-SW direction (Fig. 5-6). Vertical offset is nearly 150 m. In general, this fault system is defined as a dip-slip fault acting as a wrench fault. Fault A reaches and breaks the sea floor (Figure 5-7). The sea floor breaking zone is detected along the northeastern side of the Cay Sal Bank, not only in the seismic profiles but also in the bathymetry and parasound profiles. Detailed information about this zone will be given in the "Evidence for Neotectonics" section.

Fault B is another active deep-rooted fault system that shows wrenching. The length of the fault is approximately 115 km, and it trends in a NE-SW direction (Fig. 5-6). Typically most displacement of wrench faults is horizontal. Since it is generally hard to detect this type of displacement in our seismic sections, dashed lines are used in order to show the possible fault plane and its connection with the sea floor break (Figure 5-7). Vertical offset is around 120 m.

Fault C is observed for approximately 180 km, trending in a NE-SW direction (Fig. 5-6). It is a basement detached thrust fault system reaching Neogene strata. It is accompanied by normal faults (Figure 5-7). Vertical offset is approximately 120 m.

Fault D is observed for approximately 160 km, trending in a NE-SW direction (Fig. 5-6). It is the most easterly located deep-rooted thrust fault system reaching until Neogene strata. It is accompanied by normal faults (Figure 5-7). General offset range is nearly 90 m.

It is believed that all of these deep-rooted fault systems are related to the same detachment horizon (decollement) which was firstly detected by Masaferro (1997). Due to the insufficient depth range of the newly acquired seismic profiles, this horizon can not be documented.
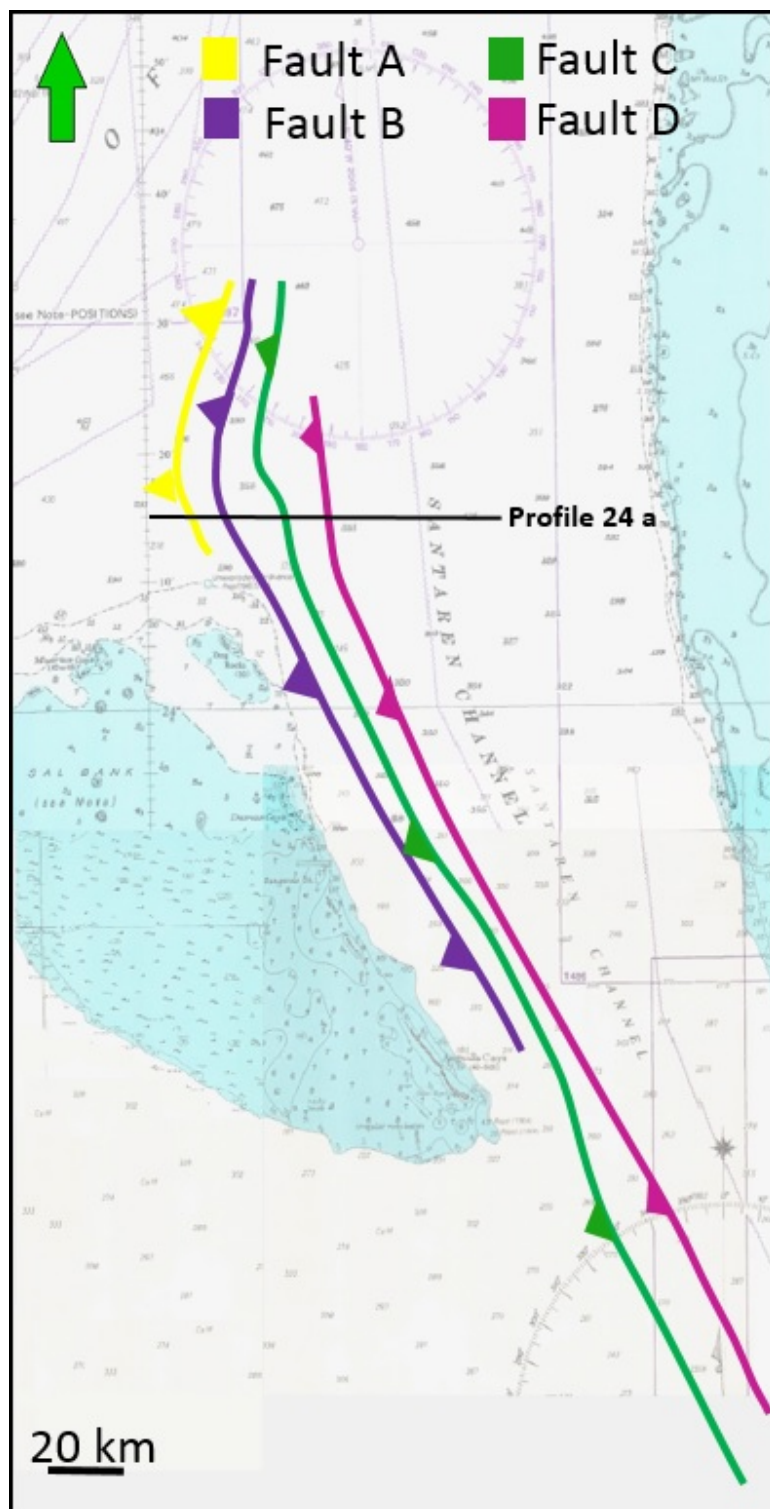
Figure 5-6. Location map of the deep-rooted fault systems. Their general trends are in a NW-SE direction. Fault A and B reach the sea floor; Fault C and D terminate in Neogene strata. Profile 24a is used in order to illustrate how the fault systems are detected in seismic data. Its location is indicated with black lines. Green arrow indicates North.
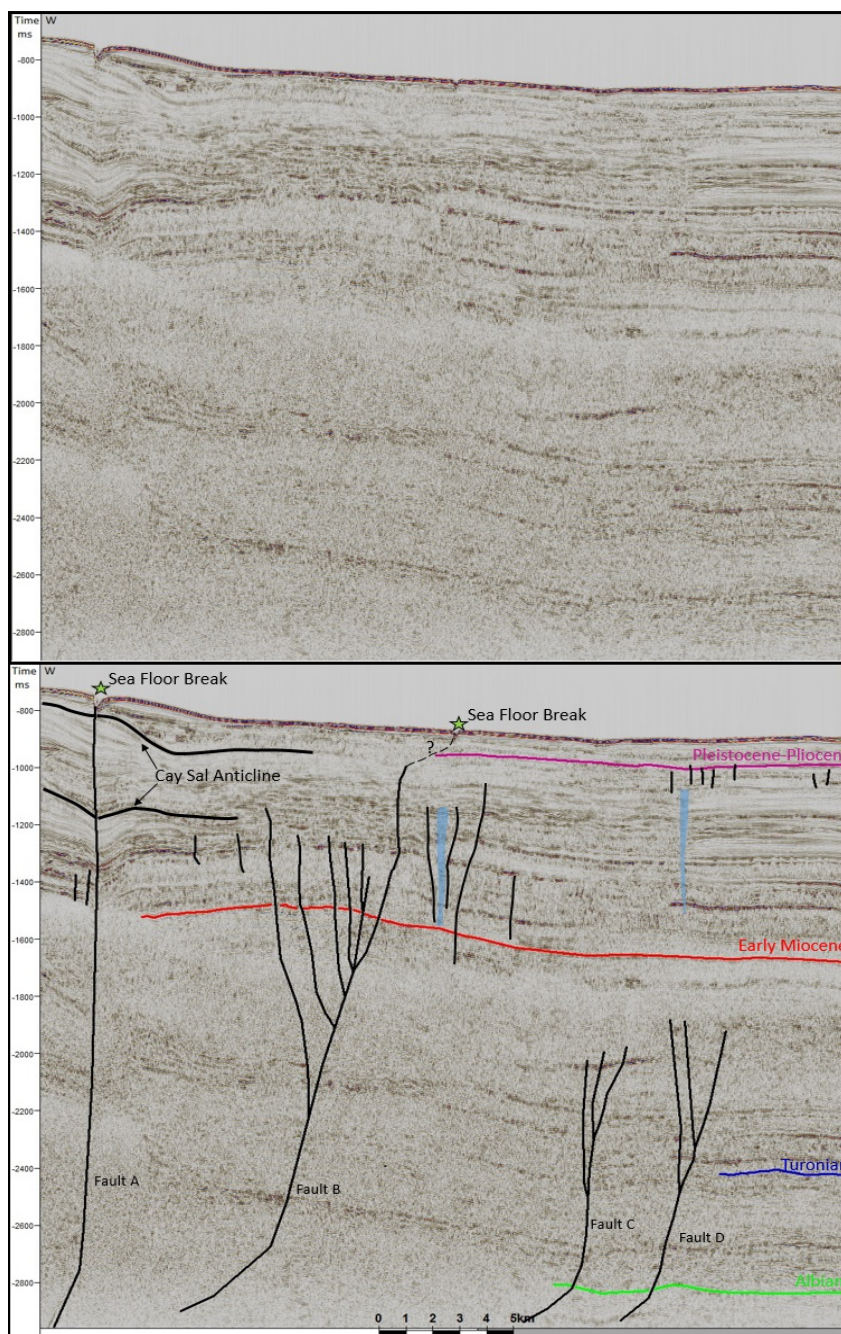
Figure 5-7. Un-interpreted and interpreted squeezed seismic section of Profile 24a. Fault A is defined as a steep-rooted dip-slip fault. Fault B is defined as steep-rooted wrench fault accompanied with small offset dip-slip faults. The other basement detached thrust fault systems Fault C and Fault D reach Pre-Neogene strata. Rather than these major fault systems residual faults are also observed within the deep-water sediment deposition. Acoustic pipes are indicated with blue strips. Cay Sal Anticline will be described in "Fold Systems" section.

5.2. Fold Systems

Two compressional structures are imaged on the newly gathered high-resolution seismic profiles. An asymmetrical, 7 km wide anticline (SantaMiocene Anticline) is detected in five lines located in the southern entrance of the Santaren Channel. A gentle, 4 km wide anticline (Cay Sal Anticline) is mapped in four lines located in the northeastern side of Cay Sal Bank.

SantaMiocene Anticline

The SantaMiocene Anticline is approximately 50 km long and 7 km wide and trends in a NW-SE direction (Figure 5-8). The anticline is imaged on four seismic profiles located in the middle of the Santaren Channel.

The SantaMiocene Anticline is a very gentle anticline with a slight asymmetry. The anticline consists of two stratigraphic units. The package showing the geometry of the anticline is defined as pre-growth strata. The younger strata, which onlaps the anticline crest and gets thinner towards the limbs, is interpreted as growth-strata (Figure 5-9).). Based on the analysis of the seismic facies, these units are composed of deep-water sediments. The growth-fold strata is of Early Miocene age. In the profiles located on the southern entrance of the Santaren Channel, Cretaceous and Early Miocene strata is folded in the anticline (Figure 5-9). Further north (Profiles 8 and 10), in the middle of the channel, only the Cretaceous strata is folded in the anticline, indicating that the growth of the anticline decreases northward. The decelerated tectonic uplift to the north is probably due to a decrease of compression in the distal portion of the Cuban Fold and Thrust Belt.
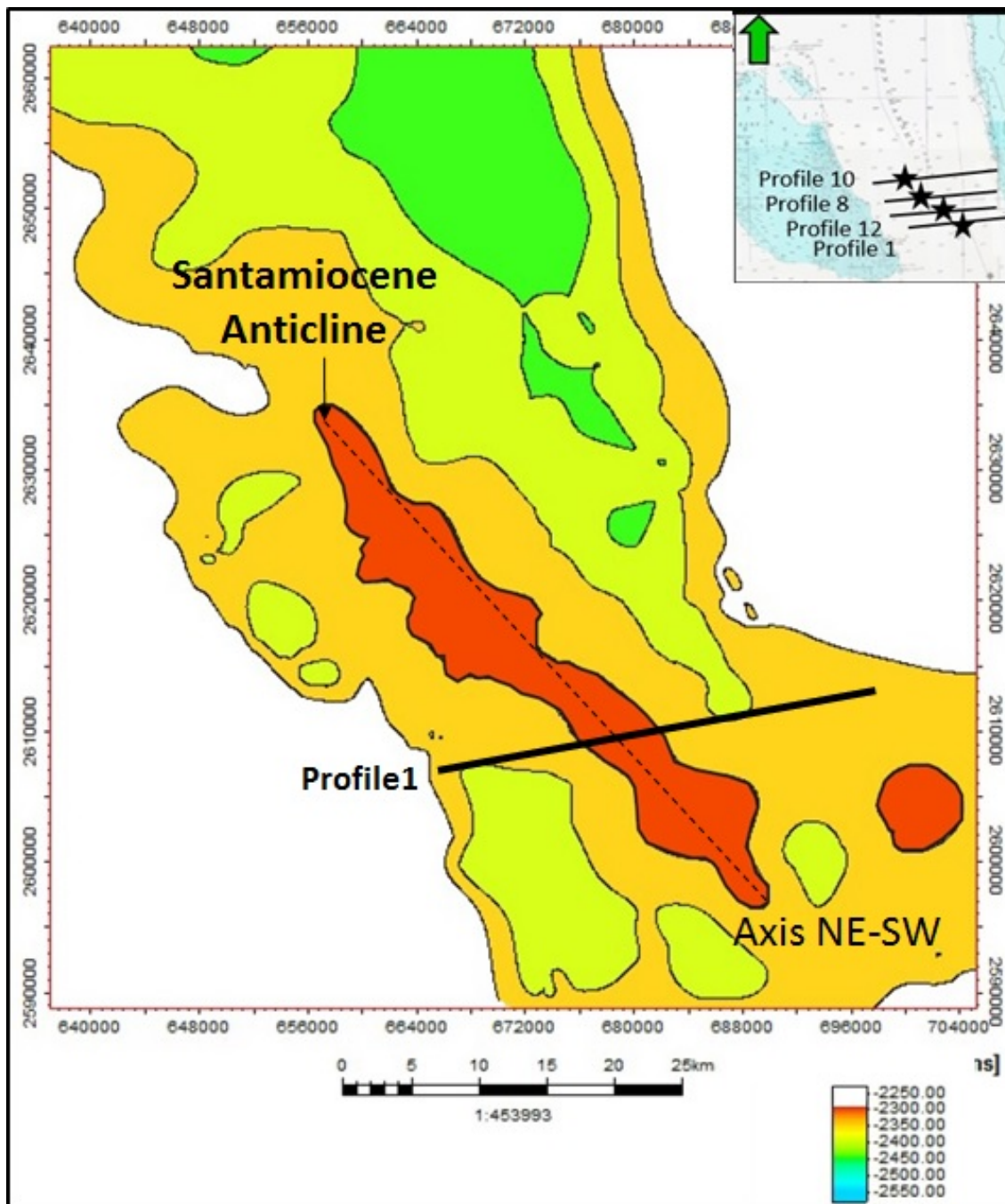
Figure 5-8. Isochron map of the SantaMiocene Anticline along the Turonian horizon. High elevation (red closure) represents the anticline. The anticline is 50 km long and at least 7 km wide. Its axis is oriented in a NW-SE direction. Inset: Location of the profiles showing the anticline structure. Black stars indicate the position where the anticline is observed in these lines. Profile 1 is the most southern located newly gathered seismic profile, which will be interpreted, in the next figure.
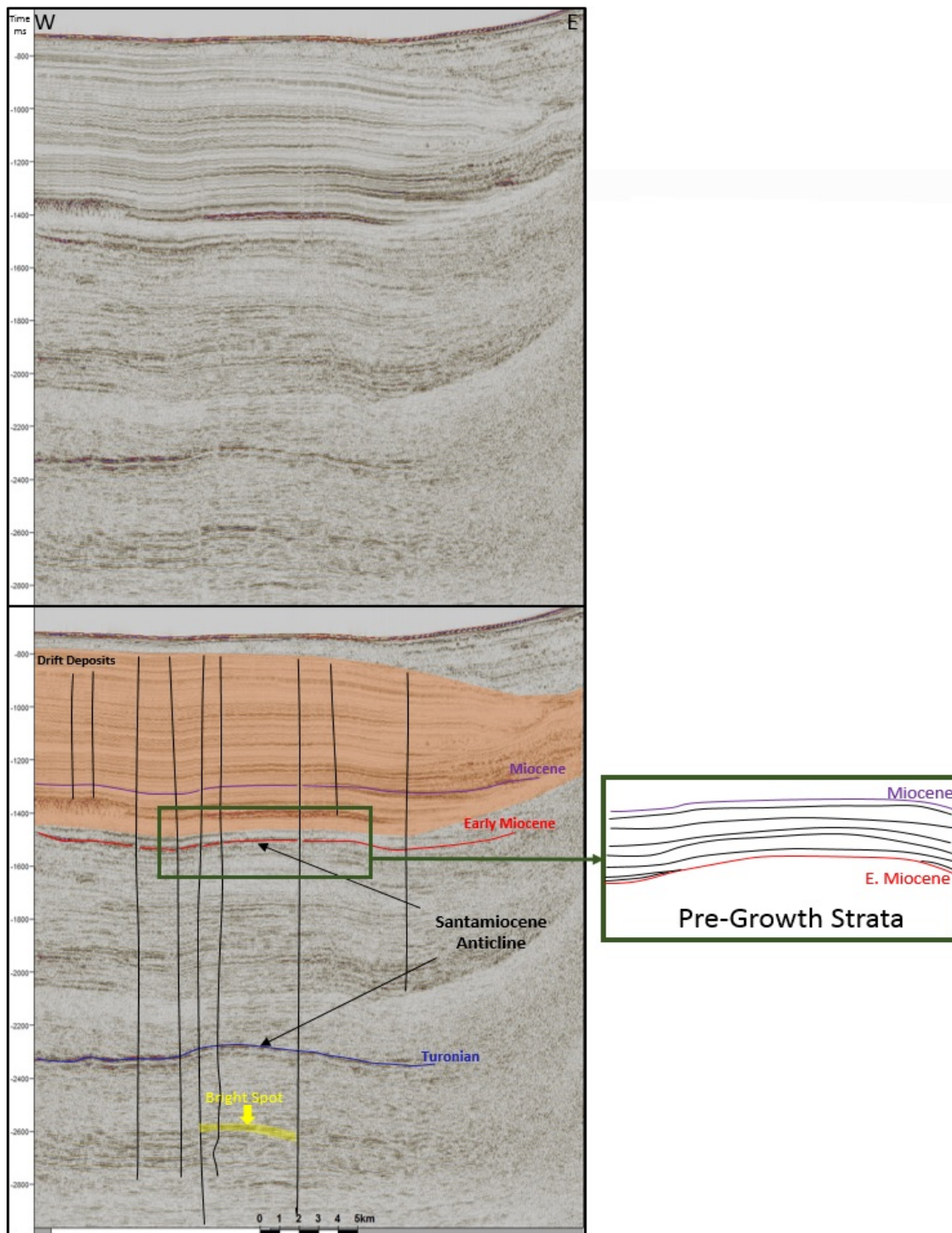
Figure 5-9. Un-interpreted and interpreted squeezed part of seismic profile 1. The asymmetric SantaMiocene anticline is observed within the Cretacous and the Early Miocene strata. Stratigraphic units are shown within the green box. Black, nearly straight lines represent a polygonal fault system which is mostly found in drift deposits. Abrupt high velocity changes in the deeper part interpreted as a bright spot which is an indicator of hydrocarbon.

Cay Sal Anticline

The Cay Sal Anticline is located northeast of Cay Sal Bank. It is a nearly symmetrical, NE-SW trending anticline that is dissected by vertical faults (Figure 5-10). The anticline is about 40 km long and at least 2 km wide. It is imaged on all profiles that cross the northeastern corner of Cay Sal Bank and adjacent basin, which allows the strike of the anticline to be mapped from the bank into the basin. Because the seismic lines do not cross the shallow portion of the bank, the southwestern continuation of the anticline cannot be documented.

Considering the growth fold characteristics in the Holocene section, the Cay Sal Anticline is defined as an active anticline (Figure 5-11). The growth stratal geometry, which contains high amplitude, semi continuous, parallel reflections onlap the anticline crest. The general reflection characteristics of the anticline shows a transition zone from high amplitude, semi continuous reflections to low amplitude and parallel reflections in the Miocene to Holocene strata. In Profile 22 the anticline crest reaches the seafloor (Figure 5-11).
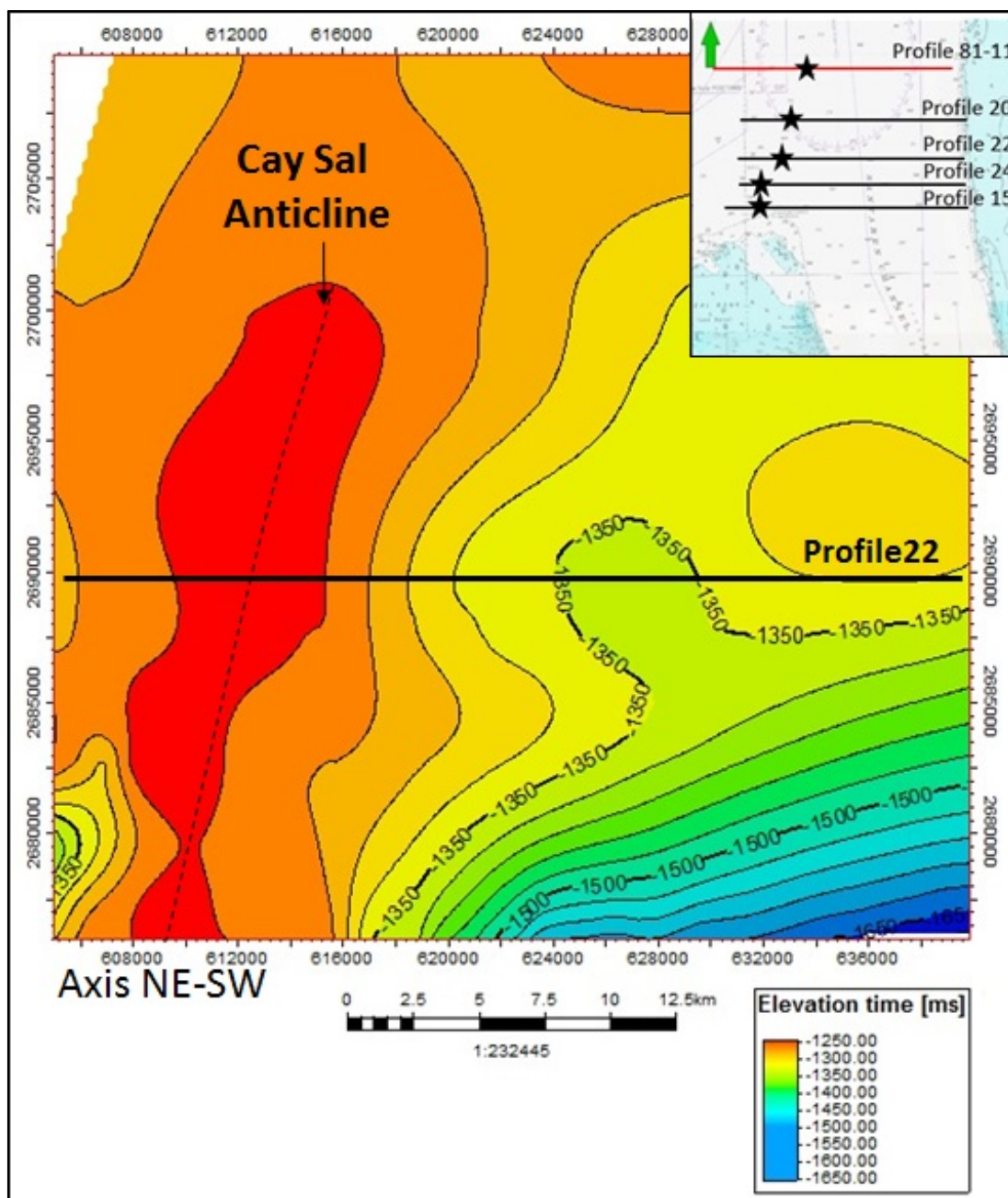
Figure 5-10. Late Miocene age isochron map of the NE-SW trending Cay Sal Anticline. Red closure indicate the high topography along the anticline crest. The location of the Profile 22, which will be interpreted in detail in next figure, is given by the black line. Inset: Location of profiles displaying the anticline structure. The black lines are the new seismic data and the red one is an old regional seismic profile. The star in each line is at the crest of anticline.
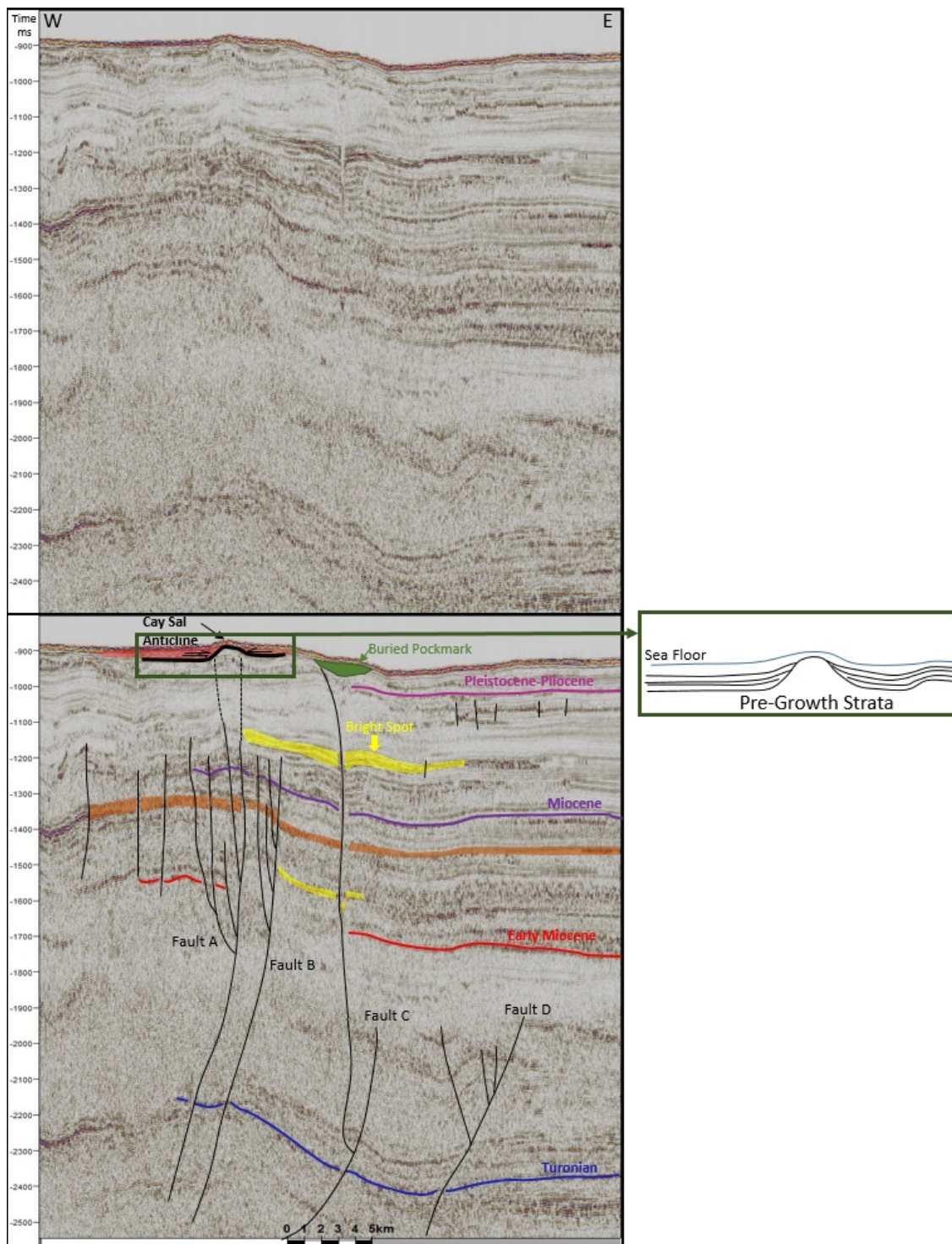
Figure 5-11. Un-interpreted and interpreted squeezed part of seismic profile 22. The Cay Sal Anticline dissected by the fault A is shown with black dashed lines. The Holocene fold-growth strata is drawn within the green box. A buried pockmark and bright spots (yellow shaded zones) indicate fluid and hydrocarbon migration along the steep-rooted faults.

5.3. Evidence for Neotectonics

5.3.1. Sea Floor Break

A sea floor break is an important indication for the presence of the neotectonic activities around the Cay Sal Bank. It is observed on all data sets; bathymetry, seismic data and parasound profiles. Bathymetry profiles reveal a sharp fracture zone. The horizontal displacement is around 50 m (Figure 5-12). The sea floor break is observed to extend for about 40 km and can be up to 1 km wide around the northeastern edge of the Cay Sal Bank (Figure 5-13). Both parasound and seismic data of Profile 15 reveal a break zone 600 m in length and 24 m deep. Highly chaotic facies and mass flow activity under this fracture zone prevent us from interpreting the direction of the throw along the fault. Another break zone is observed in seismic profile 24. The length of this break is 700 m and the depth is approximately 50 m. Seismic profile 20 also indicates that the break zone is around 1 km wide and 15 m deep and is related to an underlying fault (Figure 5-14).
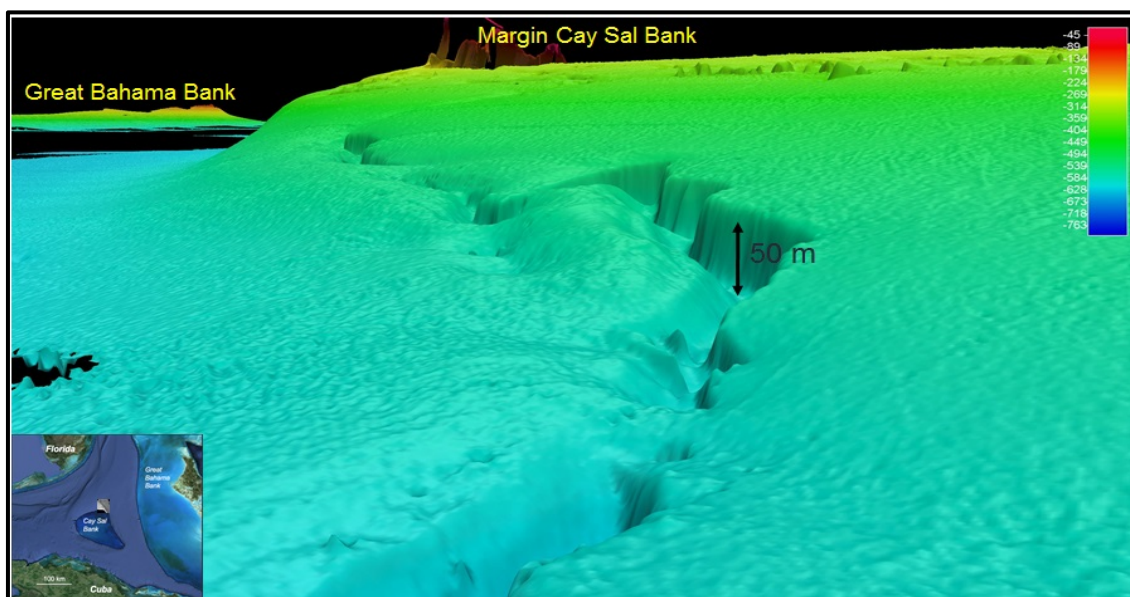
Figure 5-12. 3D view along the sea floor break on the multibeam bathymetry map along the northeastern edge of the Cay Sal Bank illustrates its irregular trace and the horizontal displacement that reaches up to 50 meters.
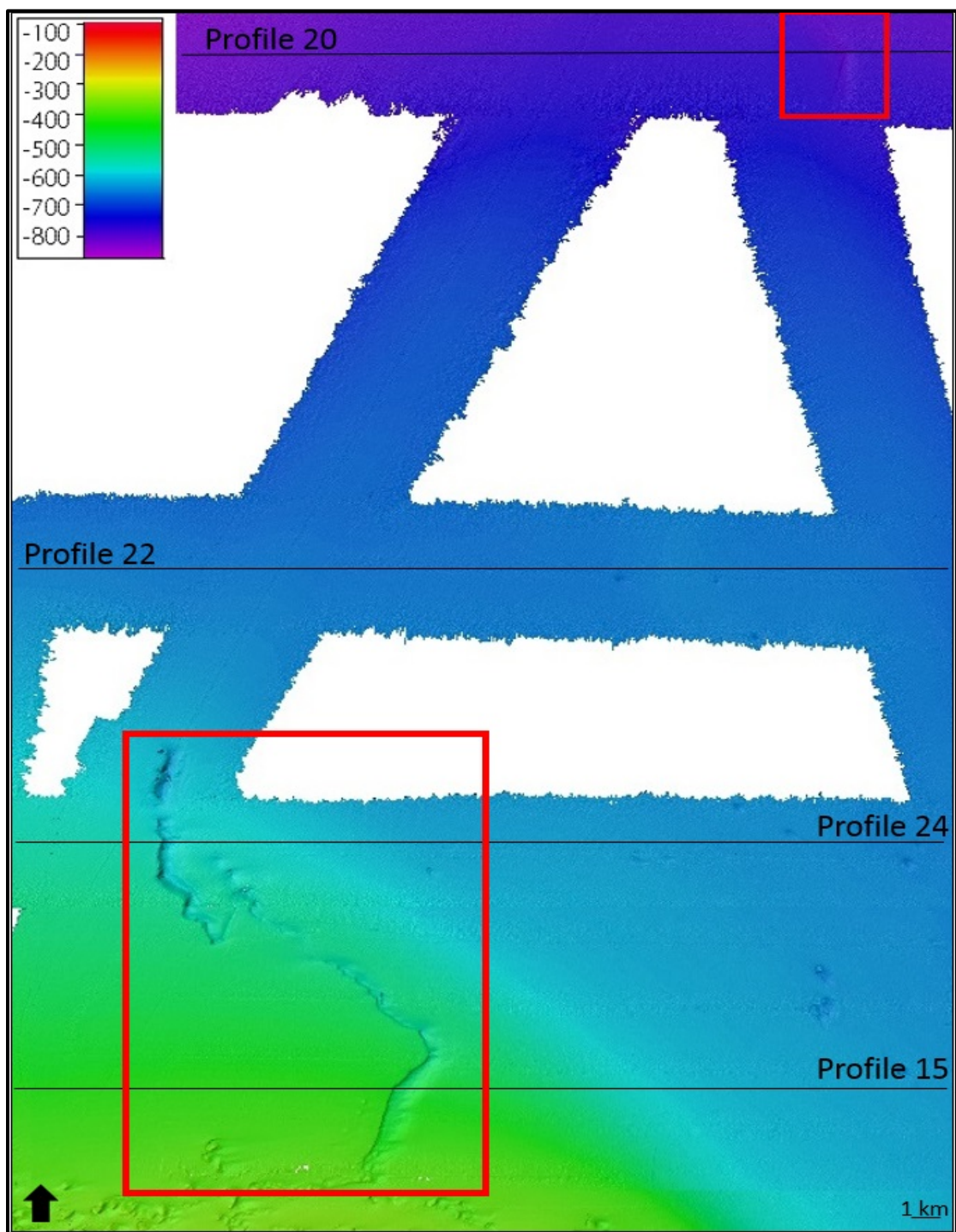
Figure 5-13. Bathymetry map of the northeastern side of Cay Sal Bank. Red boxes indicate the fracture zone that is also observed with seismic and parasound profiles.
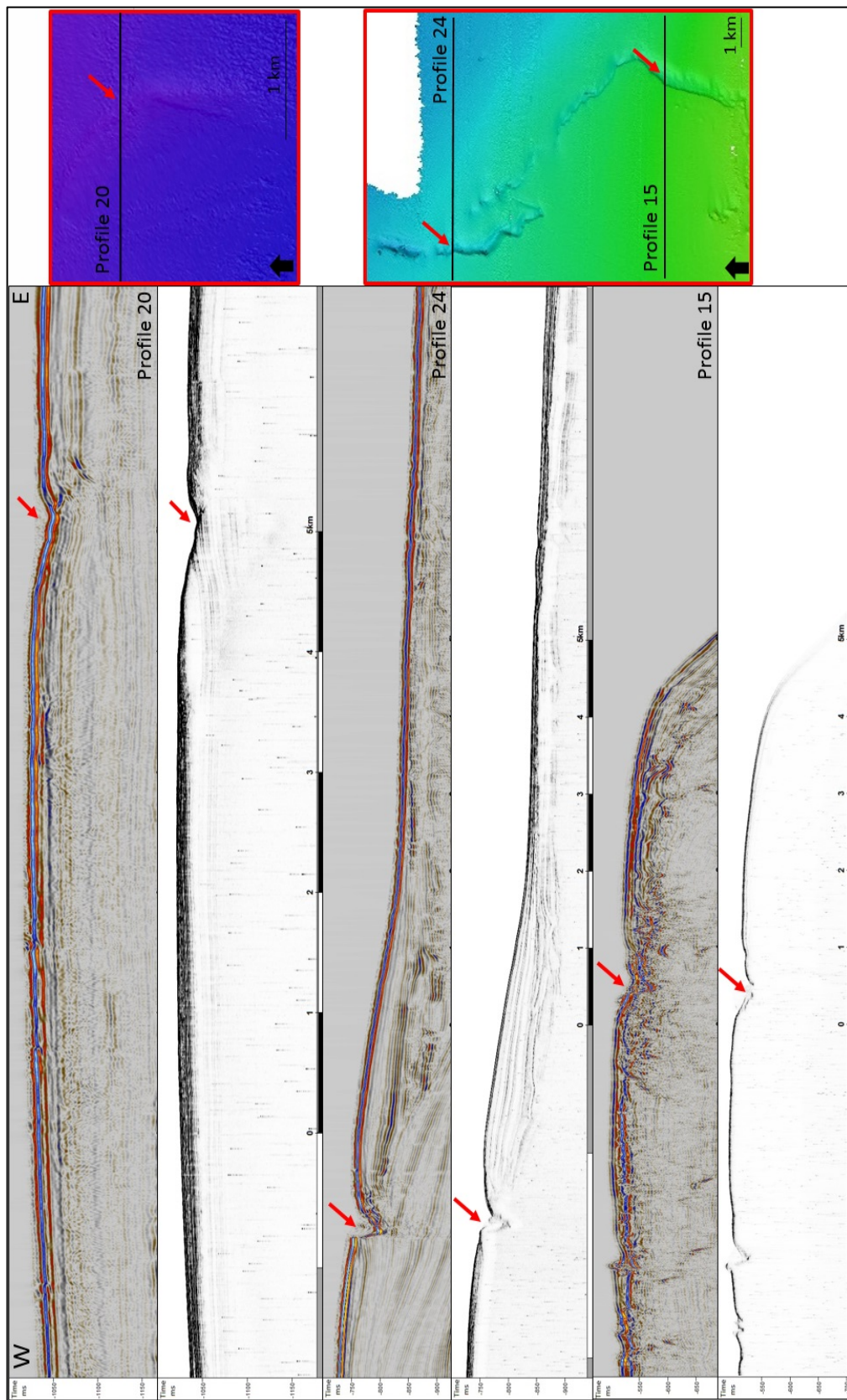
Figure 5-14. Seismic and parasound data showing the sea floor breaks. The fracture zones are indicated with red arrow.

5.3.2. Seismicity

The collision between the Greater Antilles Arc and the Bahamas in the Late Cretaceous and the Early Tertiary formed the Cuban orogenic belt. With the analysis of the fold growth strata, Masaferro (1997) documents continuous shortening between the southern Bahamas and the Cuban Fold and Thrust Belt throughout the Neogene, yet no seismic activity has been recorded in the Santaren Channel in the last 100 years. This lack of seismic activity is puzzling. It has been explained by very slow shortening rate (0.03 mm/yr) (Masaferro et al., 2002). The seismic quiet time ended recently as five large earthquakes were recorded in the northwestern side of Cuba between January and April, 2014. These are the first earthquakes observed in that region. Their magnitudes are measured as 5, 4.1, 4, 4.3 and 4.7 (Figure 5-15). The location of these new seismic events within the Cuban Fold and Thrust Belt indicates that tectonic movements are taking place in modern times.

Even though Cuba is no longer located on the collision zone of the two plates, seismic event records reveal a significant number of earthquakes around the active fault systems, which border and segment Cuba. Considering the tectonic, geophysical and seismic features, Cuba is divided into two neotectonic units: the western unit and the eastern unit (Cotilla et al, 1991). Most of the earthquakes occur in the eastern unit, which is bordered by the Barlet-Cayman (Oriente) Fault (Cotilla et al, 2007). The focal mechanism of this fault indicates a combination of strike-slip and thrust faulting (Cotilla, 1988). The Nortecubana Fault trends along the northern part of the Island of Cuba. It is an active fault system consisting of combined reverse and vertical faults that occur very close to, or sideways from, each other (Cotilla et al., 2007). Movement along this fault

caused a 5.6 magnitude earthquake that triggered a tsunami in 1939 (Rubio, 1985). La

Trocha is a Pliocene-Quaternary age transtensional fault, which is associated with an

earthquake in 1971 (Cotilla et al., 2007). The Habana-Cienfoegos Fault is defined as a

transtensional fault trending NE-SW (Saura et al, 2008). It produced an earthquake in

1693. The Guane Fault is another NE-SW trending left lateral normal fault located in the

western side of Cuba (Cotilla et al., 2007). The strongest earthquake (M=8) associated

with this fault occurred in 1980 (Cotilla et al., 2007), and strangely the record of this

event can not be found in either U.S. Geological Survey (USGS) or International

Seismological Center (ISC)'s event catalogs which means that it was in reality a much

weaker earthquake.
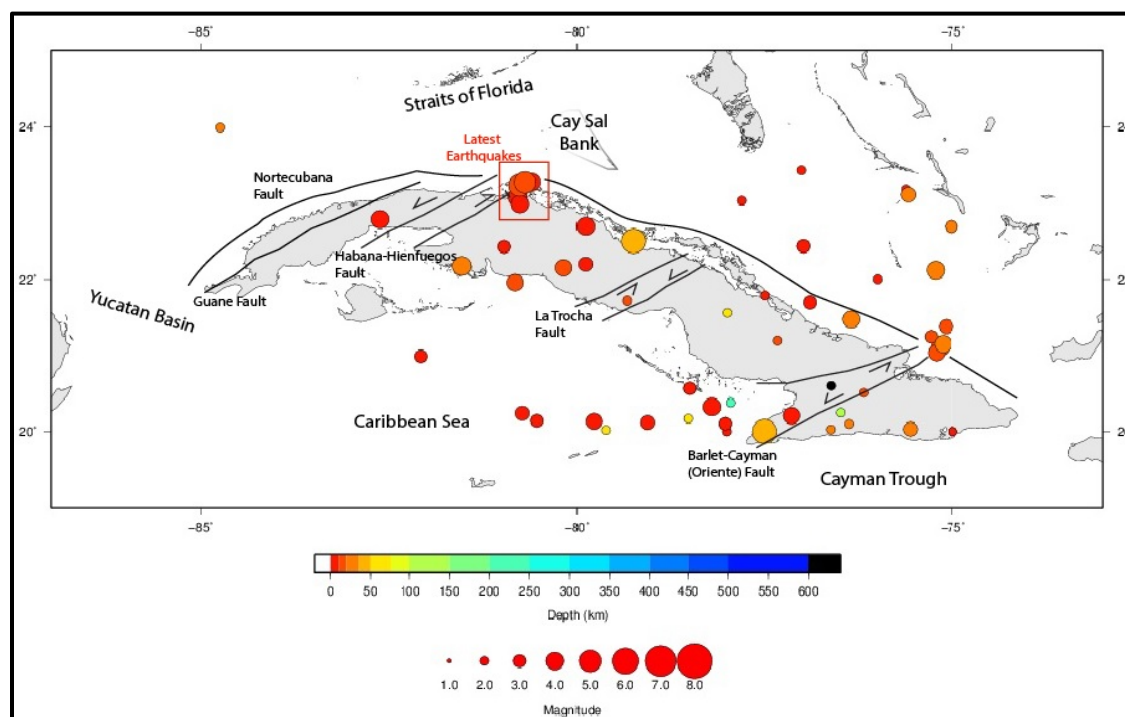
Figure 5-15. Seismological event catalogue of the Cuban area along with the active fault systems on the region. The event map is created using International Seismological Center's Online Bulletin. The latest earthquakes occurring in January-April 2014, are located in the north of Cuba alog the Nortecubana fault (red box). Fault locations are from Sauna et al. (2005) and Cotilla et al. (2007).

For a brief overview, the newly detected structural elements and evidence for neotectonic activity are illustrated in Figure 5-16. The deep-rooted fault systems associated with the sea floor break, and the growth-fold strata of the Cay Sal Anticline located on the northeastern side of the Cay Sal Bank indicate the active tectonic regime around the eastern side of the Cay Sal Bank. Considering the trend and location of these features, they are interpreted as parts of the Cuban Fold and Thrust Belt. The earthquake records are another indication for neotectonics in the region.
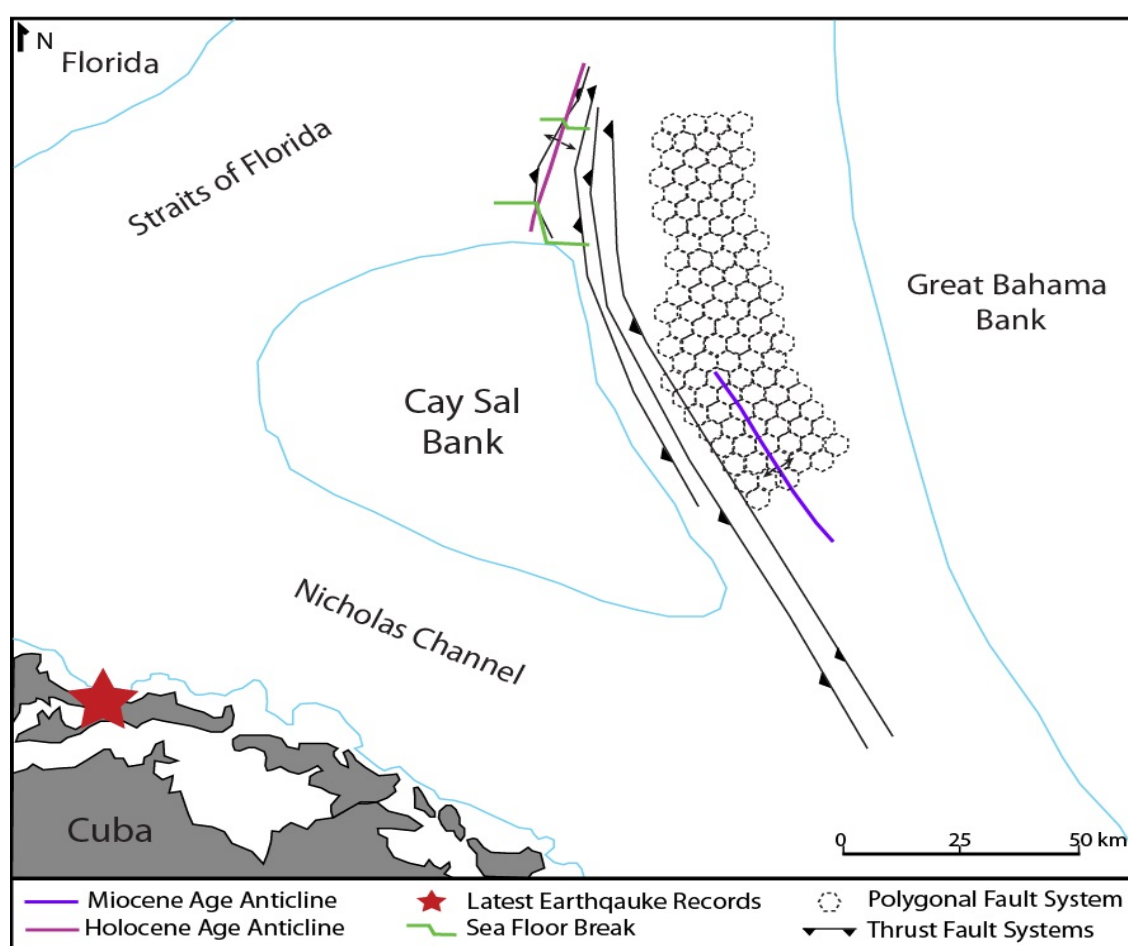
Figure 5-16. The location map of the structural units and the evidences for neotectonics. The crest of the SantaMiocene Anticline is shown as a purple line. The crest of the Cay Sal Anticline is outlined with a pink line. All the active structural features, the deep-rooted fault systems and the Cay Sal Anticline, are located at the northern edge of the Cay Sal Bank and are part of the Cuban Fold and Thrust Belt. The black dashed polygons are covering the location of the polygonal fault system which is not an expression of the tectonism of the region.

Summary and Discussion

The combination of long older regional seismic lines with new high-resolution seismic data, high-frequency sub-bottom and bathymetry profiles reveal the structural elements in the study area in great detail. Polygonal fault systems are observed throughout the Santaren Channel. They are interpreted as non-tectonic fault systems that act as a pathway for fluid flow. They are mostly found in the middle of the Santaren Channel where drift deposit is well developed. Deep-rooted fault systems are located along the eastern side of Cay Sal Bank. The two westernmost fault systems are interpreted as steep-rooted fault systems having wrench fault characteristics. Both reach and break the sea floor at several locations. The other two deep-rooted fault systems are interpreted as thrust fault systems. They reach into the Neogene strata. The trends of all these deep-rooted fault systems are NW-SE, which is the general trend of the edge of the Cuban Fold and Thrust Belt.

Two anticlines are found within the study area. The SantaMiocene Anticline is a very gentle, asymmetric anticline. It is located in the middle of the Santaren Channel and is oriented NW-SE. Cretaceous and Early Miocene strata is folded in the anticline. Younger sediments drape the anticline, indicating that the anticline is no longer active. The Cay Sal Anticline is located in the northeastern part of the Cay Sal Bank, trending in a NE-SW direction. The growth-fold strata of the anticline indicate that the anticline is presently active. A steep fault cuts through the crest of the anticline and breaks the sea floor along the northern part of the Cay Sal Bank, also indicating the presence of neotectonics in the area. New data from Jo (2013) shows that the Santaren Anticline, which is located in the southern Santaren Channel, has Holocene fold-growth strata. His

finding corroborates the speculation by Masaferro et al., (2002) that the anticline is growing in modern times. Thus, the growth geometry of both the Santaren and the Cay Sal anticlines, indicate that they are presently active and that the shortening between the southern part of the Bahamas and the Cuban Fold and Thrust Belt continues into the Holocene. This conclusion is corroborated by the 2014 earthquakes north of Cuba along the Nortecubana fault.

The structural elements mapped in this study are merged with the elements mapped by previous studies in the Santaren Channel to create a more complete map of the northern edge of the Cuban Fold and Thrust Belt (Figure 5-17). Integrating the locations of the Santaren Anticline and other structural features mapped by Masaferro (1997) with our structural location map reveals that the deep-rooted fault systems and the anticlines form the northern portion of the Cuban Fold and Thrust Belt. Breaks in the trend of the anticlines suggest that they are offset by the NE-SW trending faults. Similar trending faults dissect the structural patterns within the Island of Cuba. The dissected faults detected in our study might be related to the ones located in the Island of Cuba such as the La Trocha and Pinar faults, yet having no data in the Nicholas Channel prevents us from mapping their extent and exact location. Based on the analyzed data sets, the Cay Sal Anticline is the northeasternmost edge of the fold belt. Additional seismic data south of Cay Sal Bank in the Nicholas Channel and the Straits of Florida is required to map the trend of the fold belt along these southern regions (Figure 5-17).
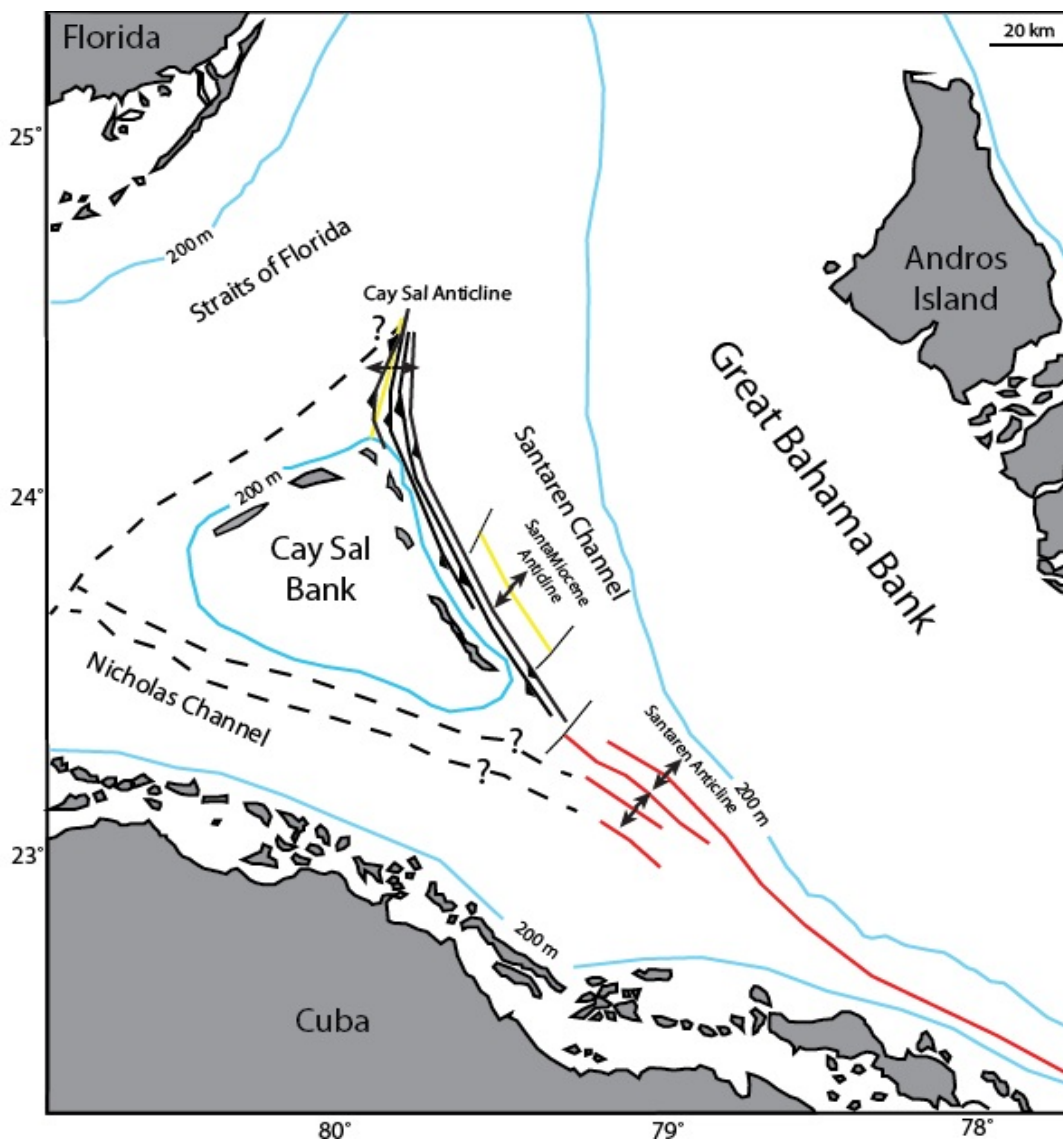
Figure 5-17. The locations of the structural elements from this study and previous studies are used to refine the location of the northern edge of the Cuban Fold and Thrust Belt. Yellow lines give the crests of two anticlines found in this study; the northern located one shows fold-growth strata. Red lines give the position of a series of anticlines, including the Santaren Anticline, drawn by Masaferro (1997). The anticlines and the deep-rooted fault systems are interpreted as part of the Cuban Fold and Thrust Belt. The Cay Sal Anticline forms the northeastern edge of the fold belt so far. Dashed lines indicate the possible trends of the belt, due to insufficient data those areas can not be documented.

The internal structure of the Cay Sal Bank indicates slightly folded strata (Figure 5-18). The mechanism behind this folding is most probably the one that creates the Cay Sal Anticline. The timing of the folding is consistent with the Cay Sal Anticline, also

both folding trends in the same direction. The eastern side of Cay Sal Bank is modified by deep-rooted fault systems. The active fault systems break the sea floor but also line the margin of the former Cay Sal Bank that bordered the deep re-entrant. Part of this bank drowned and is overlain by deep-water sediments. The easternmost fault system separates the platform from the deep-water sediment (Figure 5-18). Masaferro (1997) detected a detachment horizon underneath the anticlines further south. In the study area this detachment is not detectable due to the insufficient time depth of the newly acquired seismic profiles. As a consequence it can be proposed that the bank is a part of the Cuban Fold and Thrust Belt and that the anticline is quite likely the northeastern edge of the Cuban Fold and Thrust Belt.
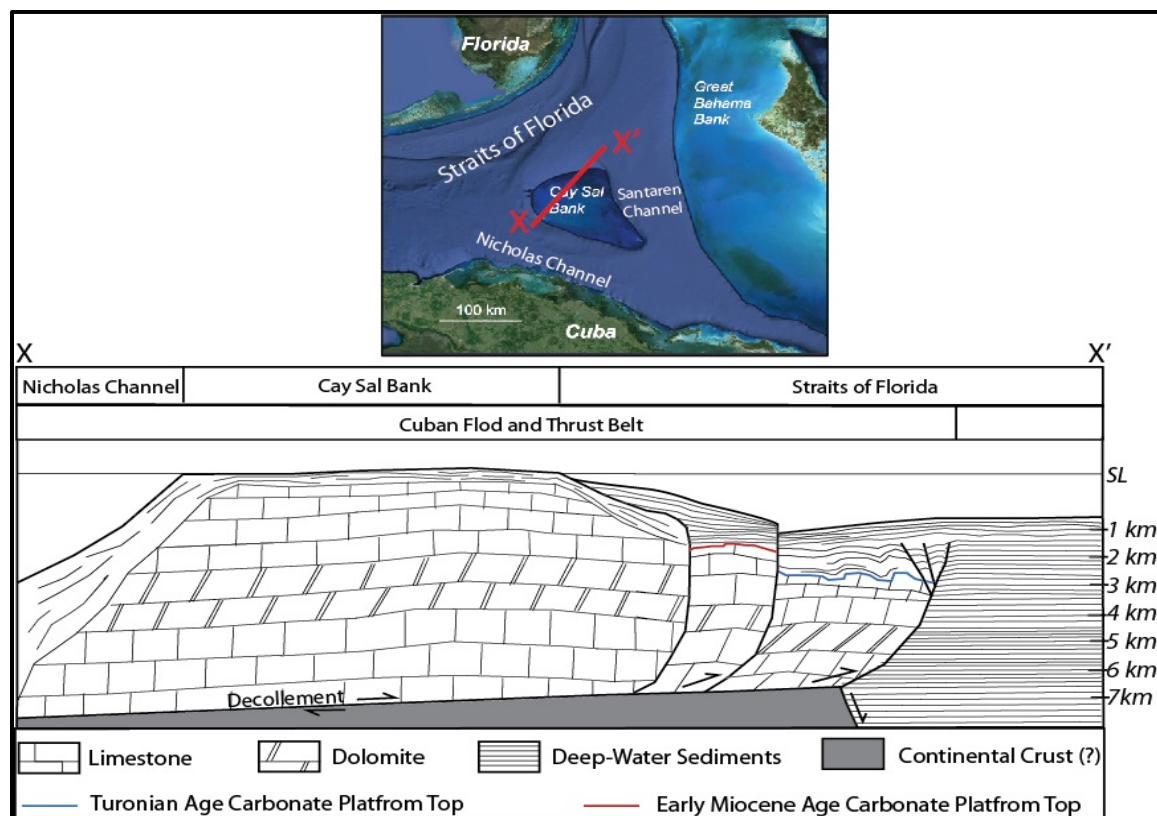
Figure 5-18. A cross-section from the Cay Sal Bank. The bending within the Cay Sal Bank indicates that the bank itself is slightly folded. Deep-rooted fault systems divide two major depositional systems: shallow-water carbonate platform and deep-water sediments and break sea floor. The 'Decollement Zone' is not observed in our data.

CHAPTER 6. CONCLUSIONS

The main goal of this study was to analyze the timing and nature of the tectonic elements around the Santaren Channel and to establish a possible connection between the Cuban Fold and Thrust Belt and the Cay Sal Bank. The interpretation of newly acquired high-resolution 2D seismic reflection and parasound profiles and bathymetric maps using a multibeam echosounder around the Santaren Channel presents new insights into the sedimentary process and tectonic modification of the region.

The high-resolution 2D seismic profiles are processed and migrated. The migrated profiles have been cleaned of all unwanted events such as multiples, noises, sea column effects etc. Five seismic horizons from Pre-Neogene and Neogene strata are used to create surface maps in order to reveal the morphological evolution of the Santaren Channel. The surface maps indicate that the Santaren Channel has been shoaling southward from Albian through Pleistocene time. Two anticlines are detected in the surface map of Horizon 4, which is Turonian in age. Surface maps from Miocene strata reveal that slope expansion modified the basin to a slightly V-shaped form. The depth of the basin decreases through time. This shallowing is probably a result of the accumulation of drift sediments.

Three main depositional systems are identified and related to the seismic facies in the area: basinal, slope, and platform system. These systems are subdivided into seven units: shallow-water carbonate platform, slope and basinal facies, sub-marine channels, deep-water sediments, drift deposits, sediment waves, and debris/slump flow. The shallow-water carbonate platforms are characterized by highly chaotic seismic facies layered by strong parallel reflections on top.

The slope and basinal seismic facies are generally the dominant facies in our seismic profiles. Their internal character indicates the effect of the sea-level changes and strong current activities along the Santaren Channel. This facies includes platform-derived material and pelagic sediments. Deep-water sediments interfinger with the basin and platform sediments at the toe of slope. The drift facies is located in the middle of the Santaren Channel. Vertical faults with little offset disturb the internal reflection characteristics of the drift facies. These strata-bound fault systems are not related to the tectonic regime in the area. The polygonal faults are generally found in deep-water sediments along the Santaren Channel. Seismic interpretation reveals that their numbers obviously increased in the middle of the Santaren Channel where the drift deposit is well developed. These faults are interpreted to be acoustic pipes and polygonal faults. Abrupt strong, discontinuous reflections known as bright spots are identified in some sections. In addition, pockmarks are present above these features. All four features, the polygonal faults, the acoustic pipes, the bright spots and the pockmarks, are most likely caused by migrating fluid and/or hydrocarbons in the Santaren Channel.

Structural evaluation reveals compressional structures, some of which are presently active. Deep-rooted fault systems are observed along the eastern side of the Cay Sal Bank and they generally trend NW-SE, following the trend of the Cuban Fault and Thrust Belt. Some of these faults reach Holocene strata and break the sea floor on the northeastern side of the Cay Sal Bank. Two anticlines are detected in different parts of the study area. The first anticline is the SantaMiocene Anticline, which is located in the middle of the Santaren Channel, trending in a NW-SE direction. Cretaceous and Early Miocene strata are folded in the anticline. The other anticline, the Cay Sal Anticline, is

located in the northeastern side of Cay Sal Bank and trends in a NE-SW direction. The Holocene strata is part of the growth-fold strata, indicating that the anticline is presently active. Sea floor breaks are evidence of neotectonic activities around the Cay Sal Bank. Having five earthquakes, ranging in magnitude between 4 and 5 within the last four months in the northwestern region of Cuba is further support for the modern movement in the area. All of these new structures are found around the northeastern and the eastern side of the Cay Sal Bank. Considering the location of these features, and the folded strata detected within the bank itself, it can be claimed that the Cay Sal Bank is a part of the Cuban Fold and Thrust Belt and that, most probably, the Cay Sal Anticline is the northern edge of the Cuban Fold and Thrust Belt (Figure 6-1).
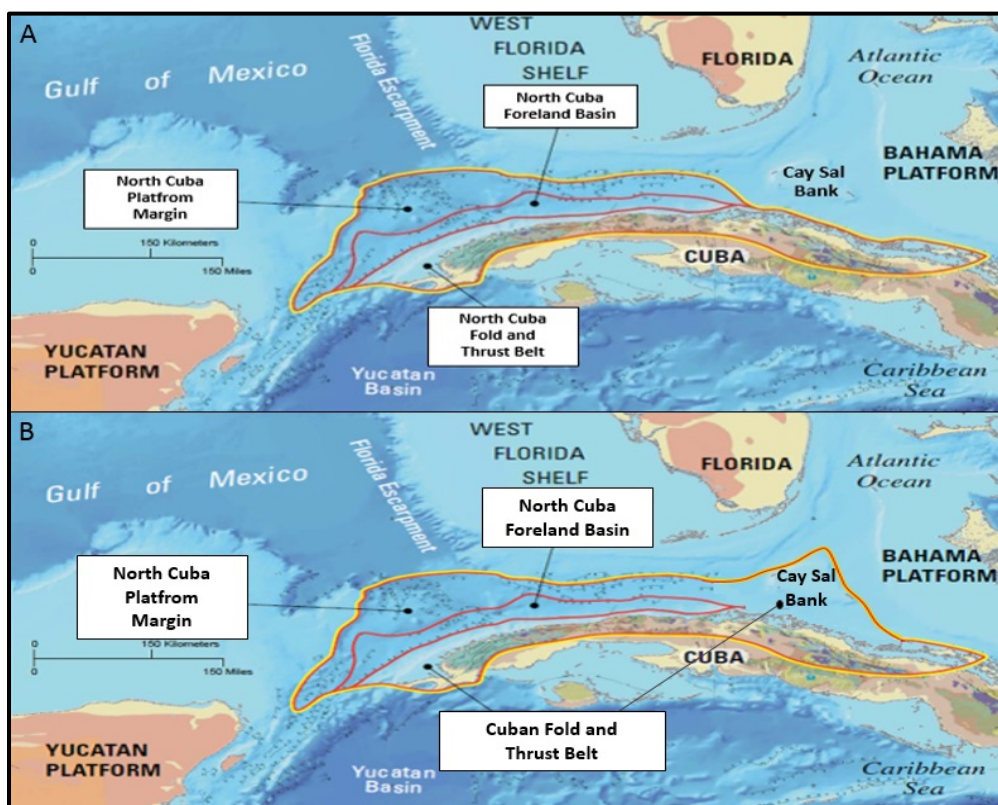

Figure 6-1. (A) shows generally accepted location map of the Cuban Fold and Thrust Belt. The fold belt is re-mapped regarding the findings of this study. (B) illustrates the final location map of the Cuban Fold and Thrust Belt.

REFERENCES

Anselmetti, F.S., G.P. Eberli, and Z. Ding, 2000, From the Great Bahama Bank into the Straits of Florida: A margin architecture controlled by sea-level fluctuations and ocean currents: Geological Society of American Bulletin, v. 112, no. 6, p. 829-844.

Austin, J.A., W. Schlager, et al., 1988, *Proceedings of the Ocean Drilling Program: Scientific Results*, Leg101: College Station, Texas, Ocean Drilling Program. v.101, 569 pp.

Austin, J.A., J.I. Ewing, J. W. Ladd, H.T. Mullins, and R. E. Sheridan, 1988a, Seismic stratigraphic implications of ODP Leg 101 site surveys. *In* J.A. Austin, Jr. and W. Schlager, et al., (Editors) *Proceedings of the Ocean Drilling Program, Scientific Results, Leg101*: College Station, Texas, Ocean Drilling Program. v.101, p. 391-424.

Austin, J.A., W. Schlager, 1988b, Leg 101- An Overview. *In* J.A. Austin, Jr. and W. Schlager (Editors) *Proceedings of the Ocean Drilling Program, scientific results, Leg101*: College Station, Texas, Ocean Drilling Program. v.101, p. 455-472.

Ball, M. M., M. R. Martin, W. Bock, R. Sylvester, R. Bowles, D. Taylor, E. Coward, J. Dodd and L. Gilbert, 1985, Seismic structure and stratigraphy of northern edge of Bahamian-Cuban collision zone: American Association of Petroleum Geologist Bulletin, v. 69, p. 1275-1294.

Bergman, K.L., H. Westphal, X. Janson, A. Poiriez, and G. P. Eberli, 2010, Controlling Parameters on Facies Geometries of the Bahamas, an Isolated Carbonate Platform Environment. *In* H. Westphal, B. Riegl, G.P. Eberli (Editors) *Carbonate Depositional Systems: Assessing Dimensions and Controlling Parameters*: Springer Science and Business Media B.V. 2010, p. 5-11.

Betzler, C., J. J. G. Reijmer, K. Bernet, G. P. Eberli, and F. S. Anselmetti, 1999, Sedimentary patterns and geometrics of the Bahamian outer carbonate ramp (Miocene-Lower Pliocene, Great Bahama Bank): Sedimentology, v. 46, no. 6, p. 1127-1143.

Bosellini, A., 1989, Dynamics of Tethyan carbonate platforms. *In* P.D. Crevello, J.L. Wilson, J.D. Sarg and J.F. Read (Editors) *Controls on carbonate platform and basin development*: SEPM Special Publication, No: 44, p. 3-13.

Burke, K., C. Cooper, J.F. Dewey, P. Mann, and J.L. Pindell, 1984, Caribbean tectonics and relative plate motions. *In* W. Bonini, R.B. Hargraves, R. Shagam (Editors) *The Caribbean–South American Plate Boundary and Regional Tectonics*: Geological Society of America Bulletin, v. 162, p. 31–63.

Betzler, C., J.J.G. Reijmer, K. Bernet, and G.P. Eberli, 1999, Sedimentary patterns and geometries of the Bahaminan outer carbonate ramp (Miocene- Lower Pliocene, Great Bahama Bank): Sedimentology, v. 46, p. 1127-1143.

Betzler, C., et al, 2013, Meteor-Berichte: Cruise Report CICARB, Cruise No. M95.

Biddle, K.T., N. Christie-Blick, 1985, *Strike-slip deformation, basin formation, and sedimentation: based on a symposium*: Society of Economic Paleontology and Mineralogy Special Publication, v. 37.

Boss, S.K., and K.A. Rasmussen, 1995, Misuse of Fischer plots as sea-level curves: Geology, v. 23, p. 221–2

Carew, J.L., J.E. Mylroie, and S.J. Schwabe, 1998, The geology of South Andros Island, Bahamas: A reconnaissance report: Cave and Karst Science, v. 25, p. 57-66.

Cartwright, J.A., and D.N. Dewhurst, 1998, Layer-bound compaction faults in fine-grained sediments: Geological Society of America Bulletin, v. 110, no. 10, p. 1242-1257.

Chen, D., S. Wu, X. Wang, and F. Lv, 2011, Seismic expression of polygonal faults and its impact on fluid flow migration for gas hydrates formation in deep water of the South China Sea: Journal of Geological Research, vol. 2011, 7 pp., Article ID 384785.

Chun, J.H., and Jacewitz C. A., 1981, Fundamentals of frequency domain migration: Geophysics, v. 46, no. 5, p. 717-733.

Cotilla, M., E. Gonzales, H.J. Franzke, J. Pilarski, J. L. Comasenas, J. Oro, F. Arteaga, L. Alvarez, 1991, Neotectonic map of Cuba, scale: 1: 1 000 000: Scientific Communications on Geophysics and Astronomy, v.22, 28 pp.

Cotilla, M., 1998, An overview on the seismicity of Cuba: Journal of Seismology, v.2, p. 323-335.

Cotilla, M., H.J. Franzke, D. Cordoba Barba, 2007, Seismicity and seismoactive faults of Cuba: Russian Geology and Geophysics, v. 48, p. 505-522.

Curran, H.A., 1997, Introduction to the geology of the Bahamas and San Salvador Island, with an overflight guide. *In* H.A. Curran (Editor) *Guide to Bahamian ichnology: Pleistocene, Holocene, and modern environments*: San Salvador, CCFL Bahamian Field Station, p. 1-10.

Denny, W.M., J.A. Austin, R.T. Buffler, 1994, Seismic Stratigraphy and geologic history of middle Cretaceous through Cenozoic rocks, Southern Straits of Florida: AAPG Bulletin, v. 78, no. 3, p. 461-487.

Dillon, P.S., J.A. Austin, N. Scanlon and K.D. Klitgord, 1987, Geology of the Caribbean: Oceanus, v. 30, p. 42-52.

Draper, G., Jackson, T.A., and Donovan, S.K., 1994, Geologic provinces of the Caribbean Region. *In* S.K. Donovan and T.A. Jackson (Editors) *Caribbean Geology: an introduction*: University of the West Indies Publishers Association/University of the West Indies Press, Kingston, Jamaica, p. 3-12.

Dondurur, D., 2009, *Deniz Sismiginde Veri-Islem*: UCTEA Chamber of Geophysical Engineers Education Series, No. 11.

Echevarria-Rodriguez, G., G. Hernandez-Perez, J. O. Lopez-Quintero, J. G. Lopez-Rivera, R. Rodriguez-Hernandez, J. R. Sanchez-Arango, R. Socorro-Trujillo, R. Tenreyro-Perez, and J. L. Yparraguirre-Pena, 1991, Oil and gas exploration in Cuba. Journal of Petroleum Geology, v. 14, 259–274.

Eberli, G.P., and R. N. Ginsburg, 1987, Segmentation and coalescence of Cenozoic carbonate platforms, northwestern Great Bahama Bank, Geology, v. 15, p. 75-79.

Eberli, G.P, 1988, Physical properties of carbonate turbidite sequences surrounding Bahamas: Implications for slope stability and fluid movements. *In* J.A. Austin, Jr. and W. Schlager (Editors) *Proceedings of the Ocean Drilling Program, scientific results, Leg101*: College Station, Texas, Ocean Drilling Program. v.101, p. 305-314.

Eberli, G.P., and R. N. Ginsburg, 1989, Cenozoic progradation of northwestern Great Bahama Bank, a record of lateral platform growth and sea-level fluctuations. *In* P. D. Crevello, J. L. Wilson, J. D. Sarg and J. F. Read (Editors) *Control on carbonate Platform and basin development*: Society of Economic Paleontology and Mineralogy Special Publication, v. 44, p. 339-351.

Eberli, G.P., 1991, Growth and demise of isolated carbonate platforms: Bahamian Controversies. *In* Müller et al. (Editors) *Controversies in Modern Geology*: Academic Press., p. 231 -248.

Eberli, G.P, P.K. Swart, M.J. Malone, et al., 1997, *Proceedings of the Ocean Drilling Program: Scientific Results*, v. 166, 850 pp.

Eberli, G.P., P.K. Swart, D.F, McNeill, J.A.M Kenter, F.S. Anselmetti, L.A. Melim, R.N Ginsburg, 1997a, A synopsis of the Bahamas Drilling Project: results from two deep core borings drilled on the great Bahama Bank. *In* G.P. Eberli, P.K. Swart, M.J. Malone, et al., (Editors) *Proceedings of the Ocean Drilling Program: Scientific Results*, v. 166, p. 23-42.

Eberli, G.P, P.K. Swart, M.J. Malone, et al., 1997b, Chapter 9. Site 1006: Shipboard scientific party. *In* G.P. Eberli, P.K. Swart, M.J. Malone, et al., (Editors) *Proceedings of the Ocean Drilling Program: Scientific Results*, v. 166, p. 233-268.

Eberli, G.P., 2000, The record of neogene sea-level changes in the prograding carbonates along the Bahamas Transect- leg 166 Synthesis. *In* P.K. Swart, G.P. Eberli, M.J. Malone, and J.F. Sarg (Editors), *Proceedings of the Ocean Drilling Program: Scientific Results*, v. 166, p.167-177.

Eberli, G.P., F.S. Anselmetti, D. Kroon, T. Sato, and J.D. Wright, 2002, The chronostratigraphic significance of seismic reflections along the Bahama Transect: Marine Geology, v. 185, p. 1-17.

Eberli, G. P, J.L. Masaferro, and J.F. Sarg, 2004, *Seismic imaging of carbonate reservoirs and systems:* American Association of Petroleum Geologists Memoir, v. 81.

Eberli, G. P., F. S. Anselmetti, C. Betzler, J. H. Van Konijnenburg, and D. Bernoulli, 2004, Carbonate platform to basin transitions on seismic data and in outcrops: Great Bahama Bank and the Maiella platform margin, Italy. *In Seismic imaging of carbonate reservoirs and systems*: American Association of Petroleum Geologists Memoir, v. 81, p. 207-250.

Eberli, G.P., and P.M. Harris, 2013, *Facies successions on Great Bahama Bank: Implications for exploration and reservoir characterization*: Comparative sedimentology Laboratory, University of Miami, Field Guide, 167 pp.

Enos, P., 1974, Map of surface sediment facies of the Florida-Bahama Plateau: Geological Society of America Map Series MC-5, Boulder/CO.

Fairbridge, R.W., R.N. Young, C.G.A. Harrison and M.M. Ball, 1974, Bahamas: *In* R.W. Fairbridge (Editor) Encyclopedia of World Regional Geology, Part I., p. 109-115.

Fulthorpe, C.G., A.J. Melillo, 1988, Middle Miocene carbonate gravity flows in the Straits of Florida at site 626. *In* J.A. Austin, Jr. and W. Schlager, et al., (Editors) *Proceedings of the Ocean Drilling Program, Scientific Results, Leg101*: College Station, Texas, Ocean Drilling Program. v.101, p. 179-191.

Gadallah, M. R., R. L. Fisher, 2005, *Applied Seismology: A Comprehensive Guide to Seismic Theory and Application*, Penn Well Publishing, 473 pp.

Gay, A. and C. Berndt, 2007, Cessation/reactivation of polygonal faulting and effects on fluid flow in the Voring Basin, Norwegian margin: Journal of the Geological Society of London, v. 164, p. 129-141.

Giunta, G. and S. Orioli, 2011, The Caribbean Plate Evolution: Trying to Resolve a Very Complicated Tectonic Puzzle, i*n* E. V. Sharkov (Editor), New Frontiers in Tectonic Research - General Problems, Sedimentary Basins and Island Arcs: Chapter 10.

Gordon, M. B., P. Mann, D. Cáceres and R. Flores, 1997, Cenozoic tectonic history of the North America-Caribbean plate boundary zone in western Cuba: Journal of Geophysical Research, v. 102, p. 10055–10082.

Harding, T.P., 1985, Seismic characteristics and identification of negative flower structures, positive flower structures, and positive flower inversion: American Association of Petroleum Geologists Bulletin, v. 69, n. 4, p. 582-600.

Harding, T.P., R.C. Vierbuchen, N. Christie-Blick, 1985, Structural styles, plate tectonic settings, and hydrocarbon traps of divergent (transtensional) wrench faults: Society of Economic Paleontologists and Mineralogists Special Publication, v. 37, p. 51-77.

Harding, T.P., A.C. Tuminas, 1988, Interpretation of footwall (lowside) fault traps sealed by reverse faults and convergent wrench faults: American Association of Petroleum Geologists Bulletin, v. 72, n. 6, p. 738-757.

Harding, T.P., 1990, Identification of wrench faults using subsurface structural data: Criteria and Pitfalls: American Association of Petroleum Geologists Bulletin, v. 74, n. 10, p. 1590-1609.

Harris, P.M., G.P. Eberli, and G.M. Grammer, 2008, Reservoirs in isolated carbonate platforms– Insight from Great Bahama Bank: Search and Discovery Article #50083.

Hine A.C., and J.C. Steinmetz, 1984, Cay Sal Bank, Bahamas- A partially drowned carbonate platform: Marine Geology, v. 59, p. 135-164.

Hovland, M., and A.G Judd, 1988, *Seabed pockmarks and seepages: Impact on geology, biology and the marine environment*: Graham& Trotman Ltd., London, 293 pp.

Hustoft, S., J. Mienert, S. Bunz, and H. Nouze, 2007, High-resolution 3D-seismic data indicate focussed fluid migration pathways above polygonal fault systems of the mid-Norwegian margin: Marine Geology, v. 245, p. 89-106.

Imbrie, J. and E. G. Purdy, 1962, Classification of modern Bahamian carbonate sediments. *In* W. E. Ham (Editor) *Classification of Carbonate Rocks*: American Association of Petroleum Geologists Memoir, v. 1, p. 253-272.

Iturralde-Vinent, M., 1994, Cuban geology: A new plate-tectonic synthesis: Journal of Petroleum Geology, v. 17, p. 39-70.

Iturralde-Vinent, M., 2003, The relationships between the ophiolites, the metamorphic terranes, the Cretaceous volcanic arcs and the Paleocene-Eocene volcanic arc: Field Guide to a geological excursion to eastern Cuba on the subject: 5th Cuban Geological and Mining Congress, IGCP Project 433 Caribbean Plate Tectonics Field Workshop, Havana, Cuba, March 18-23.

Iturralde-Vinent, M., C.D. Otero, A. García-Casco, and D.J.J. van Hinsbergen, 2010, Paleogene foredeep basin deposits of North-Central Cuba: A record of arc-continent collision between the Caribbean and North American Plates: International Geological Review, v. 50, p. 863-884.

International Seismological Centre, *On-line Bulletin*, http://www.isc.ac.uk, Internatl. Seis. Cent., Thatcham, United Kingdom, 2011.

Jo, Andrew, 2013, Carbonate slope morphology and sedimentary process along southwestern Great Bahama Bank: Master thesis, University of Miami, 122 pp.

Kenter, J.A.M., F.S. Anselmetti, P.H. Kramer, H. Westphal, M.G.M. Vandamme, 2002, Acoustic Properties of "Young" Carbonate Rocks, ODP Leg 166 and Boreholes Clino and Unda, Western Great Bahama Bank: Journal of Sedimentary Research, v. 72, p. 129-137.

Ladd, J. W. and R., E. Sheridan, 1987, Seismic stratigraphy of the Bahamas: American Association of Petroleum Geologists Bulletin, v. 71, p. 719-736.

Leroy, S., A. Mauffret, P. Patriat, and B. M. de Lepinay, 2000, An alternative interpretation of the Cayman trough evolution from a reidentification of magnetic anomalies: Geophysical Journal International, v. 141(3), p. 539–557.

Løseth, H., L. Wensaas, B. Arntsen, N. Hanken, C. Basire and K. Graue, 2001, 1000 m. lomg gas blow-out pipes: EAGE 63rd Conference& Technical Exhibition, Amsterdam, Netherlands, 11-15 June.

Lonergan, L., J. Cartwright, and R. Jolly, 1998, The geometry of polygonal fault systems in Tertiary mudrocks of the North Sea: Journal of Structural Geology, v. 20, No. 5, p. 529-548.

Mann, P. And K. Burke, 1984, Neotectonics of the Caribbean region: Reviews of Geophysics and Space Physics, v.22 (4), p. 309-362.

Mann, P., F.W. Taylor, R. Lawrence Edwards, and Teh-Lung Ku, 1995, Actively evolving microplate formation by oblique collision and sideways motion along strike-slip faults: An example from the northeastern Caribbean plate margin: Tectonophysics, v. 246, p. 1-69.

Masaferro, J.L., and G.P. Eberli, 1994, Structural Control of the evolution of a carbonate platform along a compressional plate boundary, southern Great Bahama Bank (abstr.): Geological Society of America Abstract Programs, v.26, A364-A365.

Masaferro, J.L., 1997, Interplay of tectonism and carbonate sedimentation in the Bahamas foreland basin: Ph. D. thesis, University of Miami, 146 pp.

Masaferro, J.L., and G.P. Eberli, 1999, Jurassic-Cenozoic structural evolution of the southern Great Bahama Bank. *In* K.J. Hsu, and P Mann (Editors) Sedimentary Basins of the World: v. 4, Caribbean Basins, p. 167-193.

Masaferro, J.L., J. Poblet, M. Bulnes, G.P. Eberli, T.H. Dixon and K. McClay, 1999, Palaeogene-Neogene/present day(?) growth folding in the Bahamian foreland of the Cuban Fold and Thrust Belt: Journal of Geological Society, London., v. 156, p. 617-631.

Masaferro, J.L., M. Bulnes, J. Poblet, and G.P. Eberli, 2002, Episodic folding inferred syntectonic carbonate sedimentation: the Santaren anticline, Bahamas foreland: Sedimentary Geology, v. 146, p. 11-24.

Masson, D.G, B.J. Bett, D.S.M. Billett, C.L. Jacobs, A.J. Wheeler, and R.B. Wynn, 2003, The origin of deep-water, coral-topped mounds in the northern Rockall Trough, Northeast Atlantic: Marine Geology, v. 194, p. 159-180.

Melim, L.A., J.L. Masaferro, 1997, Geology of the Bahamas: Subsurface geology of the Bahamas Banks. *In* H.L. Vacher and T. Quinn (Editors) Geology and Hydrogeology of Carbonate Islands Developments in Sedimentology: v.54, p. 161-181.

Meschede, M., and W. Frisch, 1998, A plate-tectonic model for the Mesozoic and Early Cenozoic history of the Caribbean plate: Tectonophysics, v. 296, p. 269-291.

Meyerhoff, A.A., and C.W. Hatten, 1974, Bahamas salient of North America: Tectonic framework, stratigraphy, and petroleum potential: American Association of Petroleum Geologists Bulletin, v. 58, p. 1201-1239.

Mitchum, R.M., P.R. Vail, and S. Thompson, 1977, Seismic stratigraphy and global changes of sea-level: The depositional sequence as a basic unit for stratigraphic analysis. *In* C.E. Payton (Editor) *Seismic Stratigraphy: Applications to hydrocarbon explorations*: American Association of Petroleum Geologists Memoir 26, p. 53-62.

Mountain, G.S, B.E. Tucholke, 1989, Abyssal sediment wave. *In* A.W. Bally (Editor) Atlas of seismic stratigraphy: American Association of Petroleum Geologists Studies in Geology, v.27, no.3, p. 233-236.

Mullins, H. T. and G.W. Lynts, 1977, Origin of the northwestern Bahama Platform: Geological Society of American Bulletin, v. 88, p. 1447-1461.

Mullins, H.T., A.C. Neumann, R.J. Wilber, A.C. Hine, and S.J. Chinburg, 1980, Carbonate sediment drifts in the northern Straits of Florida: American Association of Petroleum Geologists Bulletin, v. 64, p. 1701-1717.

Mullins, H.T., 1983, Modern carbonate slope and basins of the Bahamas. *In* H.E. Cook, A.C. Hine, H.T. Mullins (Editors) Platfrom margin and deepwater carbonates: Society of Economic Paleontologists and Mineralogists Course 12, p. 4.1-4.138.

Mullins, H.T., N. Breen, J. Dolan, R. Wellner, L. Petruccione, M. Gaylord, B. Andersen, A. Melillo, A. Jurgens, and D. Orange, 1992, Carbonate platforms along the southeast Bahamas-Hispaniola collision zone: Marine Geology, v. 105, p. 169-209.

Pindell, J.L., and S.F. Barrett, 1990, Caribbean plate tectonic history. *In* G. Dengo and J.E. Case (Editors), The Caribbean region: Geological Society of America, The geology of North America, v. H, p. 405-431.

Pindell, J.L. and L. Kennan, 2009, Tectonic Evolution of the Gulf of Mexico, Caribbean and northern South America in the mantle refence frame: an update. *In* K. James, M.A. Lorente and J. Pindell (Editors) *The geology and evolution of the region between North and South America*: Geological Society of London, Special Publication, v. 328, p. 1-59.

Poiriez, A., 2004, Tectonostratigraphy of the Florida Straits and northwestern Bahamian Archipelago: Master Thesis, University of Miami, 126 pp.

ProMAX® R5000.8.2.3 software Reference Manual

Purkis, S., J. Kerra, A. Dempseya, A. Calhouna, L. Metsamaaa, B. Riegla, V. Kourafaloub, A. Brucknerc, P. Renaudc, 2014, Large-scale carbonate platform development of Cay Sal Bank, Bahamas, and implications for associated reef geomorphology:Geomorphology, http://dx.doi.org/10.1016/j.geomorph.2014.03.004.

Reijmer, J.J.G., P.K. Swart, T. Bauch, R. Otto, L. Reuning, S. Roth, S. Zechel, 2009, A re-evaluation of facies on Great Bahama Bank I: new facies maps of western Great Bahama Bank: International Association of Sedimentologists Special Publication, v. 41, p. 29-46.

Rosencrantz, E., P. Mann and J. Sclater, 1988, Age and spreading history of the Cayman Through as determined from depth, heat flow and magnetic anomalies: Journal of Geophysical Research, v. 93, p. 2141-2157.

Ross, M. I. and C. R. Scotese, 1988, A hierarchical tectonic model of the Gulf of Mexico and Caribbean region: Tectonophysics, v. 155: p. 139-168.

Rowan, M.G., 2011, Structural Analysis of the Bahamian Foreland of the Cuban-Bahamian Fold-and-Thrust Belt: Bahamas Petroleum Company Plc, Southern Bahamas Licenses: Bain, Cooper, and Donaldson, p. 1-22.

Rubio, M., 1985, The assessment of seismic hazard for the republic of Cuba. *In* Proceedings of the 3rd International Symposium on the Analysis of Seismicity and on Seismic Risk, Liblice Castler, Czechoslavakia, June 17-22, p. 424-431.

Saura, E., J. Vergés, D. Brown, P. Lukito, S. Soriano, S. Torrescusa, R. García, J. R. Sánchez, C. Sosa and R. Tenreyro, 2008, Structural and tectonic evolution of western Cuba fold and thrust belt: Tectonics, v. 27, TC4002.

Schlager, W., 1981, The paradox of drowned reefs and carbonate platforms: Geological Society of America Bulletin, v. 92, p. 197-211.

Schlager, W., and R.N. Ginsburg, 1981, Bahama carbonate platforms- the deep and the past: Marine Geology, v. 44, p. 1-24.

Schlager W., F. Bourgeois, G. MacKenzie and J. Smit, 1988, Boreholes at Great Isaac and Site 626 and the history of the Florida Straits. *In* J. A. Austin, Jr., W. Schlager (Editors) *Proceedings of the Ocean Drilling Program, scientific results. Leg 101*: College Station, Texas, Ocean Drilling Program, v. 101, p. 425-437.

Sheridan, R.E., 1988, Geology and geophysics of the Bahamas, The Atlantic Continental margin: U.S. Geological Society of America, v. 1-2, p. 329-364.

Sheridan, R.E., J.T. Crosby, G.M. Bryan and P.L. Stoffa, 1981, Stratigraphy and structure of southern Blake Plateau, northern Florida straits, and northern Bahama platform from multichannel seismic reflection data: American Association of Petroleum Geologists Bulletin, v.65, p. 2571-2593.

Sheriff, R.E., 1980, *Seismic Stratigraphy*: International Human Resources Development Corporation, Edition 1.

Tator, B.A., and L.E. Hatfield, 1975a, Bahamas present complex geology: Oil and Gas Journal, v. 73, p. 172-176.

Tator, B.A., and L.E. Hatfield, 1975b, Bahamas present complex geology, part 2: Oil and Gas Journal, v. 74, p.120-122.

Tearporck, D.J., and R.E. Bischke, 1991, *Applied subsurface geological mapping*: Prentice Hall.

Uchupi E., J. D. Milliman, B.P. Luyendyk, C.O. Bowin and K.O. Emery, 1971, Structure and origin of Southeastern Bahamas: American Association of Petroleum Geologists Bulletin, v. 55, no. 5, p. 687-704.

U.S. Geological Survey, 2004, Assessment of Undiscovered Oil and Gas Resources of the North Cuban Basin: http://walrus.wr.usgs.gov/infobank/programs/html/factsheets/pdfs/2005_3009.pdf

Vail, P.R, A.G. Todd, J.B. Sangree, 1977, Chnostratigraphic significance of seismic reflections. *In* C.E. Payton (Editor) *Seismic Stratigraphy- Applications to Hydrocarbon Exploration:* American Association of Petroleum Geologists Memoir, v. 26, p. 99-116.

Walles, F.E., 1993, Tectonic and diagenetically induced seal failure within the Southwestern Great Bahama Bank: Marine and Petroleum Geology, v. 10, p. 14-27.

Westervelt, P.J., 1963, Parametric acoustic array: J. Acoust. Soc. Am., v. 35, p. 535-537.

Yilmaz, O., 2001, *Seismic Data Analysis Processing, Inversion, and Interpretation of Seismic Data Volume 1*. *In* Society of Exploration Geophysicists.